



**Max-Planck-Institut für Metallforschung**  
Stuttgart

---

## **Diffusion in Stressed Thin Films**

Jay Chakraborty

Dissertation  
an der  
**Universität Stuttgart**

---

Bericht Nr. 161  
März 2005

# Diffusion in Stressed Thin Films

Von der Fakultät für Chemie der Universität Stuttgart  
zur Erlangung der Würde eines Doktors der  
Naturwissenschaften (Dr. rer. nat.) genehmigte Abhandlung

Vorgelegt von

**Jay Chakraborty**

aus Kalkutta in Indien

Hauptberichter:	Prof. Dr. Ir. E. J. Mittemeijer
Mitberichter:	Prof. Dr. F. Aldinger
Tag der Einreichung:	28. Dezember 2004
Tag der mündlichen Prüfung:	17. März 2005

Max-Planck-Institut für Metallforschung Stuttgart,  
Institut für Metallkunde der Universität Stuttgart,

Stuttgart, 2005



## Table of Contents

<b>1. INTRODUCTION</b>	<b>7</b>
<b>2. INTERACTION OF STRESS AND DIFFUSION IN A BINARY SUBSTITUTIONAL SOLID SOLUTION</b>	<b>11</b>
ABSTRACT	11
2.1. INTRODUCTION	12
2.2. THEORETICAL BACKGROUND	14
2.2.1. Definitions: Network solid and composition variables	14
2.2.2. Diffusion potentials	15
2.2.3. Stress dependence of diffusion potentials	16
2.2.4. Basis of diffusion formalism	17
2.3. DIFFUSION FLUX EQUATIONS: SELF-, INTRINSIC-, AND INTERDIFFUSION COEFFICIENTS	19
2.3.1. Flux equations in lattice-fixed frame of reference	19
2.3.2. Flux equations in laboratory-fixed frame of reference	21
2.4. NUMERICAL SIMULATION	24
2.4.1. Diffusion equation	24
2.4.2. Dimensionless diffusion equation	25
2.4.3. Initial and boundary conditions	26
2.4.4. Considered stress profiles	27
2.4.4.1. <i>Externally applied stress profiles</i>	27
2.4.4.2. <i>Diffusion-induced, internal stress profiles</i>	27
2.4.5. Numerical procedure	28
2.4.5.1. <i>Finite difference formulation of diffusion equation</i>	28
2.4.5.2. <i>Finite difference formulation of boundary conditions</i>	29
2.4.5.3. <i>Finite difference formulation of the diffusion-induced, internal stress profiles</i>	30
2.4.6. System studied and data used	31
2.5. RESULTS AND DISCUSSION	33



2.5.1. Zero stress gradient	33
2.5.2. Externally applied Positive and negative stress gradient	34
2.5.3. Effect of internal, diffusion-induced stress on diffusion	37
2.6. SUMMARY	39
APPENDIX 2A: Derivation of equation (2.24) in section 2.3.1	40
APPENDIX 2B: Derivation of equation (2.42) in section 2.3.2	42
APPENDIX 2C: Details of finite difference methods	43
APPENDIX 2D: Finite difference versions of boundary conditions	45
<b>3. MECHANISMS OF INTER-DIFFUSION IN Pd-Cu</b>	
<b>THIN FILM DIFFUSION COUPLES</b>	<b>47</b>
ABSTRACT	47
3.1. INTRODUCTION	48
3.2. THEORY	49
3.2.1. Centre gradient (CG) method	49
3.2.2. Plateau rise (PR) method	50
3.2.3. Determination of grain boundary (gb) diffusion coefficient ( $D'$ ):	51
<i>Whipple-Le-Claire method</i>	51
3.3. EXPERIMENTAL	52
3.3.1. Deposition of thin Pd-Cu diffusion couples	52
3.3.2. Annealing of Pd-Cu diffusion couples	52
3.3.3. Characterisation of Pd-Cu bilayers before and after diffusion annealing	52
3.3.3.1. <i>Concentration-depth profiling</i>	52
3.3.3.2. <i>Phase analysis by X-ray diffraction (XRD)</i>	54
3.3.3.3. <i>Microstructure</i>	54
3.4. RESULTS AND DISCUSSION	55
3.4.1. Microstructure	55
3.4.2. Concentration-depth profiles	56
3.4.3. Determination of diffusion coefficients	59
3.4.3.1. <i>Centre-gradient (CG) method</i>	59
3.4.3.2. <i>Plateau-rise (PR) method</i>	63
3.4.3.3. <i>Whipple-Le Claire method</i>	64

3.4.4. Comparison of $\tilde{D}_{CG}$ , $\tilde{D}_{PR}$ and $D'$	69
3.4.5. <i>Determination of activation energies</i>	70
3.4.6. Comparison with literature data	72
3.4.7. Phase formation	73
3.5. SUMMARY	75
<b>4. INTERDIFFUSION, PHASE FORMATION AND STRESS</b>	
<b>DEVELOPMENT IN Pd-Cu THIN FILM DIFFUSION COUPLES</b>	<b>77</b>
ABSTRACT	77
4.1. INTRODUCTION	78
4.2. EXPERIMENTAL	79
4.2.1. Preparation of Pd-Cu diffusion couples	79
4.2.2. Annealing of Pd-Cu diffusion couples	79
4.2.3. Characterisation of Pd-Cu bilayers before and after diffusion annealing	79
4.2.3.1. <i>Concentration-depth profiling</i>	79
4.2.3.2 <i>Phase analysis and measurement of macrostress</i>	80
4.2.3.2.1. <i>'d-sin<sup>2</sup> y' method</i>	81
4.2.3.2.2. <i>Wafer curvature method</i>	82
4.2.3.3. Texture	84
4.2.3.4. Microstructure	84
4.3. RESULTS	85
4.3.1. Concentration-depth profiling	85
4.3.2. X-ray diffraction phase analysis	87
4.3.3. Residual stress	93
4.3.3.1. <i>X-ray diffraction stress analysis</i>	93
4.3.3.2. <i>Stress by wafer curvature method</i>	95
4.3.4. Texture analysis	97
4.3.5. Microstructure and selected area diffraction patterns	98
4.4. DISCUSSION	101
4.4.1. Phase formation	101
4.4.2. Stress analysis	105
4.4.2.1. <i>Discussion of stress results</i>	105

4.4.2.2. <i>Discussion of stress generation during annealing</i>	109
4.5. SUMMARY	114
APPENDIX 4A	115
1. ESTIMATION OF THERMOELASTIC SLOPES PRESENTED IN TABLE 4A	115
2. CALCULATIONS OF THERMAL STRESSES IN CU AND PD FOR THE DETERMINATION OF STRESSES AT POINTS A, B, C, D AND E (FIG.4.11)	116
APPENDIX 4B	117
DIFFUSION INDUCED STRESS DUE TO PARTIAL MOLAR VOLUME DIFFERENCE OF THE DIFFUSING SPECIES	117
<b>5. KURZFASSUNG DER DISSERTATION IN DEUTSCHER SPRACHE</b>	<b>119</b>
5.1. EINLEITUNG UND ÜBERBLICK	119
5.2. WECHSELWIRKUNG VON SPANNUNGEN UND DIFFUSION IN BINÄREN, SUBSTITUTIONELLEN LEGIERUNGEN - KAPITEL 2	121
5.2.1. Grundlagen	121
5.2.2. Exemplarische numerische Berechnungen	123
5.3. UNTERSUCHUNGEN DER DIFFUSION IN PALLADIUM-KUPFER DÜNNSCHICHT-DIFFUSIONSPAAREN: BESTIMMUNG UND DISKUSSION VON DIFFUSIONSKOEFFIZIENTEN - KAPITEL 3	125
5.3.1. Einleitung: untersuchte Proben und experimentelle Durchführung	125
5.3.2. Ergebnisse und Diskussion	125
5.4. UNTERSUCHUNGEN DER DIFFUSION IN PALLADIUM-KUPFER DÜNNSCHICHT-DIFFUSIONSPAAREN: PHASENUMWANDLUNGEN ENTWICKLUNG DER SPANNUNGEN IM SYSTEM - KAPITEL 4	129
5.4.1. Einleitung: untersuchte Proben und experimentelle Durchführung	129
5.4.2. Ergebnisse und Diskussion	130
<b>REFERENCES</b>	<b>132</b>
<b>CURRICULUM VITAE</b>	<b>137</b>
<b>ACKNOWLEDGEMENTS</b>	<b>139</b>

### 1. Introduction

Layered thin film structures are extensively used in many technologically important devices, e.g. in microelectronics. Interdiffusion in these structures may occur at temperatures as low as room temperature due to the presence of a high density of short-circuit paths for diffusion, i.e. crystalline defects and grain boundaries in polycrystalline thin films. The effects of diffusional intermixing (and, potentially, subsequent phase formation) may be beneficial or detrimental for the device performance. On the one hand, diffusion and phase formation may be desirable for tuning and optimising certain properties, as for example the conductivity. On the other hand, it may deteriorate the device performance in service and it may even lead to failure of devices. It is therefore desirable, both from a scientific and technological point of view, to arrive at a fundamental understanding of diffusion processes in thin film systems.

Whereas the effect of crystalline defects and grain boundaries in thin film system on diffusion has received considerable attention in the past [Balluffi and Blakely (1975), Gilmer and Farrell (1976), Poate *et al.* (1978), Hwang and Balluffi (1979), Bukaluk (2000)], the effect of mechanical stresses on diffusion has attracted only little attention and practically no quantitative assessments exist, though the potential effects are often invoked in the discussion of diffusion results obtained in thin film system [Balluffi and Blakely (1975), Ostrovsky *et al.* (2001), Balandina *et al.* (1998)]. The few attempts of quantitative experimental studies of the effects of mechanical stress on diffusion often suffer either from too simplistic assessments of the actual stress state or from the usage of a too simplistic theoretical background (see what follows) [Balandina *et al.* (1998), Ostrovsky *et al.* (2001)].

With respect to the theoretical background for the effect of mechanical stresses on diffusion, a rigorous re-thinking of standard textbook knowledge is required. Fick's first law, stating that the diffusion flux is proportional to the concentration (chemical potential) gradient, is usually taken as the basic equation for diffusional mass transport. Limits of its validity, in particular in a state of non-hydrostatic stress, have not been always generally recognised: In cases of non-hydrostatic stress, chemical potentials for defining equilibrium are not applicable. Following a formalism proposed by Cahn and

Larche [Larche and Cahn (1973), (1985)], the so-called diffusion potentials have to be utilised for defining equilibrium instead of the chemical potentials. Thus, the diffusional flux under non-hydrostatic states of stress is taken proportional to the gradient of a diffusion potential. The resulting equation for the diffusion flux demonstrates that the flux is not only proportional to the concentration gradient, but also proportional to the gradient of the (principal) components of the mechanical stress tensor and to the difference in the partial molar volume of the diffusing species.

Not only has the effect of stresses on diffusion to be considered: Concentration changes arising from diffusion generally lead to the build up of new stresses, so-called self-stresses. Their magnitude and distribution depends on the differences of the partial molar volumes of the diffusing species, the elastic constants of the alloy considered and the boundary conditions (e.g. if the thin film diffusion couple is freestanding or attached to a rigid substrate). The situation can be complicated by the presence of residual stresses (i.e. stresses remaining from the production of a diffusion couple), which can take very high values in thin films, and externally applied stresses (e.g. due to bending of a couple or due to a mismatch of the coefficients of thermal expansion).

Thus, one should rather consider the mutual interaction of diffusion and stresses than the effect of stresses on diffusion. The interaction of stresses and diffusion vanishes for the rarely met case that the partial molar volumes of the diffusing specie are identical.

In the **second Chapter** of this work, complete flux equations have been derived both in the lattice-fixed frame of reference and the laboratory frame of reference for the case of interdiffusion in a binary, substitutional diffusion couple.

Fick's first and second law have been solved numerically by an explicit finite difference method taking mainly Pd-Cu thin film diffusion couple having a planar, rotationally symmetric state of stress as a model example. The effects of both applied stress gradients as well as diffusion-induced stress gradients have been studied on the basis of a number of calculated concentration profiles considering both externally applied and diffusion-induced planar states of stress. A general conclusion is that the 'larger' atoms flow towards regions of tensile stress whereas 'smaller' atoms flow towards regions of compressive stress.

In the **third Chapter** of this work, investigations of interdiffusion in Pd-Cu thin (50nm thick Cu and Pd both) bilayers prepared by DC-magnetron sputtering on silicon (100) substrates coated with a thin amorphous  $\text{Si}_3\text{N}_4$  layer in the temperature range 175°C-250°C are reported. To this end, Auger electron spectroscopy in combination with X-ray diffraction phase analysis and transmission electron microscopy TEM has been employed.

The theoretical backgrounds of the various models for the determination of diffusion coefficients from laterally averaged concentration-depth profiles, as obtained by Auger electron spectroscopy in combination with sputter-depth profiling, have been summarised and their susceptibilities to errors have been discussed.

Upon annealing at relatively low temperatures (175°C to 250°C) for durations up to 10 hours, considerable diffusional intermixing occurs.

Volume interdiffusion coefficients have been determined using the so-called ‘Centre gradient’ [Hall and Morabito (1976)] and ‘Plateau rise’ methods [Hall *et al.* (1976)]. Grain boundary diffusion coefficients of Pd through Cu have been determined by the Whipple-Le Claire method [Whipple (1954)].

Both volume and grain boundary diffusion coefficients are found to decrease exponentially with increasing annealing time. Also, a corresponding increase in activation energies for both volume and grain boundary diffusion have been observed. X-ray diffraction phase analysis indicates that interdiffusion is accompanied by the sequential formation of ordered phases  $\text{Cu}_3\text{Pd}$  and  $\text{CuPd}$ . Microstructural changes (grain size, morphology etc.) after annealing have been studied by TEM.

Defect annihilation during annealing and ordering in the Pd-Cu solid solution have been proposed as potential causes for the observed decrease in diffusion coefficients (and corresponding increase in activation energies).

The evolution of the stress of the diffusion couples upon annealing will be discussed in the **fourth Chapter**. Ex-situ stress measurements by X-ray diffraction and in-situ (wafer curvature) stress measurements reveal that tensile stresses are generated during

## 1. Introduction

---

annealing. The stress results are discussed in the light of possible mechanisms of stress generation.

## **2. Interaction of stress and diffusion in a binary substitutional solid solution**

J. Chakraborty, U. Welzel and E.J. Mittemeijer

### **Abstract**

The effect of mechanical stress on interdiffusion in a binary substitutional solid solution has been investigated from a theoretical point of view. Fick's first law, stating that the diffusional flux is proportional to the concentration (chemical potential) gradient, is the basic equation for diffusional mass transport. Limits of its validity, in particular in a state of non-hydrostatic stress, have not always been generally recognised. In this work the effect of non-hydrostatic mechanical stresses on diffusion is investigated theoretically.

In cases of non-hydrostatic stress, chemical potentials for defining equilibrium are not applicable. Following a formalism proposed by Cahn and Larche [Larche and Cahn, (1973)], the so-called diffusion potentials have to be utilised for defining equilibrium instead of the chemical potentials. Thus, the diffusional flux under non-hydrostatic states of stress is taken proportional to the gradient of a diffusion potential. For the first time, complete flux equations have been derived both in the lattice-fixed frame of reference and the laboratory frame of reference. The diffusional flux is (also) proportional to the gradient of the (principal) components of the mechanical stress tensor and to the difference in the partial molar volume of the diffusing species.

Fick's first and second law have been solved numerically by an explicit finite difference method taking a Pd-Cu thin film diffusion couple having a planar, rotationally symmetric state of stress as a model example. The effects of both applied stress gradients as well as diffusion-induced stress gradients have been studied on the basis of a number of calculated concentration profiles considering both externally applied and diffusion-induced planar states of stress. A general conclusion is that the 'larger' atoms flow towards regions of tensile stress whereas 'smaller' atoms flow towards regions of compressive stress.



### 2.1. Introduction

Interdiffusion occurs in many cases under a non-hydrostatic state of mechanical stress. Such a stress state may be externally applied to the diffusion couple or it may arise as a consequence of diffusion if the partial molar volumes of the diffusing components differ. Stresses generated upon interdiffusion have been the scope of various theoretical considerations and experimental investigations [Prussin (1961), Li (1978), Wang *et al.* (2001)], but only very rarely has the effect of non-hydrostatic stresses on diffusion been considered. This is perhaps due to the fact that the phenomenological theory of diffusion in a multicomponent system, as presented in most textbooks, is limited to hydrostatic states of stress, where the gradients of the chemical potentials of the individual components are considered as driving forces for diffusion [Onsager (1931a), (1931b), Groot and Mazur (1962), Shewmon (1989)]. Such an approach requires that the chemical potential of each component in the system considered can be uniquely defined and it is constant within the system in thermodynamic equilibrium. It has to be remarked that the above mentioned concept of chemical potential and diffusion originated from fluid thermodynamics. For fluids, only hydrostatic states of stress ('pressure') can occur, whereas a solid can be also under non-hydrostatic states of stress. Already Gibbs, as early as 1879 [Gibbs (1879)] pointed out that the definition of a unique chemical potential is impossible for the case of a homogeneous, single-component solid under a homogeneous, non-hydrostatic state of stress. To arrive at this conclusion, Gibbs employed his famous Gedankenexperiment involving a solid cube in contact with fluids with three different pressures at its opposite pairs of faces. Gibbs did not define a chemical potential for such a solid, except in the hydrostatic limit.

A history of attempts to validate and define unique scalar chemical potentials for the components of a solid under non-hydrostatic states of stress followed [see, for example, McLellan (1968), Li (1966), Nolfi (1973)]. An end was put to the controversial discussions by Larche and Cahn in 1973 [Larche and Cahn (1973)], who rigorously treated the case of a (crystalline) solid under non-hydrostatic states of stress and thereby introduced the concept of a so-called network-solid and the diffusion potential [Larche and Cahn (1973)]. It has been demonstrated that the so-called diffusion potentials are

## 2. Interaction of stress and diffusion in a binary substitutional solid solution

---

constants under chemical equilibrium. Thus, gradients in the diffusion potentials should be adopted as driving forces for diffusion.

In the recent years, the theoretical approach proposed by Larche and Cahn [Larche and Cahn (1973), (1982), (1985)] has been successfully applied to investigate the effect of self stress on, for example, hydrogen diffusion in palladium and its alloys [Kandasamy (1988), Baranowski (1989), Simon and Grzywna (1992), Zhang *et al.* (2002)].

The intent of the present work is to examine the effect of applied and diffusion-induced stresses on the interdiffusion process in a substitutional binary diffusion couple. For the first time, the diffusion flux equation in the laboratory frame of reference will be rigorously derived taking gradients of diffusion potentials as driving forces for the flux of matter. Then, the solution of Fick's first and second law employing an explicit finite difference method will be outlined. A focal point of interest is the interdiffusion process in a thin film binary diffusion couple consisting of cubic materials. Examples illustrating the effect of diffusion-induced and applied non-hydrostatic stresses will be presented and discussed.

## 2.2. Theoretical background

### 2.2.1. Definitions: Network solid and composition variables

In the following, the analysis will focus on crystalline solid materials. A so-called network is associated with the solid, which is embedded in the solid and allows the definition of displacements and hence strains. For the case of a substitutional solid solution, considered in the following, in which atoms diffuse by a vacancy mechanism, the substitutional lattice sites can serve as the network. It is assumed in the following that the network (i.e. the number of lattice sites) is conserved.

For defining strain in the ‘actual’ state, it is necessary to introduce the so-called ‘reference’ state, which may be a real or hypothetical state of the solid considered. The strain can be due to changes in composition (‘compositional strain’, if changes of composition lead to volume effects, i.e. if the partial molar volumes of the diffusion species differ) or due to mechanical stresses (‘elastic strain’).

In the following, the analysis will focus on a binary (elements A and B) substitutional diffusion couple. The reference state will be chosen as stress free and homogenous in composition. The dimensionless composition at a certain point in the couple can be expressed as

$$c = c_B = \left( \frac{\mathbf{r}'_B}{\mathbf{r}'_0} \right) = \left( \frac{\mathbf{r}_B}{\mathbf{r}_0} \right) \quad (2.1)$$

where  $\mathbf{r}'_B$  and  $\mathbf{r}_B$  are the molar densities of B atoms in the reference state and in the actual state, respectively, and  $\mathbf{r}'_0$  and  $\mathbf{r}_0$  are the molar density of lattice sites in the reference state and actual state, respectively. For ‘A’ atoms, the above relation can be written as (assuming that the vacancy concentration is negligible):

$$c_A = 1 - c = \left( \frac{\mathbf{r}'_A}{\mathbf{r}'_0} \right) = \left( \frac{\mathbf{r}_A}{\mathbf{r}_0} \right). \quad (2.2)$$

For the case that the network is conserved, it holds that

$$\mathbf{r}'_0 = \mathbf{r}'_A + \mathbf{r}'_B = \text{constant} \quad (2.3)$$

and

## 2. Interaction of stress and diffusion in a binary substitutional solid solution

---

$$\mathbf{r}_0 = \mathbf{r}_A + \mathbf{r}_B \quad (2.4)$$

therefore,

$$c_A + c_B = 1. \quad (2.5)$$

The molar densities are therefore not independent: only one independent molar density occurs in a binary system as a consequence of the existence of the network.

It is possible to calculate quantities  $\Upsilon'$  (e.g. molar densities, energy density and entropy density) in the reference state from the respective quantities in the actual state as:

$$\Upsilon' = \Upsilon (1 + \mathbf{e}_{kk}^t) \quad (2.6)$$

and vice versa, where  $\mathbf{e}_{kk}^t$  is the trace of the strain tensor [Larche and Cahn (1985)] (note that the Einstein Convention is adopted throughout the paper: the summation symbol of repeated indices is omitted; a summation over indices appearing twice is implicit). Note that the strain tensor  $\mathbf{e}_{ij}^t$  generally contains compositional ( $\mathbf{e}_{ij}^c$ ) and elastic strain ( $\mathbf{e}_{ij}$ ) contributions (see also Section 2.2.3).

### 2.2.2. Diffusion potentials

Larche and Cahn investigated the equilibrium conditions of multicomponent solids subject to network constraints under non-hydrostatic states of stress. To this end, they followed an approach proposed first by Gibbs: the total internal energy of an isolated system is minimised subject to the constraints of constant entropy and constant mass of all components. These constraints are taken into consideration in the energy minimisation in terms of the so-called Lagrange multipliers, which are constants. The analysis leads to the conclusion that for chemical equilibrium, the chemical potentials, equal to the Lagrange multipliers, of all components are constant within the system, provided that the local compositions of the components can be varied independently. If, however, a network constraint holds for the system, the local compositions of  $N$  substitutional components are not independent: only  $(N-1)$  independent compositional variables and thus  $(N-1)$  Lagrange multiplier differences (which are constants), associated with compositional variables, occur. These differences, relevant for defining chemical equilibrium, are then called diffusion potentials. Only for cases of hydrostatic

## 2. Interaction of stress and diffusion in a binary substitutional solid solution

---

states of stress, the diffusion potentials can be associated with differences of chemical potentials for a binary substitutional solid solution (AB):

$$M_{BA} = m_B - m_A. \quad (2.7)$$

The case of non-hydrostatic states of stress will be considered next.

### 2.2.3. Stress-dependence of diffusion potentials

The following Maxwell-type relation reveals the stress dependence of the diffusion potential [Larche and Cahn (1985)]:

$$\left( \frac{\partial \mathbf{e}_{ij}^t}{\partial c} \right)_{\mathbf{s}_{ij} = \text{const.}} = - \frac{1}{V'} \left( \frac{\partial M_{BA}}{\partial \mathbf{s}_{ij}} \right)_{\mathbf{s}_{kl \neq ij}^c = \text{const.}} \quad (2.8)$$

Equation (2.8) is valid under the small strain approximation [Larche and Cahn (1973)]<sup>1</sup>.

$V'$  is the molar volume of the solid solution in the reference state. The total strain in the system  $\mathbf{e}_{ij}^t$  is the sum of a contribution  $\mathbf{e}_{ij}^c$  due to the composition changes with respect to the reference state and a contribution  $\mathbf{e}_{ij}$  due to the mechanical stress  $\mathbf{s}_{ij}$ :

$$\mathbf{e}_{ij}^t = \mathbf{e}_{ij}^c + S_{ijkl} \mathbf{s}_{kl} \quad (2.9)$$

where the  $S_{ijkl}$  are the elastic compliances of the solid considered.

Assuming that the elastic compliances  $S_{ijkl}$  are independent of composition it follows that [Larche and Cahn (1985)]:

$$- \frac{1}{V'} \left( \frac{\partial M_{BA}}{\partial \mathbf{s}_{ij}} \right)_{\mathbf{s}_{kl \neq ij}^c = \text{const.}} = \mathbf{h}_{ij} \quad (2.10)$$

with

$$\mathbf{h}_{ij} = \left( \frac{\partial \mathbf{e}_{ij}^c}{\partial c} \right)_{\mathbf{s}_{ij} = \text{const.}}. \quad (2.11)$$

$\mathbf{h}_{ij}$  is the chemical expansion coefficient tensor which generally depends on composition.

---

<sup>1</sup> In small-strain approximation,  $\frac{\partial u}{\partial x'} \approx \frac{\partial u}{\partial x}$  where,  $\mathbf{u}$  is the displacement vector.  $x'$  is the coordinate in reference state and  $x$  is the coordinate in actual state.

## 2. Interaction of stress and diffusion in a binary substitutional solid solution

---

In cubic binary materials,  $\mathbf{e}_{ij}^c$  is isotropic and in this case, it holds that

$$\mathbf{h}_{ij} = \mathbf{h}_{BA} \mathbf{d}_{ij} . \quad (2.12)$$

In cubic materials  $\mathbf{h}_{BA}$  is related to the partial molar volumes of the two components ( $\bar{V}_A$  and  $\bar{V}_B$  for 'A' and 'B' respectively) by the relation [Larche and Cahn (1985)]:

$$\mathbf{h}_{BA} = \frac{\bar{V}_B - \bar{V}_A}{3V'} \quad (2.13)$$

In case of cubic binary materials, by integrating equation (2.10) from zero stress to an actual stress state  $\mathbf{s}_{ij}$ , it follows that:

$$M_{BA}(\mathbf{s}_{ij}, c) - M_{BA}(0, c) = -V' \mathbf{h}_{BA} \{ \mathbf{s}_{kk} \} \quad (2.14)$$

where it has been assumed that  $\mathbf{h}_{BA}$  is independent of the stress state.  $M_{BA}(0, c)$  denotes the diffusion potential in the absence of stress which, using Eq. (2.7), can be expressed in terms of the difference between the chemical potentials of the two components A and B describing the equilibrium of the solid in the absence of stress:

$$M_{BA}(0, c) = \mathbf{m}_B(c) - \mathbf{m}_A(1-c). \quad (2.15)$$

According to Eq. (2.14), the diffusion potential depends on the trace of stress tensor which appears obvious because the trace of the stress tensor expresses the dilation associated with the stress state  $\mathbf{s}_{ij}$ . The state of stress can be completely due to composition-induced stresses (so-called self-stresses) or due to stresses which have been externally imposed (external stresses). Evidently, the stress influences the diffusion potential via the dependence of compositional strain on composition (as  $S_{ijkl}$  is assumed to be composition independent). Hence, if  $\mathbf{h}_{BA}$  is zero, then there is no stress effect on the diffusion potential: both not for an externally applied and not for internally induced stress. However, the diffusion *coefficient* may be affected.

### 2.2.4. Basis of diffusion formalism

The equilibrium of an isolated multicomponent solid (1,2,...,N) in the absence of non-hydrostatic stress  $\mathbf{s}_{ij}$  (but under hydrostatic pressure) is uniquely determined by specifying temperature ( $T$ ), pressure ( $P$ ) and the chemical potentials  $\mathbf{m}_1, \mathbf{m}_2, \dots, \mathbf{m}_N$ . If

## 2. Interaction of stress and diffusion in a binary substitutional solid solution

---

the system is displaced ‘slightly’ from equilibrium, it may be assumed that the rate of return to equilibrium is proportional to the (energy) deviation from the equilibrium. Then, the flux of the  $i$ -th component is proportional to the gradients of temperature, pressure and chemical potentials  $\mathbf{m}_k$ . The resulting flux equations thus are phenomenological equations with proportionality constants as the so-called phenomenological coefficients [Shewmon (1989)].

Analogously, for a multi-component network-solid in a state of (non-hydrostatic) stress, it may be assumed that the flux is proportional to the gradients of each of the diffusion potentials in the system [Larche and Cahn (1983), (1985)]. Then the flux of the  $k$ -th component can be written as [Larche and Cahn (1985)]:

$$\vec{J}_k = - \sum_{j=1}^N B_{kj} \nabla M_{jl}, k = 1, \dots, N. \quad (2.16)$$

Note that vacancies can also be treated as a component.

The following restrictions for  $J$ ,  $B$  and  $M$  hold [Larche and Cahn (1983)]:

$$\sum_k J_k = 0 \quad (2.17)$$

$$\sum_k B_{kj} = 0 \quad (2.18)$$

$$\sum_j B_{kj} = 0 \quad (2.19)$$

$$M_{kj} + M_{jl} + M_{lk} = 0 \quad (2.20)$$

$$M_{kj} = -M_{jk} \quad (2.21)$$

$$M_{kk} = 0 \quad (2.22)$$

Fluxes ( $J_k$ ) are defined in the lattice (network) frame of reference.  $B_{kj}$  are the phenomenological coefficients (see above).  $B_{kj}$  is second rank tensor. In general, the  $B_{kj}$  depend on composition, stress and temperature. In the present case, the  $B_{kj}$  are assumed to be independent of stress. For a cubic material the  $B_{kj}$  are scalar quantities. It follows that there are (N-1) independent fluxes with (N-1) independent diffusion potentials and (N-1)<sup>2</sup> independent phenomenological quantities. The choice of ‘ $l$ ’ as a reference component is arbitrary. ‘ $l$ ’ can be vacancy or any other chemical species: the fluxes and

the phenomenological coefficients are independent of the choice of the species ' $l$ '. Although the choice of ' $l$ ' is arbitrary, it is recommended to choose ' $l$ ' as one of the major species instead of vacancies because of the large uncertainty in the vacancy concentration within the solid.

### 2.3. Diffusion flux equations: self-, intrinsic- and interdiffusion coefficients

On the basis of the theoretical background described in Section 2.2, in this section, diffusion flux equations for a stressed binary substitutional solid solution will be derived for both the lattice-fixed and laboratory-fixed frames of reference. The analysis will be performed such that dilatation changes due to composition changes are included. Hence, the effect of self-stress is incorporated. Expressions for self and intrinsic diffusion coefficients will be given in the lattice reference frame; an expression for the chemical, interdiffusion coefficient is derived for the laboratory frame of reference.

#### 2.3.1. Flux equations in lattice-fixed frame of reference

For a binary substitutional solid solution of components 'A' and 'B' following the vacancy as diffusion mechanism,  $N$  is equal to 3. Choosing 'A' as ' $l$ ', the flux expressions for  $J_A$  and  $J_B$  can straightforwardly be given for the lattice-fixed reference frame using Eq. (2.16). As  $M_{AA} = 0$ , it follows for the diffusion flux of A atoms:

$$J_A = -[B_{AB} \nabla M_{BA} + B_{Av} \nabla M_{vA}]. \quad (2.23)$$

In case of one dimensional diffusion, the derivatives of  $M_{BA}$  and  $M_{vA}$  with respect to position have been calculated using equations (2.14) and (2.15).  $B_{AB}$  has been replaced by  $-(B_{Av} + B_{AA})$  using equation (2.19).

As in the classical Darken treatment for diffusion in a stress-free state [Darken (1948) and Shewmon (1989)], it is assumed that the vacancy concentration is negligible compared to the concentration of 'A' or 'B' and it is maintained at a local equilibrium value everywhere within the diffusion zone. Thus, the potential effect of vacancy generation and annihilation on interdiffusion is ignored in this treatment.



## 2. Interaction of stress and diffusion in a binary substitutional solid solution

---

It is further assumed that  $\mathbf{h}_{BA}$  is independent of composition.

Under the above assumptions, the following expression for the diffusion flux equation can be derived (See Appendix 2A):

$$J_A = - \left[ B_{AA} \left\{ RT \mathbf{j} \left( \frac{1}{c} + \frac{1}{1-c} \right) \frac{\partial(1-c)}{\partial x} + V \mathbf{h}_{BA} \frac{\partial \mathbf{s}_{kk}}{\partial x} \right\} \right] \quad (2.24)$$

where  $c$  is the mole fraction of B (see equation (2.1)),  $\mathbf{j}$  is the thermodynamic factor (using the Gibbs-Duhem relation, it follows that  $\mathbf{j}_A = \mathbf{j}_B = \mathbf{j}$ , where  $\mathbf{j}_A$  and  $\mathbf{j}_B$  are the thermodynamic factors of 'A' and 'B' respectively [Philibert (1991)]),  $R$  is the Gas constant and  $T$  is the absolute temperature.

At this stage, it is necessary to define an intrinsic diffusion coefficient and to express the flux equation in terms of the concentration gradient (instead of the gradient of mole fraction) so that equation (2.24) is isomorphic to Fick's first law.

If it is assumed that the elastic strain is negligible and that the partial molar volumes of A,  $\bar{V}_A$ , and B,  $\bar{V}_B$ , are constant, then by differentiating equation (2), the following relation can be derived [Philibert (1991)]:

$$\frac{\partial(1-c)}{\partial x} = \frac{V^2}{\bar{V}_B} \frac{\partial \mathbf{r}_A}{\partial x}. \quad (2.25)$$

Use has been made of the following relations:

$$V = (1-c)\bar{V}_A + c\bar{V}_B \quad (2.26)$$

and

$$\mathbf{r}_A \bar{V}_A + \mathbf{r}_B \bar{V}_B = 1. \quad (2.27)$$

Insertion of Eq. (2.25) into Eq. (2.24) results in:

$$J_A = - \left[ B_{AA} RT \mathbf{j} \left( \frac{1}{c} + \frac{1}{1-c} \right) \frac{V^2}{\bar{V}_B} \frac{\partial \mathbf{r}_A}{\partial x} + B_{AA} V \mathbf{h}_{BA} \frac{\partial \mathbf{s}_{kk}}{\partial x} \right]. \quad (2.28)$$

Upon inspection of Eq. (2.28) and comparison with the usual form of Fick's first law, a self diffusion coefficient ( $D_A$ ) may be defined as,

$$D_A = \frac{B_{AA} RT}{c(1-c)} \frac{V^2}{\bar{V}_B}. \quad (2.29)$$

and thus equation (2.28) can be written as:

$$J_A = - \left[ D_A \mathbf{j} \frac{\partial \mathbf{r}_A}{\partial x} + \frac{D_A c(1-c)}{RT} \left( \frac{\bar{V}_B}{V^2} \right) V' \mathbf{h}_{BA} \frac{\partial \mathbf{s}_{kk}}{\partial x} \right]. \quad (2.30)$$

By introducing the intrinsic diffusion coefficient  $\bar{D}_A = D_A \mathbf{j}$ , equation (2.30) reads

$$J_A = - \left[ \bar{D}_A \frac{\partial \mathbf{r}_A}{\partial x} + \frac{\bar{D}_A c(1-c)}{\mathbf{j} RT} \left( \frac{\bar{V}_B}{V^2} \right) V' \mathbf{h}_{BA} \frac{\partial \mathbf{s}_{kk}}{\partial x} \right]. \quad (2.31)$$

The first term in the flux equation (equation (2.31)) agrees exactly with the flux usually defined in the lattice-fixed reference frame with the intrinsic diffusion coefficient.

The ratio  $\left( \frac{\bar{V}_B}{V^2} \right)$  appears in the second term, because of the change in the molar volume of the solid solution with changing composition in the actual state.

Now, maintaining, 'A' as 'l' the following expression for ' $J_B$ ' in one dimension can be obtained:

$$J_B = - [B_{BB} \nabla M_{BA} + B_{Bv} \nabla M_{vA}] \quad (2.32)$$

In a similar manner (see above) earlier, it can be shown that,

$$J_B = - \left[ \bar{D}_B \frac{\partial \mathbf{r}_B}{\partial x} - \frac{\bar{D}_B c(1-c)}{\mathbf{j} RT} \left( \frac{\bar{V}_A}{V^2} \right) V' \mathbf{h}_{BA} \frac{\partial \mathbf{s}_{kk}}{\partial x} \right] \quad (2.33)$$

where use has been made of:

$$\frac{\partial c}{\partial x} = \frac{V^2}{\bar{V}_A} \frac{\partial \mathbf{r}_B}{\partial x} \quad (2.34)$$

and  $\bar{D}_B = D_B \mathbf{j}$  is the intrinsic diffusion coefficient for 'B' with the self diffusion coefficient for the 'B' component

$$D_B = \frac{B_{BB} RT V^2}{c(1-c) \bar{V}_A}. \quad (2.35)$$

### 2.3.2. Flux equations in laboratory-fixed frame of reference

For a general state of stress (misfit stress, stress due to compositional heterogeneity and/or externally applied stress) equations (2.31) and (2.33) are the diffusion flux equations for the components 'A' and 'B' in the lattice-fixed frame of reference respectively. Evidently, in general  $J_A \neq J_B$  and consequently, there is a net vacancy flux in case of substitutional diffusion. In the lattice-fixed frame of reference, it holds that:

## 2. Interaction of stress and diffusion in a binary substitutional solid solution

---

$$J_A + J_B = -J_V . \quad (2.36)$$

In the treatment proposed by Larche and Cahn [Larche and Cahn (1973)] and adopted in this work, the lattice network is conserved and the presence of sources and sinks of vacancies (dislocations and grain boundaries) is not allowed within the network, i.e. vacancy creation and annihilation is not allowed. The effect of the presence of sources and sinks for vacancies is thus ignored in their work.

It should be recognised that during interdiffusion, the molar volume of the solid solution changes with composition, although the total volume of the system remains constant as the partial molar volumes of the components are assumed to be constants. Therefore, the so-called ‘mean-volume fixed frame of reference’ coincides with the laboratory-fixed frame of reference.

In the following, the so-called interdiffusion coefficient  $\tilde{D}$  will be introduced. Generally, it is necessary to distinguish the so-called mean volume frame of reference, where the interdiffusion coefficient  $\tilde{D}$  is defined, and the laboratory-fixed frame of reference [Philibert (1991)]. However, for the case that the partial molar volumes are constants (i.e. are independent of composition), this distinction is not necessary and the two frames of reference coincide.

The expressions for the diffusion fluxes in the laboratory-fixed frame of reference,  $J_A^{(0)}$  and  $J_B^{(0)}$ , are:

$$J_A^{(0)} = J_A + \mathbf{r}_A \mathbf{n} \quad (2.37)$$

$$J_B^{(0)} = J_B + \mathbf{r}_B \mathbf{n} \quad (2.38)$$

where  $\mathbf{n}$  is the velocity of the lattice-fixed frame of reference with respect to the laboratory frame of reference. The velocity  $\mathbf{n}$  can be determined using the conservation of A and B masses in the laboratory-fixed frame of reference which leads to:

$$\frac{\partial \mathbf{r}_A}{\partial t} = -\frac{\partial J_A^{(0)}}{\partial x} = -\frac{\partial}{\partial x}(J_A + \mathbf{r}_A \mathbf{n}) \quad (2.39)$$

and

$$\frac{\partial \mathbf{r}_B}{\partial t} = -\frac{\partial J_B^{(0)}}{\partial x} = -\frac{\partial}{\partial x}(J_B + \mathbf{r}_B \mathbf{n}) \quad (2.40)$$

## 2. Interaction of stress and diffusion in a binary substitutional solid solution

---

Now,  $J_A$  and  $J_B$  can be substituted from equations (2.31) and (2.33) on the right-hand sides of equations (2.39) and (2.40) respectively. The time and position derivatives of  $\mathbf{r}_A$  and  $\mathbf{r}_B$  can be substituted (determined from equation (2.27)) on the left-hand and right-hand sides of equations (2.39) and (2.40) respectively. Assuming that the intrinsic diffusion coefficients ( $\bar{D}_A$  and  $\bar{D}_B$ ) are independent of concentration (and thus position), it follows from the resulting expressions that (See Appendix 2B):

$$\mathbf{n} = \bar{D}_A \bar{V}_A \frac{\partial \mathbf{r}_A}{\partial x} - \bar{D}_B \bar{V}_B \frac{\partial \mathbf{r}_B}{\partial x} + \frac{\bar{V}_A \bar{D}_A c(1-c)}{\mathbf{j} RT} \frac{\bar{V}_B}{V^2} V' \mathbf{h}_{BA} \frac{\partial \mathbf{s}_{kk}}{\partial x} - \frac{\bar{D}_B \bar{V}_B c(1-c)}{\mathbf{j} RT} \frac{\bar{V}_A}{V^2} V' \mathbf{h}_{BA} \frac{\partial \mathbf{s}_{kk}}{\partial x}. \quad (2.41)$$

The flux equations for 'A' and 'B' in the laboratory-fixed frame of reference can be obtained by replacing  $\mathbf{n}$  in equations (2.37) and (2.38) by equation (2.41) and by replacing  $J_A$  and  $J_B$  employing equations (2.31) and (2.33). For the component A, the flux equation reads (See Appendix 2B):

$$J_A^{(0)} = -(\bar{D}_A \mathbf{r}_B \bar{V}_B + \bar{D}_B \mathbf{r}_A \bar{V}_A) \frac{\partial \mathbf{r}_A}{\partial x} - \left( \frac{\bar{V}_B}{V^2} \right) V' \frac{c(1-c)}{\mathbf{j} RT} \mathbf{h}_{BA} \frac{\partial \mathbf{s}_{kk}}{\partial x} (\bar{D}_A \mathbf{r}_B \bar{V}_B + \bar{D}_B \mathbf{r}_A \bar{V}_A). \quad (2.42)$$

Now, adopting the usual definition of the interdiffusion coefficient  $\tilde{D}$ :

$$\tilde{D} = \bar{D}_A \mathbf{r}_B \bar{V}_B + \bar{D}_B \mathbf{r}_A \bar{V}_A \quad (2.43)$$

the flux equations for 'A' and 'B' can be written as:

$$J_A^{(0)} = -\tilde{D} \frac{\partial \mathbf{r}_A}{\partial x} - \tilde{D} \left( \frac{\bar{V}_B}{V^2} \right) \frac{c(1-c)}{\mathbf{j} RT} V' \mathbf{h}_{BA} \frac{\partial \mathbf{s}_{kk}}{\partial x} \quad (2.44)$$

$$J_B^{(0)} = -\tilde{D} \frac{\partial \mathbf{r}_B}{\partial x} + \tilde{D} \left( \frac{\bar{V}_A}{V^2} \right) \frac{c(1-c)}{\mathbf{j} RT} V' \mathbf{h}_{BA} \frac{\partial \mathbf{s}_{kk}}{\partial x}. \quad (2.45)$$

If the stress effects are neglected in equations (2.44) and (2.45), by putting  $\bar{V}_A = \bar{V}_B$ , Darken's flux equation in laboratory-fixed frame of reference is obtained [Darken (1948)]:

$$J_A^{(0)} + J_B^{(0)} = 0 \quad (2.46)$$

with

$$\tilde{D} = c \bar{D}_A + (1-c) \bar{D}_B. \quad (2.47)$$

## 2.4. Numerical simulation

### 2.4.1. Diffusion equation

Fick's second law can be written down as follows:

$$\frac{\partial \mathbf{r}_B}{\partial t} = - \frac{\partial J_B^{(0)}}{\partial x}. \quad (2.48)$$

Using the flux equation (2.45), and the relationships,

$$\frac{\partial \mathbf{r}_B}{\partial x} = \frac{\bar{V}_A}{V^2} \frac{\partial c}{\partial x} \quad (2.49)$$

and

$$\frac{\partial \mathbf{r}_B}{\partial t} = \frac{\bar{V}_A}{V^2} \frac{\partial c}{\partial t} \quad (2.50)$$

the following equation can be derived :

$$\begin{aligned} \frac{\partial c}{\partial t} = & \tilde{D} \frac{\partial^2 c}{\partial x^2} + \frac{2\tilde{D}(\bar{V}_A - \bar{V}_B)}{V} \left( \frac{\partial c}{\partial x} \right)^2 - \frac{\tilde{D} V' c (1-c)}{j RT} \mathbf{h}_{BA} \frac{\partial^2 \mathbf{s}_{kk}}{\partial x^2} \\ & - \frac{\tilde{D} V'}{j RT} \mathbf{h}_{BA} \frac{\partial \mathbf{s}_{kk}}{\partial x} \frac{\partial c}{\partial x} \left( 1 - \frac{2c\bar{V}_B}{V} \right) + \frac{\partial \tilde{D}}{\partial c} \frac{\partial c}{\partial x} \left[ \frac{\partial c}{\partial x} - \frac{V' c (1-c)}{j RT} \mathbf{h}_{BA} \frac{\partial \mathbf{s}_{kk}}{\partial x} \right]. \end{aligned} \quad (2.51)$$

If  $\bar{V}_B = \bar{V}_A$ , the term associated with  $\left( \frac{\partial c}{\partial x} \right)^2$  vanishes.

In deriving equation (2.51), it has been assumed that the thermodynamic factor is independent of composition  $\left( \frac{\partial \mathbf{s}}{\partial c} = 0 \right)$ . However, in practice, thermodynamic factor is composition dependent and therefore it also varies with position. For a planar, rotationally symmetric state of stress,  $\mathbf{s}_{kk}$  can be replaced by  $2\mathbf{s}_{\parallel}$  where,  $\mathbf{s}_{\parallel}$  is the rotationally symmetric biaxial stress.

Equation (2.51) is partial differential equation for the concentration as a function of time and position. Analytical solutions are generally infeasible. In the following, equation (2.51) will be solved numerically, considering both diffusion-induced and externally applied states of stress.

### 2.4.2. Dimensionless diffusion equation

Using non-dimensional variables has certain advantages while solving a differential equation by numerical methods. To convert the equation (2.51) into a dimensionless diffusion equation, the following non-dimensional variables  $X_1, T', c', \mathbf{s}'_{\parallel}$  and  $K$  are introduced:

$$X_1 = \frac{x}{L} \quad (2.52)$$

$$T' = \frac{\tilde{D}t}{L^2} \quad (2.53)$$

$$c' = \frac{c}{c_0} \quad (2.54)$$

$$\mathbf{s}'_{\parallel} = \frac{\mathbf{s}_{\parallel}}{\mathbf{s}_0} \quad (2.55)$$

$$K = 2V'h_{BA}\mathbf{s}_0 \frac{1}{jRT} \quad (2.56)$$

$$\tilde{D}' = \frac{\tilde{D}}{D_0} \quad (2.57)$$

where  $L$  is total length of the couple,  $c_0$  is a certain maximum concentration,  $D_0$  is a constant diffusion coefficient and  $\mathbf{s}_0$  is a constant stress, respectively. Thus, the non-dimensional position  $X_1$  can vary from 0 to 1 and the non-dimensional concentration  $c'$  can also vary from 0 to 1. Fig. 2.1 shows a schematic view of the diffusion geometry. The diffusion flux is directed along the x-axis. Stress can be externally applied during diffusion or the stress can result from interdiffusion, but in both case, the stress state is planar, rotationally symmetric (i.e.  $\mathbf{s}_{zz} = \mathbf{s}_{yy} = \mathbf{s}_{\parallel}$  and

$$\mathbf{s}_{xy} = \mathbf{s}_{yx} = \mathbf{s}_{xz} = \mathbf{s}_{zx} = \mathbf{s}_{xx} = \mathbf{s}_{zy} = \mathbf{s}_{yz} = 0).$$

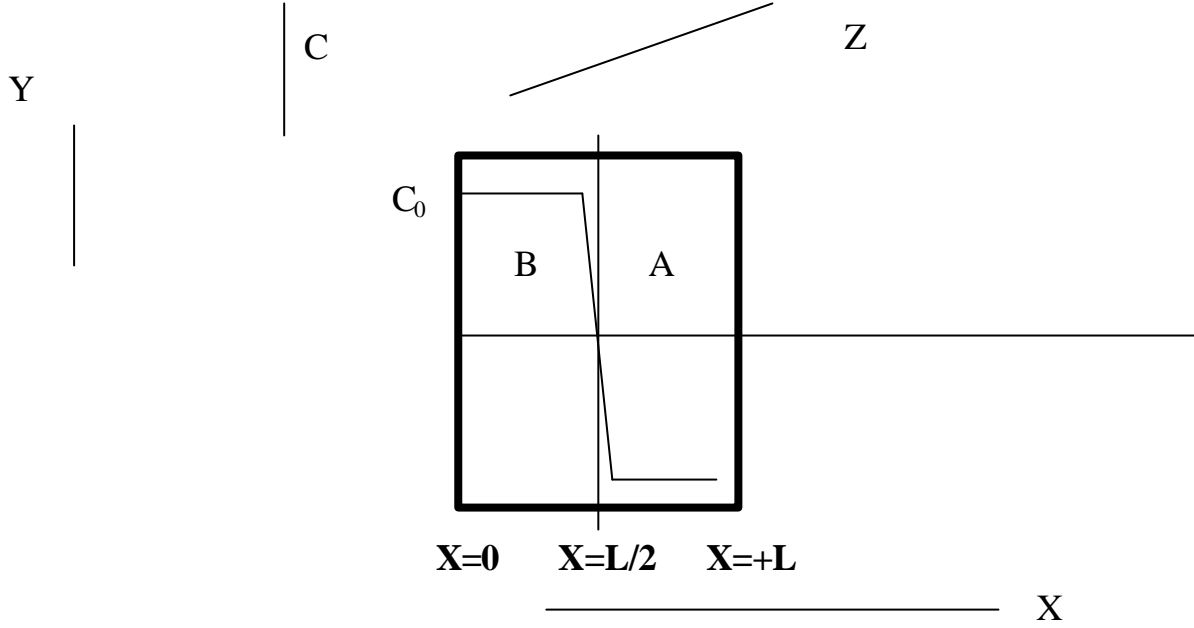


Fig. 2.1: Schematic sketch of the diffusion geometry.

The dimensionless diffusion equation can be written as follows

$$\begin{aligned} \frac{\partial c'}{\partial T'} = & \frac{\partial^2 c'}{\partial X_1^2} - Kc'(1-c'_0) \frac{\partial^2 \mathbf{s}'_{\parallel}}{\partial X_1^2} - K \left( 1 - \frac{2c'_0 \bar{V}_B}{(1-c'_0) \bar{V}_A + c'_0 \bar{V}_B} \right) \frac{\partial c'}{\partial X_1} \frac{\partial \mathbf{s}'_{\parallel}}{\partial X_1} \\ & + \frac{2(\bar{V}_A - \bar{V}_B)c_0}{(1-c'_0) \bar{V}_A + c'_0 \bar{V}_B} \left( \frac{\partial c'}{\partial X_1} \right)^2 + \frac{1}{\tilde{D}'} \frac{\partial \tilde{D}'}{\partial c'} \frac{\partial c'}{\partial X_1} \left[ \frac{\partial c'}{\partial X_1} - Kc'(1-c'_0) \frac{\partial \mathbf{s}'_{\parallel}}{\partial X_1} \right] \end{aligned} \quad (2.58)$$

The above equation can be solved by an explicit finite difference method [Crank (1973), Smith (1965)]. To this end, boundary conditions are required. These will be introduced in the following.

### 2.4.3. Initial and boundary conditions

Two sets of initial ( $t=0$ ) concentration profiles have been considered:

$$\begin{aligned} \text{Set-1} \quad & c' = 1 \quad \text{for } 0 \leq X_1 < 0.5 \\ & c' = 0.5 \quad \text{at } X_1 = 0.5 \\ & c' = 0 \quad \text{for } 0.5 < X_1 \leq 1 \end{aligned}$$

## 2. Interaction of stress and diffusion in a binary substitutional solid solution

---

$$\begin{aligned} \text{Set-2} \quad c' &= 0.5 \quad \text{for } 0 \leq X_1 < 0.5 \\ c' &= 0.5 \quad \text{at } X_1 = 0.5 \\ c' &= 0.5 \quad \text{for } 0.5 < X_1 \leq 1 \end{aligned}$$

Considering the geometry of the diffusion couple, the boundary conditions are that the diffusion flux must be zero at the surfaces ( $X_1 = 0$  and  $X_1 = 1$ ).

After non-dimensionalisation of the flux-equation (2.45), these two conditions are expressed as:

$$X_1 = 0 : \quad \left( \frac{\partial c'}{\partial X_1} \right)_{X_1=0} = K c' (1 - c_0 c') \left( \frac{\partial \mathbf{s}'_{\parallel}}{\partial X_1} \right)_{X_1=0} \quad (2.59)$$

$$X_1 = 1 : \quad \left( \frac{\partial c'}{\partial X_1} \right)_{X_1=1} = K c' (1 - c_0 c') \left( \frac{\partial \mathbf{s}'_{\parallel}}{\partial X_1} \right)_{X_1=1} . \quad (2.60)$$

### 2.4.4. Considered stress profiles

#### 2.4.4.1. Externally applied stress profiles

In case of externally applied stress, the following dimensionless stress profile has been adopted for the stress ( $\mathbf{s}'_{\parallel} \times \mathbf{s}_0$ ) (cf. equation (2.55)):

$$\mathbf{s}'_{\parallel}(X_1) = R \cdot \text{erf} \left( \frac{X_1 - 0.5}{W} \right). \quad (2.61)$$

If  $\mathbf{s}_0 = 600\text{MPa}$  and  $R=5$ , then the maximum magnitude of actual, externally applied stress  $\mathbf{s}_{\parallel}$  is 3GPa.

#### 2.4.4.2. Diffusion-induced, internal stress profiles

After interdiffusion and in case of a freestanding diffusion couple (i.e. a thin bilayer) the corresponding diffusion induced stress profile is given by the following equation [Larche and Cahn (1982), (1992)]:

$$\mathbf{s}_{zz} = \mathbf{s}_{yy} = \mathbf{s}_{\parallel} = -\mathbf{h}_{BA} Y \left[ (c - c'_0) - \frac{1}{L} \int_0^L (c - c'_0) dx - \frac{12(x - \frac{L}{2})}{L^3} \int_0^L (c - c'_0) (x - \frac{L}{2}) dx \right] \quad (2.62)$$

and



## 2. Interaction of stress and diffusion in a binary substitutional solid solution

$$s_{xx} = 0. \quad (2.63)$$

$c'_0$  is the average composition of 'B' atoms (measured in mole fraction) and  $c$  is the local composition. The last term in equation (2.62) describes the bending of the film. For a thin film diffusion couple on the substrate, one can neglect the bending of the couple and the third term within the square bracket can be neglected.

Non-dimensionalisation of this stress profile has been done by putting:

$$s'_{\parallel} = \frac{s_{\parallel}}{Y h_{B A} c'_0}. \quad (2.64)$$

### 2.4.5. Numerical procedure

#### 2.4.5.1. Finite difference formulation of diffusion equation

The dimensionless diffusion equation (2.58) has been discretized using the explicit finite difference method [Crank (1973), Smith (1965)]. In this method, a number of rectangular grids occupy the space  $0 \leq X_1 \leq L$  in the  $X_1 - T'$  diagram (see Fig. 2.2). Let the range of  $X_1$  be divided into equal interval  $dX_1$  and the time into intervals  $dT'$ . Let the coordinates of a representative grid point be  $(i dX_1, j dT')$  where  $i$  and  $j$  are integers.

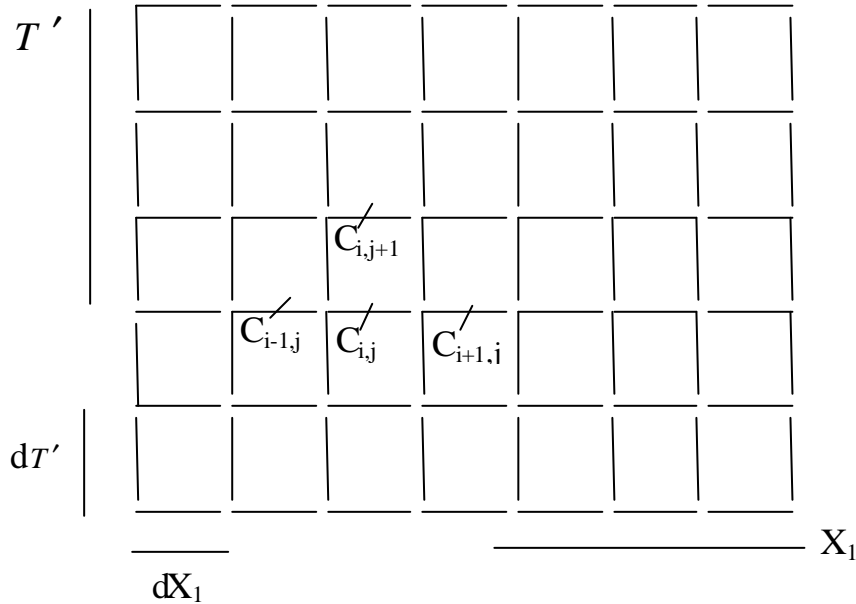


Fig. 2.2 Finite difference grid employed for the numerical calculations.

## 2. Interaction of stress and diffusion in a binary substitutional solid solution

---

The value of concentration, at the representative grid point can be denoted by  $c_{i,j}$ . If the  $c_{i,j}$ 's are known for a particular  $i$  and  $j$ , then it is possible to calculate the  $c_{i,j+1}$ 's. In the case of an externally applied stress,  $\mathbf{s}'_{\parallel}$  only depends on the space coordinates whereas in the case of diffusion induced stress,  $\mathbf{s}'_{\parallel}$  depends on both the space and time coordinates. The resulting finite difference version of the dimensionless diffusion equation reads (for details see Appendix 2C):

$$\begin{aligned}
 c'_{i,j+1} = & c'_{i,j} + r \left( c'_{i+1,j} + c'_{i-1,j} - 2c'_{i,j} \right) - \\
 & r K c'_{i,j} (1 - c'_{i,j} c_0) \left( \mathbf{s}'_{\parallel+1,j} + \mathbf{s}'_{\parallel-1,j} - 2\mathbf{s}'_{\parallel,j} \right) \\
 & - \frac{rK}{4} \left( 1 - \frac{2c'_{i,j}c_0\bar{V}_B}{(1 - c_0c'_{i,j})\bar{V}_A + c_0c'_{i,j}\bar{V}_B} \right) (c'_{i+1,j} - c'_{i-1,j}) (\mathbf{s}'_{\parallel+1,j} - \mathbf{s}'_{\parallel-1,j}) + \quad (2.65) \\
 & \frac{2(\bar{V}_A - \bar{V}_B)c_0}{(1 - c_0c'_{i,j})\bar{V}_A + c_0c'_{i,j}\bar{V}_B} \frac{r}{4} (c'_{i+1,j} - c'_{i-1,j})^2 + \frac{P_{i,j}}{\tilde{D}'_{i,j}} \frac{r}{4} (c'_{i+1,j} - c'_{i-1,j}) \times \\
 & \left\{ c'_{i+1,j} - c'_{i-1,j} - K c'_{i,j} (1 - c_0c'_{i,j}) (\mathbf{s}'_{\parallel+1,j} + \mathbf{s}'_{\parallel-1,j}) \right\}
 \end{aligned}$$

where,

$$P_{i,j} \equiv \frac{\partial \tilde{D}'_{i,j}}{\partial c'_{i,j}} \quad (2.66)$$

and the ratio

$$r \equiv \frac{dT'}{(dX_1)^2} \quad (2.67)$$

The maximum value of  $r$  can be taken as 1/2. A value greater than 1/2 leads to the divergence of the solution [Smith (1965)].

Using equation (2.65) the concentration at grid points at a time  $T' + dT'$  can be calculated if the concentrations at time  $T'$  are known.

Calculations have been done for a maximum of 10000 time steps and 200 position steps.

### 2.4.5.2. Finite difference formulation of boundary conditions

The conditions of zero diffusion flux at the two boundaries at  $X_1 = 0$  (or  $i = 1$ ) and at

$X_1 = 1$  ( $i = NMAX$ ) can be expressed as follows:

## 2. Interaction of stress and diffusion in a binary substitutional solid solution

---

At  $i = 1$ :

$$c'_{1,j+1} = c'_{1,j} + 2r(c'_{2,j} - c'_{1,j}) - rKc'_{1,j}(1 - c'_{1,j}c_0)(s'_{\parallel 2,j} - s'_{\parallel 1,j}) \times \left(2 - \frac{K}{4}(1 - 2c_0c'_{1,j})(s'_{\parallel 2,j} - s'_{\parallel 1,j})\right) \quad (2.68)$$

and at  $i = NMAX$ :

$$c'_{NMAX,j+1} = c'_{NMAX,j} + 2r(c'_{NMAX-1,j} - c'_{NMAX,j}) + rKc'_{NMAX,j}(1 - c'_{NMAX,j}c_0)(s'_{\parallel NMAX,j} - s'_{\parallel NMAX-1,j}) \times \left(2 - \frac{K}{4}(1 - 2c_0c'_{NMAX,j})(s'_{\parallel NMAX,j} - s'_{\parallel NMAX-1,j})\right) \quad (2.69)$$

In deriving equations (2.68) and (2.69), the following approximations have been applied:

$$s'_{\parallel 0,j} \approx s'_{\parallel 1,j}, \quad (2.70)$$

$$s'_{\parallel NMAX+1,j} \approx s'_{\parallel NMAX,j} \quad (2.71)$$

These approximations were necessary because of the absence of any boundary condition for the stress state.

In the following results are presented which have been obtained using equations (2.65), (2.68) and (2.69) taking the diffusion coefficient concentration independent, i.e

$$P_{i,j} \equiv \frac{\partial \tilde{D}'_{i,j}}{\partial c'_{i,j}} \equiv 0. \quad (2.72)$$

### 2.4.5.3. Finite difference formulation of the diffusion-induced, internal stress profiles

The finite difference formulation of the non-dimensional stress profile can be written as follows:

$$(s'_{\parallel})_{i,j} = -\left(\frac{c_0c'_{i,j}}{c'_0} - 1\right) + \int_0^1 \left(\frac{c_0c'_{i,j}}{c'_0} - 1\right) dX_{li} + 12 \times (X_{li} - 1/2) \int_0^1 \left(\frac{c_0c'_{i,j}}{c'_0} - 1\right) (X_{li} - 1/2) dX_{li} \quad (2.73)$$

### 2.4.6. System studied and data used

Evidently, the effect of (non-hydrostatic) stress on diffusion can be pronounced if the factor  $K$  and/or the stress gradient are significant (cf. equation (2.58)). Hence:

- (i) in case of externally applied stress, the response of diffusion on stress increases if the absolute value of the stress and/or  $h_{BA}$  increase and/or  $j$  decreases (at a given temperature). Note that in thin films the residual biaxial stress (growth stress and thermal stress) occurring after layer production can be of the order of GPa.
- (ii) in case of diffusion induced stress, the response of diffusion on stress increases if  $s_0 (=Yh_{BA}c'_0)$  increases. This can be achieved by increasing the biaxial modulus  $Y$  and/or  $h_{BA}$ .

$h_{BA}$  varies widely from binary system to binary system and can depend strongly on composition. The thermodynamic factor  $j$  is composition-dependent (at a particular temperature);  $j > 1$  for solutions with a negative heat of mixing and  $j < 1$  in the opposite case. Table 2.1 shows the value of  $h_{BA}$  and  $j$  for some binary cubic systems and the temperature range for which complete solid solubility exists. In these cases,  $h_{BA}$  is practically independent of composition (i.e. Vegard's law is obeyed). Values given for  $h_{BA}$  have been calculated using the lattice-parameter data [Pearson (1967)] and  $j$  values have been calculated using thermodynamic data [Hultgren *et al.* (1973)] for different systems.

Two systems have been chosen for numerical simulations: the Copper-Palladium (Cu-Pd) system and the Gold-Nickel (Au-Ni) system

(i) Cu-Pd system:

For the Cu-Pd system, complete solid solubility prevails over the whole composition range. However, ordered phases occur at temperatures below 500°C. The formation of phases has not been considered in this work.  $\bar{V}_{Cu}$  and  $\bar{V}_{Pd}$  are 7.12cm<sup>3</sup>/mole and 8.91 cm<sup>3</sup>/mole, respectively and the partial molar volumes do not depend on composition. For simplicity,  $j$  is taken as 1, although from the available thermodynamic data for Cu-Pd

## 2. Interaction of stress and diffusion in a binary substitutional solid solution

---

system,  $j$  is greater than one almost throughout the whole composition range (at 1077°C).

(ii) Au-Ni system:

For the Au-Ni system, complete solid solubility prevails over the whole composition range at temperatures above 1100°C. Potential phase formation has not been considered in this work.

$\bar{V}_{Au}$  and  $\bar{V}_{Ni}$  are 10.27 cm<sup>3</sup>/mole and 6.65 cm<sup>3</sup>/mole respectively and the partial molar volumes do not depend on composition. For simplicity,  $j$  has been taken as constant (neglecting the composition dependence), equal to 0.5 (cf. Table 2.1) at 877°C.

Table 2.1: Thermodynamic factor ( $j$ ) and chemical expansion coefficient ( $h_{BA}$ ) for various binary cubic solid solutions [Pearson (1967) and Hultgren *et al.* (1973)] .

System	$j$	$h_{BA}$
Pd-Cu (T> 500°C)	>1 (c=0 to 1) (> 500°C)	0.0744
Ag-Pd (at all Temp.)	>1 (c=0 to 1) (At 927°C)	0.0458
Mo-Nb (at all Temp.)	>1 (c=0 to 1) (At >500°C)	0.0488
Pd-Ni (at all Temp.)	<1 (0.11 ≤ c ≤ 0.265) (At 1000°C)	0.098
Au-Ni (T>1100°C)	<1 (c=0 to 1) (At 877°C)	0.1426
Mo-Cr (T>850°C)	<1 (c=0 to 1) (At 1198°C)	0.0859

## 2.5. Results and discussion

### 2.5.1. Zero stress gradient

If the applied stress does not depend on location (see Fig. 2.3(a); i.e. the stress gradient vanishes), equation (2.58) reduces to the ‘usual’ diffusion equation. An example for the concentration profiles developing in this case in a Pd-Cu couple is shown in Fig. 2.3(b), where the Pd concentration (in mole fraction) is plotted versus the dimensionless position. Concentration profiles similar to error functions are obtained. The deviations with respect to error functions are (mainly) due to the zero-flux boundary conditions at the surfaces. However, also the term proportional to  $(\partial c'/\partial X_1)^2$  in equation (2.58) leads to a deviation of the concentration profile from an error function.

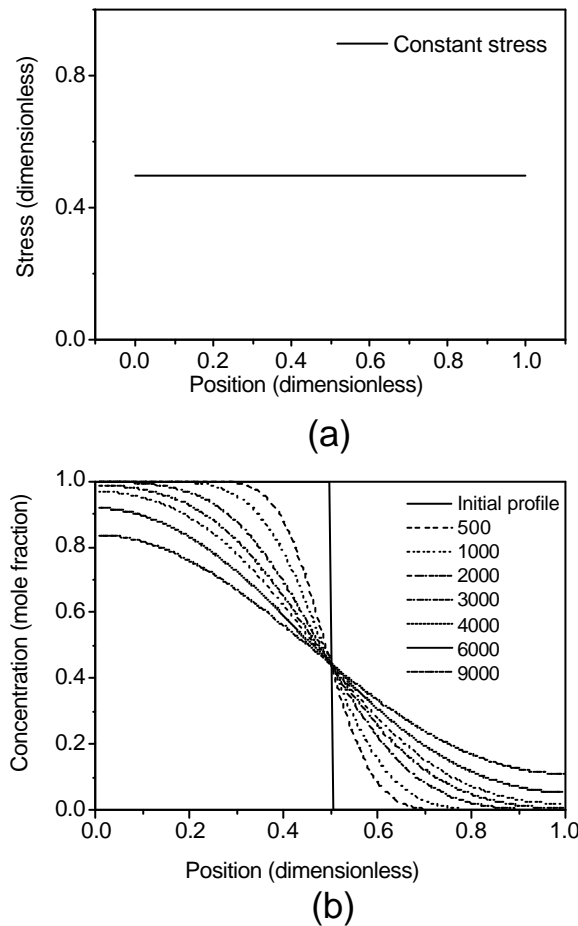


Fig. 2.3: (a) Externally applied stress profile with zero gradient. (b) Resulting Pd concentration profiles in the absence of stress gradients.

### 2.5.2. Externally applied positive and negative stress gradient

First, the case of a Pd-Cu couple is considered. An externally applied stress profile with a positive stress gradient is shown in Fig. 2.4(a). (equation (2.61);  $W$  has been taken as 0.05,  $R$  has been taken as 5). Therefore, initially, B (Pd) atoms are under compressive planar stress and A (Cu) atoms will be under tensile planar stress. The resulting concentration profile is shown in Fig. 2.4(b). Qualitatively, the peculiar shape of the resulting concentration profile can be understood as follows. Palladium atoms are bigger (partial molar volume  $8.91 \text{ cm}^3/\text{mole}$ ) than copper atoms (partial molar volume  $7.12 \text{ cm}^3/\text{mole}$ ). The bigger atoms (Pd) would prefer a state of

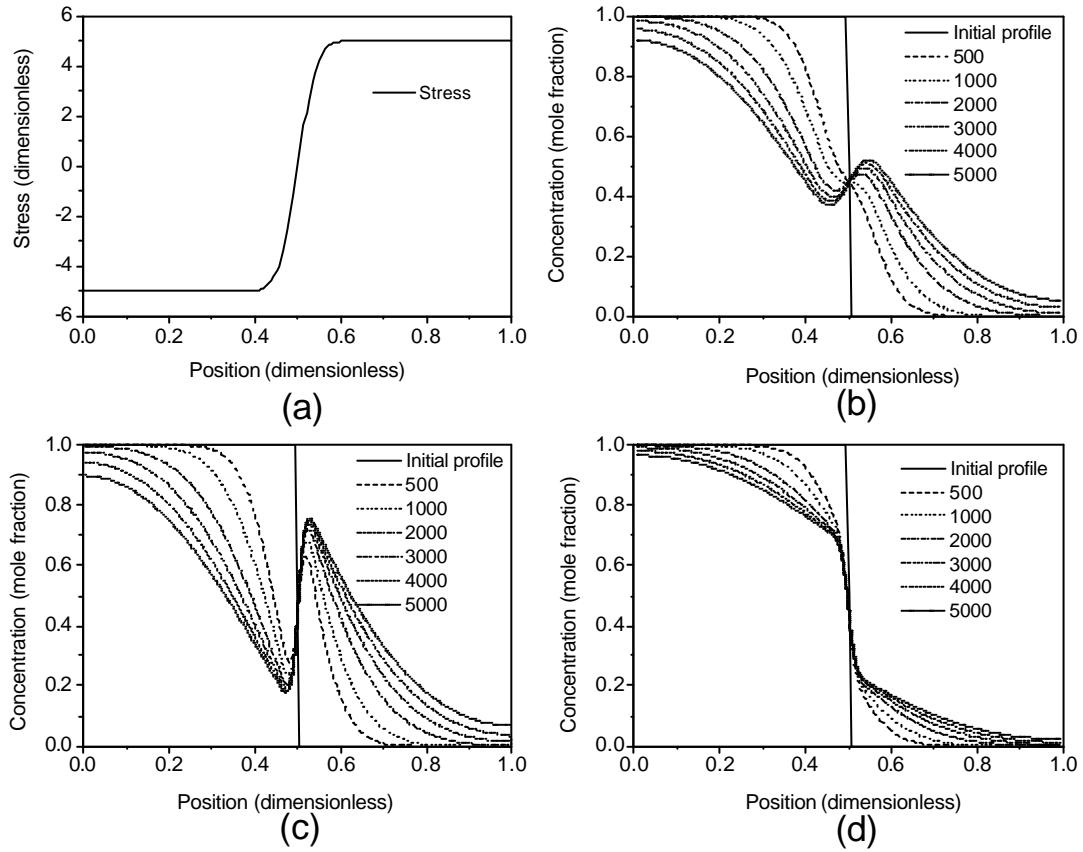


Fig. 2.4: (a) Externally applied stress profile with positive stress gradient ( $R=5, W=0.05$ ). (b) Resulting Pd concentration profiles. (c) Resulting Pd concentration profiles ( $R=10, W=0.02$ ). (d) Resulting Pd concentration profiles in case of a negative stress gradient ( $R=-5, W=0.02$ ).

## 2. Interaction of stress and diffusion in a binary substitutional solid solution

tensile stress and the smaller atoms (Cu) would prefer a state of compressive stress within the couple (thereby lowering the total energy of the system). As a consequence, the stress-gradient related terms in the diffusion equation result in a flux of the bigger atoms (Pd) towards the tensile region and vice versa.

As the stress gradient has been constrained to the proximity of the initial interface in the simulations, a high flux occurs there. However, the atoms also have to be transported away from the proximity of the interface and this can only occur due to concentration gradients. As a consequence, an ‘atom jam’ develops at those points in the couple, where the stress gradient decreases to zero. Note that the flux driven by the stress gradient more than counterbalances the back-flux arising from the concentration gradient at the interface.

The magnitude of the peculiar concentration profile is enhanced if the magnitude of the stress gradient increases. See Fig. 2.4(c), which has been calculated with  $W = 0.02$  and  $R=10$ . Evidently, the ‘atom jam’ in the neighbourhood is now more pronounced.

If the stress profile (with  $W = 0.02$ ,  $R=-5$ ) is inverted (i.e., a negative stress gradient then prevails at the initial interface), the concentration profiles shown in Fig. 2.4(d) develop. Now, the stress-gradient related flux counteracts the concentration-gradient driven flux. As a consequence, a very steep concentration profile develops in the proximity of the initial interface and a suppression of interdiffusion occurs.

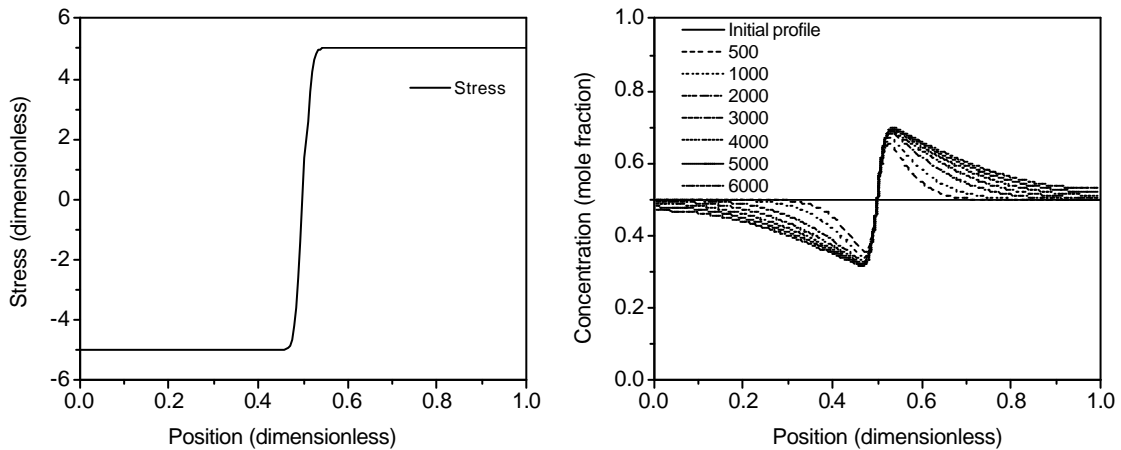


Fig. 2.5: (a) Externally applied stress profile with positive stress gradient ( $R=5$ ,  $W=0.02$ ). (b) Resulting Pd concentration profiles for an initially homogeneous couple.



## 2. Interaction of stress and diffusion in a binary substitutional solid solution

If an initially homogeneous couple is subjected to a positive stress gradient ( $W = 0.02$  and  $R=5$ ), the result shown in Fig. 2.5(b) develops.

This result can be understood as follows. Initially, only the stress gradient drives the diffusion flux: Pd atoms are pushed towards the region with a planar tensile stress (i.e. to the right-hand side in Fig. 2.5(b) and vice versa in the proximity of the interface. As a consequence, concentration gradients develop. In order to maintain the flux at the interface, dominated by the stress gradient, concentration gradients driving flux of Pd atoms to and from the neighborhood of the interface develop. Note that in the immediate proximity of the interface, the flux driven by the concentration is more than counterbalanced by the flux driven by the stress gradient.

Finally, a comparison has been made between Pd-Cu system and Au-Ni system where the simulation has been performed for the same externally applied stress gradient for both systems (in Fig. 2.6,  $W$  has been taken as 0.02,  $R$  has been taken as 5). Clearly, comparing, Figs. 2.6(a) and 2.6(b), it is seen that the stress effect is more significant in case of Au-Ni system which has bigger  $h_{BA}$  and smaller  $j$  compared to Pd-Cu system.

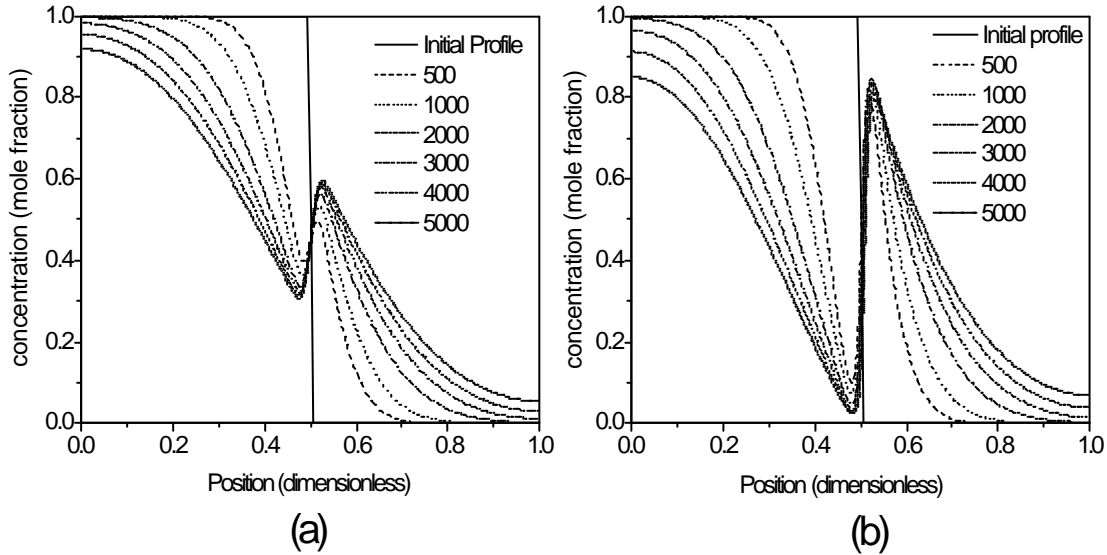


Fig. 2.6: (a) Externally applied stress profile with positive stress gradient ( $R=5$ ,  $W=0.02$ ) in case of Pd-Cu system for an initial concentration profile given by condition 1.

(b) Externally applied stress profile with positive stress gradient ( $R=5$ ,  $W=0.02$ ) in case of Au-Ni system for an initial concentration profile given by condition 1.

### 2.5.3. Effect of internal, diffusion-induced stress on diffusion

Even if no stress is externally applied to the diffusion couple and if no residual stresses resulting from the production of e.g. a thin film diffusion couple exist, stress will be generated from concentration redistributions upon interdiffusion. These stresses can be calculated from equation (2.62) for the case of a free-standing couple and from equation (2.64) for the case of a couple attached to a rigid substrate and they will be called ‘self-stress’ in the following. These self-stresses, in turn, affect the diffusion process and new (self-stress affected) concentration profiles develop etc.

For the case of an initial concentration profile of type ‘1’, in the absence of externally applied stresses, the self-stress profiles and the concentration profiles are shown in Figs. 2.7(a) and 2.7(b), respectively, for the condition of a free-standing layer and for the condition of a layer attached to a rigid substrate in Figs. 2.7(c) and 2.7(d), respectively.

The stress profiles have been calculated assuming that the stresses are zero throughout the couple upon complete homogenisation. The calculated stress profile in the initial condition then serves to match the lattices of Cu and Pd coherently at the initial interface. Note that the oscillatory behaviour of the stress profile is thus most pronounced for the given initial condition and that the stress will be zero throughout the couple upon complete homogenisation.

The calculations of the concentration profiles have also been repeated neglecting stress-gradient related terms in the diffusion equation, i.e. without considering stress effects. The results can be compared in Fig. 2.7(b) and 2.7(d) with the results containing the stress effects. Obviously, self-stresses enhance diffusional intermixing.

The enhancement of intermixing is more pronounced for the case of the couple bound to the substrate. This is a consequence of the fact that the stress profile changes monotonically with position in this case: the stress gradient always serves the diffusional intermixing, whereas this is not the case for the free-standing couple.

## 2. Interaction of stress and diffusion in a binary substitutional solid solution

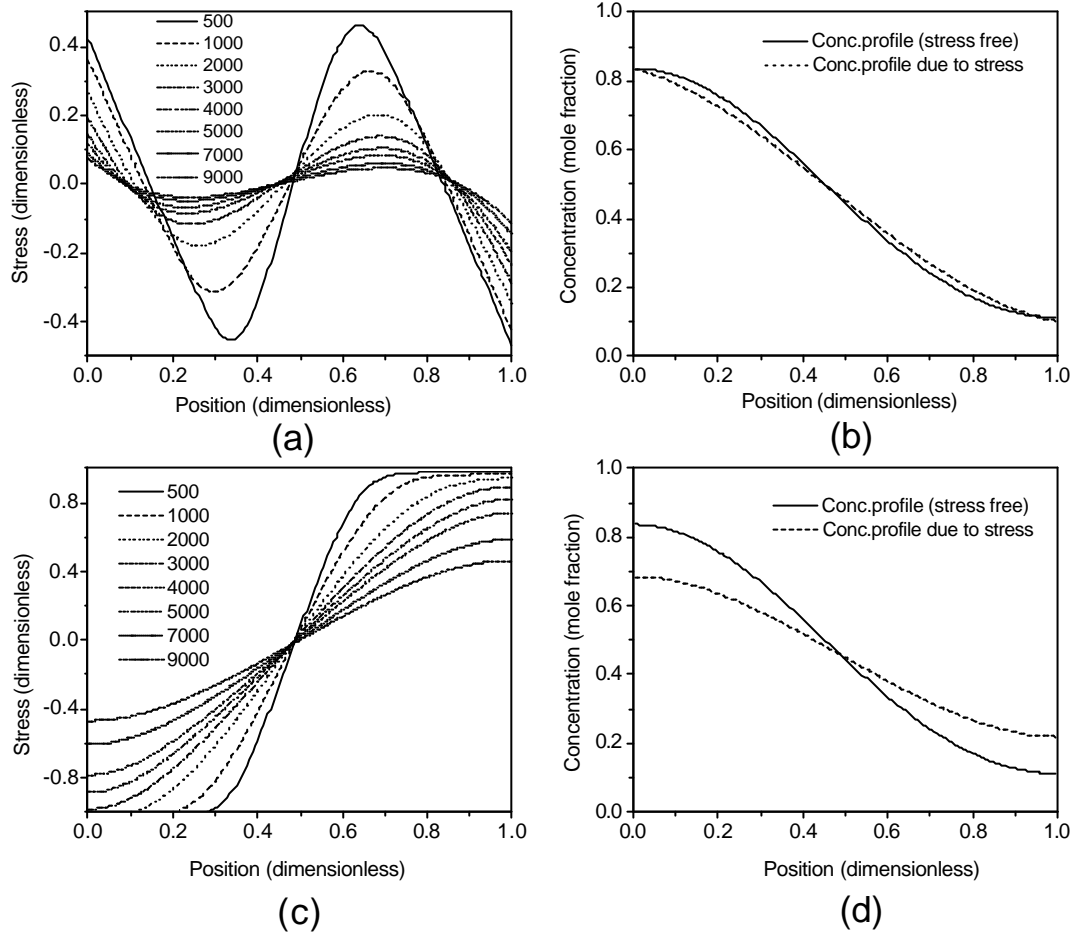


Fig. 2.7: (a) Diffusion induced (self) stress profiles for the free-standing thin Pd-Cu diffusion couple. (b) Stress free concentration profile for Pd and also the concentration profile due to diffusion induced stress (time step is 9000 in both cases) in case of free-standing couple. (c) Diffusion induced (self) stress profiles for the diffusion couple on a rigid substrate. (d) Stress free Pd concentration profile and also the concentration profile due to diffusion induced stress in case the diffusion couple is on a rigid substrate (time step is 9000 in both cases).

### 2.6 Summary

- Following a treatment proposed by Larche and Cahn [Larche and Cahn (1973), (1983), (1985)], i.e. adopting gradients of so-called diffusion potentials as driving forces for diffusion fluxes, flux equations analogous to Fick's first law have been derived in the laboratory frame of reference for binary substitutional diffusion couples for cases of non-hydrostatic (in particular planar) states of stress.
- The role of non-hydrostatic stress for substitutional diffusion in crystalline solids cannot be expressed by a (simple) modification of the chemical, interdiffusion coefficient, as is possible for hydrostatic stress.
- The flux equations demonstrate that stress gradients can act as significant driving forces for diffusion, provided that the partial molar volumes of the diffusing species differ.
- For numerical solutions of the diffusion equations (flux equations plus continuity equation, Fick's 2<sup>nd</sup> law), explicit finite difference formulations have been given.
- Taking the Cu-Pd and Au-Ni systems as examples, numerical simulations of concentration and stress profiles in initially layered and initially homogenous couples subjected to externally applied or diffusion-induced stresses have been obtained.
- The results show that stress profiles can lead to peculiar effects in concentration-depth profiles developing upon diffusion, which ask for experimental verification.

## Appendix 2A

### Derivation of equation (2.24)

In equation (2.23) (in the text), the derivatives of  $M_{BA}$  and  $M_{wA}$  can be determined using equation (2.14) and (2.15) as follows:

By taking the derivative of equation (2.14) with respect to position, the gradient of diffusion potential in one dimension can be written as follows:

$$\frac{\partial M_{BA}(\mathbf{s}_{ij}, c)}{\partial x} = \frac{\partial M_{BA}(0, c)}{\partial x} - V' \mathbf{h}_{BA} \frac{\partial \mathbf{s}_{kk}}{\partial x} - V' \mathbf{s}_{kk} \frac{\partial \mathbf{h}_{BA}}{\partial x} \quad (2A1)$$

Now, equation (2.15) (in text) has to be differentiated with respect to position in one dimension to determine the first term on the right-hand side of equation (2A1). It is well known that the standard chemical potentials of 'B' and 'A' atoms in the absence of stress can be written as:

$$\mathbf{m}_B(c) = \mathbf{m}_B^{(0)} + RT \ln \mathbf{g}_B c \quad (2A2)$$

Where,  $c$  is the concentration of 'B' atoms, measured in mole fraction. Also,

$$\mathbf{m}_A(1-c) = \mathbf{m}_A^{(0)} + RT \ln \mathbf{g}_A (1-c) \quad (2A3)$$

Where,  $c_A (=1-c)$  is the composition of 'A' atoms measured in mole fraction, if the vacancy concentration is much small compared to the concentration of 'A' or 'B'.  $\mathbf{g}_A$  and  $\mathbf{g}_B$  are the activity coefficients of 'A' and 'B' respectively.

Hence, differentiating equation (2A2) and (2A3) with respect to position in one dimension the following expressions can be obtained.

$$\frac{\partial \mathbf{m}_B(c)}{\partial x} = RT \mathbf{j}_B \frac{1}{c} \frac{\partial c}{\partial x} \quad (2A4)$$

$$\frac{\partial \mathbf{m}_A(1-c)}{\partial x} = RT \mathbf{j}_A \frac{1}{(1-c)} \frac{\partial (1-c)}{\partial x} \quad (2A5)$$

When these expressions are substituted in the equation (2A1), then it follows that:

$$\frac{\partial M_{BA}(\mathbf{s}_{ij}, c)}{\partial x} = -RT \mathbf{j} \left( \frac{1}{c} + \frac{1}{1-c} \right) \frac{\partial (1-c)}{\partial x} - V' \mathbf{h}_{BA} \frac{\partial \mathbf{s}_{kk}}{\partial x} - V' \mathbf{s}_{kk} \frac{\partial \mathbf{h}_{BA}}{\partial x} \quad (2A6)$$

where  $\mathbf{j}_A$  and  $\mathbf{j}_B$  are the thermodynamic factors for the component 'A' and 'B' respectively.

## 2. Interaction of stress and diffusion in a binary substitutional solid solution

---

$$j_A = \left(1 + \frac{\partial \ln g_A}{\partial \ln(1-c)}\right) \quad (2A7)$$

$$j_B = \left(1 + \frac{\partial \ln g_B}{\partial \ln c}\right) \quad (2A8)$$

From the Gibbs-Duhem relation it can be proved that:

$$j_A = j_B = j \quad (2A9)$$

(i.e. thermodynamic factors for both the chemical species are same)

Similarly, derivative of  $M_{vA}(\mathbf{s}_{ij}, c_v)$  in one dimension can be written down as follows:

$$\frac{\partial M_{vA}(\mathbf{s}_{ij}, c_v)}{\partial x} = -RTj \frac{1}{(1-c)} \frac{\partial(1-c)}{\partial x} - V' \mathbf{h}_{vA} \frac{\partial \mathbf{s}_{kk}}{\partial x} - V' \mathbf{s}_{kk} \frac{\partial \mathbf{h}_{vA}}{\partial x} \quad (2A10)$$

where,  $c_v$  is the vacancy composition. Also it has been assumed that vacancy concentration is small and it is maintained at a local equilibrium value everywhere within the diffusion zone. Therefore, to derive equation (2A10), the following relationships have been used.

$$\mathbf{m}_v(c_v) = \mathbf{m}_v(\bar{c}_v) \approx 0 \quad (2A11)$$

$$\text{Therefore, } M_{vA}(0, c_v) = -\mathbf{m}_A(1-c) \quad (2A12)$$

To derive the flux equation (2.24) we eliminate  $B_{AB}$  from the equation (2.19) (in text) by using the relation:

$$B_{AB} = -(B_{Av} + B_{AA}) \quad (2A13)$$

Therefore, in one dimension, the diffusion flux equation for the component 'A' is as follows when equation (2A6), (2A10) and (2A13) have been put in equation (2.23) (in text). :

$$J_A = - \left[ B_{AA} \left\{ RTj \left( \frac{1}{c} + \frac{1}{1-c} \right) \frac{\partial(1-c)}{\partial x} + V' \mathbf{h}_{BA} \frac{\partial \mathbf{s}_{kk}}{\partial x} + V' \mathbf{s}_{kk} \frac{\partial \mathbf{h}_{BA}}{\partial x} \right\} + B_{Av} \left\{ RTj \frac{1}{c} \frac{\partial(1-c)}{\partial x} - V' \mathbf{h}_{vA} \frac{\partial \mathbf{s}_{kk}}{\partial x} - V' \mathbf{s}_{kk} \frac{\partial \mathbf{h}_{vA}}{\partial x} + V' \mathbf{h}_{BA} \frac{\partial \mathbf{s}_{kk}}{\partial x} - V' \mathbf{s}_{kk} \frac{\partial \mathbf{h}_{BA}}{\partial x} \right\} \right] \quad (2A14)$$

Neglecting the contributions associated with the cross effects (arising out of the second term with  $B_{Av}$ ) to the diffusion flux, the following can be written:

$$J_A = - \left[ B_{AA} \left\{ RTj \left( \frac{1}{c} + \frac{1}{1-c} \right) \frac{\partial(1-c)}{\partial x} + V' \mathbf{h}_{BA} \frac{\partial \mathbf{s}_{kk}}{\partial x} + V' \mathbf{s}_{kk} \frac{\partial \mathbf{h}_{BA}}{\partial x} \right\} \right] \quad (2A15)$$

If it is assumed that  $\mathbf{h}$  is independent of composition or position, then for a general state of stress (may be applied externally or due to internal or self stress), equation (2A15) can be written as:

$$J_A = - \left[ B_{AA} \left\{ RTj \left( \frac{1}{c} + \frac{1}{1-c} \right) \frac{\partial(1-c)}{\partial x} + V \mathbf{h}_{BA} \frac{\partial \mathbf{s}_{kk}}{\partial x} \right\} \right] \quad (2A16)$$

which is exactly equation (2.24) in the text.

## Appendix 2B

### Derivation of equation (2.42)

$J_A$  and  $J_B$  in equation (2.38) and (2.39) (in the text) can be replaced by their corresponding expressions from equations (2.31) and (2.33) which results in the following equations:

$$\frac{\partial \mathbf{r}_A}{\partial t} = \frac{\partial}{\partial x} \left( \bar{D}_A \frac{\partial \mathbf{r}_A}{\partial x} \right) + \frac{\partial}{\partial x} \left( \frac{\bar{D}_A c(1-c)}{j RT} \frac{\bar{V}_B}{V^2} V \mathbf{h}_{BA} \frac{\partial \mathbf{s}_{kk}}{\partial x} \right) - \frac{\partial}{\partial x} (\mathbf{r}_A \mathbf{n}) \quad (2B1)$$

$$\text{and } \frac{\partial \mathbf{r}_B}{\partial t} = \frac{\partial}{\partial x} \left( \bar{D}_B \frac{\partial \mathbf{r}_B}{\partial x} \right) - \frac{\partial}{\partial x} \left( \frac{\bar{D}_B c(1-c)}{j RT} \frac{\bar{V}_A}{V^2} V \mathbf{h}_{BA} \frac{\partial \mathbf{s}_{kk}}{\partial x} \right) - \frac{\partial}{\partial x} (\mathbf{r}_B \mathbf{n}) \quad (2B2)$$

Now, following expressions for the position and time derivatives of  $\mathbf{r}_A$  and  $\mathbf{r}_B$  can be obtained by differentiating equation (2.27) (see in the text) with respect to position and time.

$$\frac{\partial \mathbf{r}_B}{\partial t} = - \frac{\bar{V}_A}{\bar{V}_B} \frac{\partial \mathbf{r}_A}{\partial t} \quad (2B3)$$

$$\bar{V}_A \frac{\partial \mathbf{r}_A}{\partial x} = - \bar{V}_B \frac{\partial \mathbf{r}_B}{\partial x} \quad (2B4)$$

Now, using equation (2B3) and (2B4) we can transform equation (2B2) as follows:

$$- \frac{\bar{V}_A}{\bar{V}_B} \frac{\partial \mathbf{r}_A}{\partial t} = - \frac{\partial}{\partial x} \left( \bar{D}_B \frac{\bar{V}_A}{\bar{V}_B} \frac{\partial \mathbf{r}_A}{\partial x} \right) - \frac{\partial}{\partial x} \left( \frac{\bar{D}_B c(1-c)}{j RT} \frac{\bar{V}_A}{V^2} V \mathbf{h}_{BA} \frac{\partial \mathbf{s}_{kk}}{\partial x} \right) - \frac{\partial \mathbf{n}}{\partial x} \mathbf{r}_B - \mathbf{n} \frac{\partial \mathbf{r}_B}{\partial x} \quad (2B5)$$

Eliminating  $\frac{\partial \mathbf{r}_A}{\partial t}$  from (2B5) using (2B1) and simplifying, it follows that:

$$\begin{aligned} \frac{\partial \mathbf{n}}{\partial x} = & \bar{V}_A \frac{\partial}{\partial x} \left( \bar{D}_A \frac{\partial \mathbf{r}_A}{\partial x} \right) - \bar{V}_B \frac{\partial}{\partial x} \left( \bar{D}_B \frac{\bar{V}_A}{\bar{V}_B} \frac{\partial \mathbf{r}_A}{\partial x} \right) + \bar{V}_A \frac{\partial}{\partial x} \left( \frac{\bar{D}_A c(1-c)}{j RT} \frac{\bar{V}_B}{V^2} V \mathbf{h}_{BA} \frac{\partial \mathbf{s}_{kk}}{\partial x} \right) - \\ & \bar{V}_B \frac{\partial}{\partial x} \left( \frac{\bar{D}_B c(1-c)}{j RT} \frac{\bar{V}_A}{V^2} V \mathbf{h}_{BA} \frac{\partial \mathbf{s}_{kk}}{\partial x} \right) \end{aligned} \quad (2B6)$$

## 2. Interaction of stress and diffusion in a binary substitutional solid solution

---

As the partial molar volumes are independent of position, they can be taken inside the partial derivatives. Then simply integrating equation (2B6) or lifting the partial derivatives on both sides of equation (2B6), the expression for velocity can be obtained which is as following:

$$\mathbf{n} = \bar{D}_A \bar{V}_A \frac{\partial \mathbf{r}_A}{\partial x} - \bar{D}_B \bar{V}_B \frac{\partial \mathbf{r}_B}{\partial x} + \frac{\bar{V}_A \bar{D}_A c(1-c)}{\mathbf{j} RT} \frac{\bar{V}_B}{V^2} V' \mathbf{h}_{BA} \frac{\partial \mathbf{s}_{kk}}{\partial x} - \frac{\bar{D}_B \bar{V}_B c(1-c)}{\mathbf{j} RT} \frac{\bar{V}_A}{V^2} V' \mathbf{h}_{BA} \frac{\partial \mathbf{s}_{kk}}{\partial x} \quad (2B7)$$

The flux equations for ‘A’ and ‘B’ in the laboratory reference frame can be obtained by putting the velocity expression in equation (2.37) and (2.38) and replacing  $J_A$  and  $J_B$  by their corresponding expressions (equations (2.31 and 2.33) which are as follows:

$$J_A^{(0)} = -(\bar{D}_A \mathbf{r}_B \bar{V}_B + \bar{D}_B \mathbf{r}_A \bar{V}_A) \frac{\partial \mathbf{r}_A}{\partial x} - \left( \frac{\bar{V}_B}{V^2} \right) V' \frac{c(1-c)}{\mathbf{j} RT} \mathbf{h}_{BA} \frac{\partial \mathbf{s}_{kk}}{\partial x} (\bar{D}_A \mathbf{r}_B \bar{V}_B + \bar{D}_B \mathbf{r}_A \bar{V}_A) \quad (2B8)$$

Which is exactly the equation (2.42) in text.

## Appendix 2C

### Details of finite difference methods

In this section of the appendix, a relationship (see Fig.2.2) between  $c'_{i,j}$  and  $c'_{i,j+1}$  has been established. To do that first,  $c'_{i,j}$  is expanded in a Taylor's series in ‘ $T'$ ’ direction keeping  $X_1$  constant, which is as follows:

$$c'_{i,j+1} = c'_{i,j} + dT \left( \frac{\partial c'}{\partial T'} \right)_{i,j} + \frac{1}{2} (dT')^2 \left( \frac{\partial^2 c'}{\partial T'^2} \right)_{i,j} + \text{higherorder} \quad (2C1)$$

Neglecting the higher order terms and also the term associated with  $(dT')^2$ , the following can be written:

$$\frac{c'_{i,j+1} - c'_{i,j}}{dT'} = \left( \frac{\partial c'}{\partial T'} \right)_{i,j} \quad (2C2)$$

Similarly, expanding  $c'_{i,j}$  in  $X_1$  direction keeping ‘ $T'$ ’ constant, it follows:

$$c'_{i-1,j} = c'_{i,j} - dX_1 \left( \frac{\partial c'}{\partial X_1} \right)_{i,j} + \frac{1}{2} (dX_1)^2 \left( \frac{\partial^2 c'}{\partial X_1^2} \right)_{i,j} + \text{higherorder} \quad (2C3)$$

$$\text{and } c'_{i+1,j} = c'_{i,j} + dX_1 \left( \frac{\partial c'}{\partial X_1} \right)_{i,j} + \frac{1}{2} (dX_1)^2 \left( \frac{\partial^2 c'}{\partial X_1^2} \right)_{i,j} + \text{higherorder} \quad (2C4)$$



## 2. Interaction of stress and diffusion in a binary substitutional solid solution

Therefore, adding (2C3) and (2C4), and neglecting higher order terms, it follows that,

$$\frac{c'_{i+1,j} + c'_{i-1,j} - 2c'_{i,j}}{(dX_1)^2} = \left( \frac{\partial^2 c'}{\partial X_1^2} \right)_{i,j}. \quad (2C5)$$

Again subtracting (2C3) from (2C4), and neglecting higher order terms, it follows that,

$$\frac{c'_{i+1,j} - c'_{i-1,j}}{2(dX_1)} = \left( \frac{\partial c'}{\partial X_1} \right)_{i,j}. \quad (2C6)$$

Also, in general space and time variation of  $\mathbf{s}'_{\parallel}$  can be written by the following expression:

$$\frac{\mathbf{s}'_{\parallel i+1,j} + \mathbf{s}'_{\parallel i-1,j} - 2\mathbf{s}'_{\parallel i,j}}{(dX_1)^2} = \left( \frac{\partial^2 \mathbf{s}'_{\parallel}}{\partial X_1^2} \right)_{i,j} \quad (2C7)$$

$$\text{and} \quad \frac{\mathbf{s}'_{\parallel i+1,j} - \mathbf{s}'_{\parallel i-1,j}}{2(dX_1)} = \left( \frac{\partial \mathbf{s}'_{\parallel}}{\partial X_1} \right)_{i,j} \quad (2C8)$$

Using equation (2C2), (2C5), (2C6), (2C7) and (2C8) the finite difference version of equation (2.58) (in the text), can be written as follows:

$$\begin{aligned} \frac{c'_{i,j+1} - c'_{i,j}}{dT} = & \frac{c'_{i+1,j} + c'_{i-1,j} - 2c'_{i,j}}{(dX_1)^2} - Kc'_{i,j}(1 - c'_{i,j}c_0) \frac{\mathbf{s}'_{\parallel i+1,j} + \mathbf{s}'_{\parallel i-1,j} - 2\mathbf{s}'_{\parallel i,j}}{(dX_1)^2} \\ & - K \left( 1 - \frac{2c'_{i,j}c_0\bar{V}_B}{(1 - c_0c'_{i,j})\bar{V}_A + c_0c'_{i,j}\bar{V}_B} \right) \left( \frac{c'_{i+1,j} - c'_{i-1,j}}{2(dX_1)} \right) \left( \frac{\mathbf{s}'_{\parallel i+1,j} + \mathbf{s}'_{\parallel i-1,j}}{2(dX_1)} \right) + \\ & \frac{2(\bar{V}_A - \bar{V}_B)c_0}{(1 - c_0c'_{i,j})\bar{V}_A + c_0c'_{i,j}\bar{V}_B} \left( \frac{c'_{i+1,j} - c'_{i-1,j}}{2(dX_1)} \right)^2 + \frac{P_{i,j}}{\tilde{D}'_{i,j}} \frac{1}{4(dX_1)^2} (c'_{i+1,j} - c'_{i-1,j}) \times \\ & \{ c'_{i+1,j} - c'_{i-1,j} - Kc'_{i,j}(1 - c_0c'_{i,j})(\mathbf{s}'_{\parallel i+1,j} + \mathbf{s}'_{\parallel i-1,j}) \} \end{aligned} \quad (2C9)$$

where,  $P_{i,j} = \frac{\partial \tilde{D}'_{i,j}}{\partial c'_{i,j}}$  which is equation (2.66) in the text. Then using equation (2.66) of the

text, and after rearranging the equation (2C9), the following expression can be written:

$$\begin{aligned} c'_{i,j+1} = & c'_{i,j} + r(c'_{i+1,j} + c'_{i-1,j} - 2c'_{i,j}) - \\ & rKc'_{i,j}(1 - c'_{i,j}c_0)(\mathbf{s}'_{\parallel i+1,j} + \mathbf{s}'_{\parallel i-1,j} - 2\mathbf{s}'_{\parallel i,j}) \\ & - \frac{rK}{4} \left( 1 - \frac{2c'_{i,j}c_0\bar{V}_B}{(1 - c_0c'_{i,j})\bar{V}_A + c_0c'_{i,j}\bar{V}_B} \right) (c'_{i+1,j} - c'_{i-1,j})(\mathbf{s}'_{\parallel i+1,j} - \mathbf{s}'_{\parallel i-1,j}) + \\ & \frac{2(\bar{V}_A - \bar{V}_B)c_0}{(1 - c_0c'_{i,j})\bar{V}_A + c_0c'_{i,j}\bar{V}_B} \frac{r}{4} (c'_{i+1,j} - c'_{i-1,j})^2 + \frac{P_{i,j}}{\tilde{D}'_{i,j}} \frac{r}{4} (c'_{i+1,j} - c'_{i-1,j}) \times \\ & \{ c'_{i+1,j} - c'_{i-1,j} - Kc'_{i,j}(1 - c_0c'_{i,j})(\mathbf{s}'_{\parallel i+1,j} + \mathbf{s}'_{\parallel i-1,j}) \} \end{aligned} \quad (2C10)$$

Which is exactly equation (2.65) in the text.

## Appendix 2D

### Finite difference version of the boundary conditions

To determine the finite difference formulation of the boundary conditions (Zero diffusion flux at  $X_1=0$  or  $i=1$  and  $X_1=1$  or  $i=NMAX$ ) the following finite difference formulations of equations (2.59) and (2.60) (see the text) at  $i=1$  and  $i=NMAX$  respectively have been performed which are as follows:

$$c'_{2,j} - c'_{0,j} = K c'_{1,j} (1 - c_0 c'_{1,j}) (s'_{\parallel 2,j} - s'_{\parallel 0,j}) \quad (2D1)$$

$$c'_{NMAX+1,j} - c'_{NMAX-1,j} = K c'_{NMAX,j} (1 - c_0 c'_{NMAX,j}) \times (s'_{\parallel NMAX+1,j} - s'_{\parallel NMAX-1,j}) \quad (2D2)$$

Please note that in course of this, equations (2C6) and (2C8) (from Appendix 2C) have been used. Now, neglecting the concentration dependence of the diffusion coefficient equation (2.65) (in the text) can be written at  $i=1$  and at  $i=NMAX$  as follows:

At  $i=1$ ,

$$\begin{aligned} c'_{1,j+1} = & c'_{1,j} + r (c'_{2,j} + c'_{0,j} - 2c'_{1,j}) - \\ & r K c'_{1,j} (1 - c'_{1,j} c_0) (s'_{\parallel 2,j} + s'_{\parallel 0,j} - 2s'_{\parallel 1,j}) \\ & - \frac{rK}{4} \left( 1 - \frac{2c'_{1,j} c_0 \bar{V}_B}{(1 - c_0 c'_{1,j}) \bar{V}_A + c_0 c'_{1,j} \bar{V}_B} \right) (c'_{2,j} - c'_{0,j}) (s'_{\parallel 2,j} - s'_{\parallel 0,j}) + \\ & \frac{2(\bar{V}_A - \bar{V}_B) c_0}{(1 - c_0 c'_{1,j}) \bar{V}_A + c_0 c'_{1,j} \bar{V}_B} \frac{r}{4} (c'_{2,j} - c'_{0,j})^2 \end{aligned} \quad (2D3)$$

and at  $i=NMAX$ ,

$$\begin{aligned} c'_{NMAX,j+1} = & c'_{NMAX,j} + r (c'_{NMAX+1,j} + c'_{NMAX-1,j} - 2c'_{NMAX,j}) - \\ & r K c'_{NMAX,j} (1 - c'_{NMAX,j} c_0) (s'_{\parallel NMAX+1,j} + s'_{\parallel NMAX-1,j} - 2s'_{\parallel NMAX,j}) \\ & - \frac{rK}{4} \left( 1 - \frac{2c'_{NMAX,j} c_0 \bar{V}_B}{(1 - c_0 c'_{NMAX,j}) \bar{V}_A + c_0 c'_{NMAX,j} \bar{V}_B} \right) (c'_{NMAX+1,j} - c'_{NMAX-1,j}) \times \\ & (s'_{\parallel NMAX+1,j} - s'_{\parallel NMAX-1,j}) + \\ & \frac{2(\bar{V}_A - \bar{V}_B) c_0}{(1 - c_0 c'_{NMAX,j}) \bar{V}_A + c_0 c'_{NMAX,j} \bar{V}_B} \frac{r}{4} (c'_{NMAX+1,j} - c'_{NMAX-1,j})^2 \end{aligned} \quad (2D4)$$

## 2. Interaction of stress and diffusion in a binary substitutional solid solution

---

$c'_{0,j}$  can be eliminated from equation (2D3) using equation (2D1) and using equation (2.70) of the text whereas  $c'_{NMAX+1,j}$  can be eliminated from equation (2D4) using equation (2D2) and using equation (2.71) of the text. After eliminating these two terms and simplifying, the two boundary conditions can be written as follows:

At  $i=1$ ,

$$c'_{1,j+1} = c'_{1,j} + 2r(c'_{2,j} - c'_{1,j}) - rKc'_{1,j}(1 - c'_{1,j}c_0)(s'_{\parallel 2,j} - s'_{\parallel 1,j}) \times \left(2 - \frac{K}{4}(1 - 2c_0c'_{1,j})(s'_{\parallel 2,j} - s'_{\parallel 1,j})\right) \quad (2D5)$$

and at  $i=NMAX$ ,

$$c'_{NMAX,j+1} = c'_{NMAX,j} + 2r(c'_{NMAX-1,j} - c'_{NMAX,j}) + rKc'_{NMAX,j}(1 - c'_{NMAX,j}c_0)(s'_{\parallel NMAX,j} - s'_{\parallel NMAX-1,j}) \times \left(2 - \frac{K}{4}(1 - 2c_0c'_{NMAX,j})(s'_{\parallel NMAX,j} - s'_{\parallel NMAX-1,j})\right) \quad (2D6)$$

Equations (2D5) and (2D6) are exactly same as equations (2.68) and (2.69) in the text.

### **3. Mechanisms of interdiffusion in Pd-Cu thin film diffusion couples**

J. Chakraborty, U. Welzel and E.J. Mittemeijer

#### **Abstract**

Interdiffusion in thin polycrystalline Pd-Cu bilayers (thickness of each sublayer 50nm) has been studied in the temperature range 175°C-250°C by sputter-depth profiling in combination with Auger electron spectroscopy. X-ray diffraction and transmission electron microscopy investigations reveal that the layers are polycrystalline, consisting of columnar grains separated by grain boundaries oriented more or less perpendicular to the film surface. It has been found that considerable diffusional intermixing occurs in the studied temperature range, which is accompanied by the sequential formation of (ordered) phases Cu<sub>3</sub>Pd and CuPd.

Theoretical backgrounds of different models for the determination of diffusion coefficients have been summarised and their limitations have been discussed.

Volume interdiffusion coefficients have been determined using the so-called 'Centre gradient' and 'Plateau rise' methods. Grain boundary diffusion coefficients of Pd through Cu have been determined by the Whipple-Le Claire method.

Both volume and grain boundary diffusion coefficients are found to decrease roughly exponentially with annealing time. Activation energies for volume and grain boundary diffusion have been determined; the activation energies increase slightly upon annealing.

Defect annihilation upon continued annealing and the formation of new phases have been proposed as potential causes for the observed decrease in diffusion coefficients and corresponding increase in activation energies.

#### 3.1. Introduction

Interdiffusion plays an important role in thin film structures where diffusion is much faster than in the bulk due to high concentrations of crystalline defects and grain boundaries [Balluffi and Blakely (1975)].

Cu is often preferred over Al for metallization in microelectronics due to its higher conductivity and higher resistance to electromigration [Ohring, (2002)]. However, Cu has poor adhesion to many dielectrics and higher tendency to react with adjacent metals or silicon substrates via interdiffusion [Li *et al.* (1992)]. Noble metals like Pd or Pt can act as diffusion barriers in microelectronic circuits [Pretorius (1984)]. Apart from these structures consisting of Pd and Cu thin films have also been established as materials for catalytic applications [Sinfelt (1983)].

In recent years, interdiffusion in bi- and multilayer structures has been studied by Auger electron spectroscopy (AES) extensively [Bukaluk (1999) and (2001), Jeon *et al.* (1994)]. Nevertheless, systematic investigations of interdiffusion processes, taking into account also microstructural changes occurring upon annealing, as for example the formation of new phases, still are lacking.

In the present work interdiffusion in thin Pd-Cu bilayer specimens (thickness of each sublayer 50nm) has been studied by AES in combination with ion sputter profiling in the annealing temperature range 175°C-250°C. Volume and grain boundary diffusion coefficients have been determined by using various models described rigorously in the theoretical section of this paper. Advantages and drawbacks of different models have been highlighted with respect to the determined values of diffusion coefficients and activation energies.

Both the as-deposited and annealed specimens have been investigated by transmission electron microscopy (TEM) and X-ray diffraction (XRD).

## 3.2. Theory

In the following, the theoretical background for the determination of both volume and grain boundary diffusion coefficients in binary diffusion couples from laterally averaged concentration-depth profiles will be outlined. For such analyses presented in the following, idealized microstructures of the specimens are assumed: (i) the microstructure of the layers consists of columnar grains separated by equally spaced, parallel grain boundaries oriented perpendicular to the film surface/interface, (ii) only two constant diffusion coefficients (i.e. the diffusion coefficients are time and position-independent), a volume and a grain-boundary diffusion coefficient, occur, (iii) the diffusion fluxes from adjacent grain boundaries into the grain interior do not interact and (iv) the couple is double semi-infinite.

### 3.2.1. Centre gradient (CG) method

Hall and Morabito [Hall and Morabito (1976)] developed a formalism for extracting the volume interdiffusion coefficient  $\tilde{D}$  from the slope of the concentration profile (as measured, for example, by Auger electron spectroscopy (AES)) in the proximity of the initial interface. If the concentration changes arising from grain boundary diffusion are negligible near the interface and if the above mentioned assumptions (ii) (with respect to the volume diffusion coefficient) and (iv) hold, the concentration profiles have complementary error function dependence near the interface:

$$c(y, t) = 0.5 \left( \operatorname{erfc} \left( \frac{y}{2\sqrt{\tilde{D}t}} \right) \right) \quad (3.1)$$

where  $y$  is the distance from the initial interface and  $t$  is the annealing time. If these assumptions are fulfilled can be checked by plotting the measured concentration profiles of the annealed specimens on a linear probability scale; this should result in a linear plot close to the initial interface (cf. Section 3.4.3).

The concentration-depth profile of the as-deposited specimen obtained by AES sputter-depth profiling is not sharp. The broadening can be due to the roughness of the interface, interdiffusion in the as-deposited state and instrumental effects [Hofmann, (1992) and (1994)]. The concentration profile after annealing has to be considered as the convolution of

### 3. Mechanisms of interdiffusion in Pd-Cu thin film diffusion couples

---

a concentration profile due to diffusion with a resolution function defined by the concentration profile obtained for the unannealed specimen.

If both the measured concentration profiles before and after annealing obey equation (3.1) near the interface, the interdiffusion coefficient can be determined from the following formula [Lo and Schuele (1975); Hall and Morabito (1976)]:

$$\tilde{D} = \left[ \left( \frac{G_0}{G_t} \right)^2 - 1 \right] (4pG_0^2t)^{-1} \quad (3.2)$$

where,  $G_0$  and  $G_t$  are the concentration gradients at the interfaces in the as-deposited and annealed concentration profiles respectively. Concentration gradient at the interface can be determined from the linear region of the probability plot of the concentration profile. The presence of  $G_0$  in equation (3.2) corrects for the broadening of the as-deposited concentration profiles.

#### 3.2.2. Plateau rise (PR) method

The volume interdiffusion coefficient  $\tilde{D}$  can also be determined using another formalism developed by Hall et.al. [ Hall et.al. 1976 ]. This approach is based on Whipple's theory [Whipple (1954)] of coupled grain boundary diffusion ( $D'$  is the grain boundary (GB) diffusion coefficient) and sideways lattice diffusion in a semi-infinite medium. All above mentioned assumptions have to be valid. Additionally, it is assumed that the grains have the dimensions  $L \times L$  in the plane of the film and infinitely fast diffusion of solute through grain boundaries ( $D' \gg \tilde{D}$ ) occurs.

Under these assumptions, the laterally averaged concentration  $\bar{C}$  of diffusant in the plane of the film is:

$$\frac{\bar{C}}{C_0} = \frac{8\sqrt{\tilde{D}t}}{L\sqrt{p}} + \left( 1 - \frac{8\sqrt{\tilde{D}t}}{L\sqrt{p}} \right) \operatorname{erfc} \left( \frac{y}{2\sqrt{\tilde{D}t}} \right) \quad (3.3)$$

$C_0$  is the time independent concentration at  $y=0$ , where  $y$  is the distance from the interface. It has to be remarked that assumption (iii) above can be made explicit as:  $L \gg 4\sqrt{\tilde{D}t}$ .

### 3. Mechanisms of interdiffusion in Pd-Cu thin film diffusion couples

---

The concentration profile consists of two so-called plateau regions far from the interface in which the concentration  $\bar{C}$  is independent of  $y$  and increases proportional to  $\sqrt{t}$  in a region close to the initial interface, where the broadening of the concentration profile is due to volume diffusion across the initial interface and sideways volume diffusion from the grain boundary.

The volume diffusion coefficient  $\tilde{D}$  can be determined from the concentration in the plateau region, where  $\bar{C}$  is independent of  $y$ . For the plateau with  $y > 0$ , it holds that

$$\tilde{D} = \frac{pL^2}{64t} \left( \frac{\bar{C}}{C_0} \right)^2. \quad (3.4)$$

Thus, in principle, one annealing time suffices. However, in view of error minimization, usually the ‘rise’ of the plateau concentration is followed as a function of annealing time and  $\tilde{D}$  is then determined from the slope of a plot of  $\bar{C}$  versus  $\sqrt{t}$ . It has to be remarked that this approach is problematic should the diffusion coefficient vary as a function of time.

#### 3.2.3. Determination of grain boundary (gb) diffusion coefficient ( $D'$ ): Whipple-Le-Claire method

If the grain-boundary diffusion coefficient  $D'$  is finite (and not infinite, as assumed for the PR method), a small (non-constant) slope prevails in the plateau region. From the concentration variation in the plateau region,  $D'$  can be determined using the Whipple-Le-Claire equation [Whipple (1954) and Le Claire (1963)]:

$$D'sd_{gb} = 0.66 \left[ -\frac{\partial \ln \bar{C}}{\partial y^{\frac{6}{5}}} \right]^{\frac{5}{3}} \left( \frac{4\tilde{D}}{t} \right)^{0.5}, \quad (3.5)$$

where,  $d_{GB}$  is the effective grain boundary width and  $s$  is the solute segregation factor (assumed to be 1 in the present case). Equation (3.5) has been derived under the above idealized assumptions (i) to (iv). For the determination of  $D'$  the knowledge of  $\tilde{D}$  is a prerequisite.



## 3.3. Experimental

### 3.3.1. Deposition of thin Pd-Cu diffusion couples

Polycrystalline thin film Pd-Cu diffusion couples were deposited onto Si/SiO<sub>2</sub>/Si<sub>3</sub>N<sub>4</sub> substrates in a dc magnetron sputtering chamber evacuated to a base pressure of  $1 \times 10^{-10}$  mbar. The Cu and Pd layers each had a thickness 50nm. The Pd layer was chosen as the top layer due to superior mechanical and chemical stability as compared to Cu. Commercially available single crystalline silicon (100) wafers of thickness 500 $\mu$ m with amorphous silicon oxide (50nm thickness) and amorphous silicon nitride (50nm thickness) layers on it were used as substrate materials. Prior to deposition, the substrates were sputter cleaned for 1 minute with Ar<sup>+</sup> ions accelerated with -100V. During film deposition, the sample holder was rotated at 12 rpm and the chamber pressure was maintained at  $2 \times 10^{-4}$  mbar using Argon gas for producing a plasma. A magnetron power of 200W for the deposition of the Cu layer and 100W for the deposition of the Pd layer has been used. The substrate temperature increased slightly during the deposition due to the atomic bombardment. The maximum temperature, however, did not exceed 40°C.

### 3.3.2. Annealing of Pd-Cu diffusion couples

Annealing of Pd-Cu diffusion couples was performed in an oil bath at 175°C, 200°C, 225°C and 250°C annealing temperatures for various durations (0.5 hours to 10 hours). To this end, the specimens were encapsulated in quartz ampoules initially evacuated to a pressure of  $1 \times 10^{-6}$  mbar and subsequently filled with Ar gas at a pressure of 300 mbar in order to avoid oxidation.

### 3.3.3. Characterisation of Pd-Cu bilayers before and after diffusion annealing

#### 3.3.3.1. Concentration-depth profiling

Concentration-depth profiles have been measured employing ion sputter profiling combined with Auger Electron spectroscopy (AES) in a JEOL JAMP 7830F field emission Auger microprobe. Argon ions of energy 1keV was used for sputter-depth profiling and a primary electron beam with energy 10keV was used for AES. These sputter conditions resulted in the

### 3. Mechanisms of interdiffusion in Pd-Cu thin film diffusion couples

---

best compromise of depth resolution and sputter time for the samples under investigation. Auger lines of Cu (LMM, 920eV) and Pd (MNN, 330eV) were monitored for the determination of the Cu and Pd concentrations. The concentrations of Cu and Pd atoms were calculated using the following relationships [Grant (1989), Bukaluk, (1983)]:

$$C_i = \frac{\frac{I_i}{S_i}}{\sum_{j=1}^n \frac{I_j}{S_j}} \quad (3.6)$$

Where  $C_i$  is the concentrations of  $i$ th element (Cu, Pd etc.).  $S_i$  is the ( $S_{Cu}=0.574$  and  $S_{Pd}=0.923$ ) relative Auger yield of  $i$ th element (Cu, Pd etc.) with respect to pure copper [JEOL JAMP 7830F database].  $I_i$  is the measured Auger peak-to-peak heights (APPH) of corresponding Auger line of  $i$ th element (Cu, Pd etc.). If  $n$  is the total number of elements, then  $j$  runs over all the elements.

The ratio of the sputter rates for pure elements (Pd and Cu) determined from the sputter-depth profiles of unannealed (as-deposited) specimens is 0.96. Sputter time can be converted into sputter depth if the sputter rate is known. However, the sputter rate can change with changing composition in a binary system when inter-diffusion takes place. In order to evaluate the sputter rate of the Pd-Cu binary system a simple kinetic sputter model originally developed by Ho *et. al* [Ho P. S, J.E. Lewis, L.K. Howard 1977] has been applied. In order to avoid errors related to possible changes of the sputter rate for different specimens, the sputter rate was re-calibrated individually for each specimen. Two approaches were followed for this calibration:

- (i) All theories for extracting diffusion coefficients from measured concentration-depth profiles discussed in Section 3.2 presume that a concentration of 50 at.% prevails at the initial interface. For the determination of diffusion coefficients, the sputter rate was adjusted such that the point of 50 at.% Pd (or Cu) concentration occurred at a sputter-depth of 500Å.
- (ii) Within the temperature range investigated, the  $Si_3N_4$  layer on the substrate can be considered as a diffusion barrier. A calibration of the sputter rate thus can also be achieved by adjusting the sputter rate such that the point of 50 at.% Cu concentration at the interface to the  $Si_3N_4$  layer of the substrate occurred at a sputter-depth of 1000Å.

Generally, the sputter rates obtained by these two approaches are not exactly equal. This will be discussed in Sections 3.4.

#### 3.3.3.2. Phase analysis by X-ray diffraction (XRD)

Both unannealed and annealed bilayer specimens have been characterised by X-ray diffraction to check the formation of ordered phases in the Pd-Cu system, which are predicted by the equilibrium phase diagram [Subramanian and Laughlin, Binary Alloy Phase Diagram, 1990,]. The phase analysis has been carried out using Cu K $\alpha$  radiation in a Philips X'Pert MRD diffractometer equipped with an Eulerian cradle and parallel beam optics and also using Cu K $\alpha_1$  radiation in a Philips X'Pert MPD diffractometer in Bragg-Brentano geometry with a position sensitive detector (Panalytical X'Pert Accelerator) in the secondary side.

#### 3.3.3.3. Microstructure

Both as-deposited and annealed specimens have been investigated in a JEOL FX 2000 transmission electron microscope (TEM). For the preparation of cross-sectional specimens, two pieces have been cut from the bilayer/substrate specimen and have been sandwiched (bilayer films faces each other from both pieces) with epoxy glue. The sandwiches have been embedded into a specially designed cylindrical polycrystalline Al<sub>2</sub>O<sub>3</sub> tube of 3mm diameter as a holder for the cross-sectional sample. Then the tube has been cut into slices of thickness ~350 $\mu$ m. The slices underwent mechanical grinding, dimpling from both sides and finally ion thinning (Ar<sup>+</sup> ions with 3.5 keV energy and 1mA ion current in BAL-TEC RES 010 with liquid nitrogen cooling) for several hours to achieve electron transparency (for details of the sample preparation, see also [Strecker *et al.* (2003)]). Bright field (BF) images have been taken using a 200keV electron beam. The thicknesses of the films have been verified from the cross-sectional TEM micrographs.

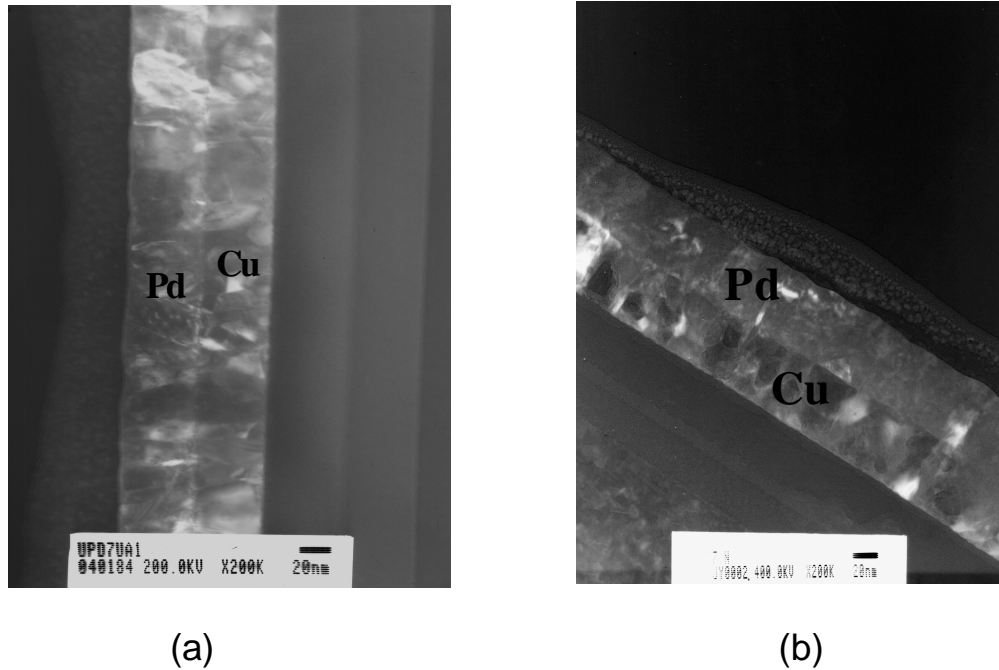


Fig. 3.1: (a) TEM micrograph of an unannealed Pd-Cu bilayer. (b) TEM micrograph of an annealed Pd-Cu bilayer; annealing temperature: 225°C, annealing time: 6 hours.

## 3.4. Results and discussion

### 3.4.1. Microstructure

Microstructures of both as-deposited and annealed specimens (cross-sectional) have been investigated by TEM. Fig. 3.1(a) shows for example, one of the cross-sectional micrographs of an unannealed specimen. It has been found from the inspection of a number of micrographs that a columnar microstructure prevails in both sublayers. However, a more irregular microstructure is also observed in some portions of the Cu sublayer. The interface of the two sublayers is clearly visible. The in-plane grain-sizes fall in the range from 10 nm to 25 nm (average: 22nm) for the Cu sublayer and in the range from 15 nm to 25 nm (average: 21 nm) for the Pd sublayer.

However, upon annealing at 200°C for 6 hours a little increase of the average grain size (about 5 nm to 6 nm) has been noticed and the interface of the two sublayers is still clearly visible (not shown in Figures). Annealing at 225°C, (Fig. 3.1(b)) leads to the formation of

new phase (for details see Section 3.4.7) in the immediate vicinity of the grain boundaries and similar growth of Cu and Pd grains (like 200°C annealing). Nevertheless, the interface is still clearly visible. After annealing at 250°C, neither the columnar microstructure nor the location of the initial interface can be observed. This indicates that extensive interdiffusion has taken place, which is potentially accompanied by the migration of grain boundaries, extensive grain growth and the formation of new phases.

#### 3.4.2. Concentration-depth profiles

Figs. 3.2(a)-(d) show Pd concentration-depth profiles for the unannealed and annealed Pd-Cu bilayer specimens in the temperature range 175°C-250°C for various annealing durations (0.5hours-10hours). Cu concentration-depth profiles can be generated by subtracting the Pd concentration values (atom fraction) at each depth from unity. The sputter rate has been calibrated following approach (i) discussed in Section 3.3.3.1.

The sputter-depth profile of the as-deposited sample does not show a sharp interface. This is due to instrumental effects and the roughness of the interface. Interdiffusion in the as-deposited state can be safely ignored because the temperature during deposition did not exceed 40°C.

At 175°C, only very small changes of the concentration profiles occur upon annealing. A rigorous analysis demonstrates that the concentration gradient at the initial interface decreases slightly and, gradually, a plateau region develops on the Cu-rich side of the couple. At temperatures of 200°C and above, considerable diffusional intermixing occurs. The concentration gradient at the initial interface decreases and the plateau concentration on the Cu-rich side increases considerably. It is, however, remarkable that no Cu plateau develops on the Pd-rich side of the diffusion couple, even at elevated temperatures and long annealing times.

The development of a plateau region is due to the combined occurrence of grain-boundary diffusion and volume diffusion from the grain boundary into the grain interior following the so-called ‘B’ kinetics ( $d_{gb} \ll \sqrt{\tilde{D}t} < L$ ) of Harrison’s classification [Harrison (1961)]. Two

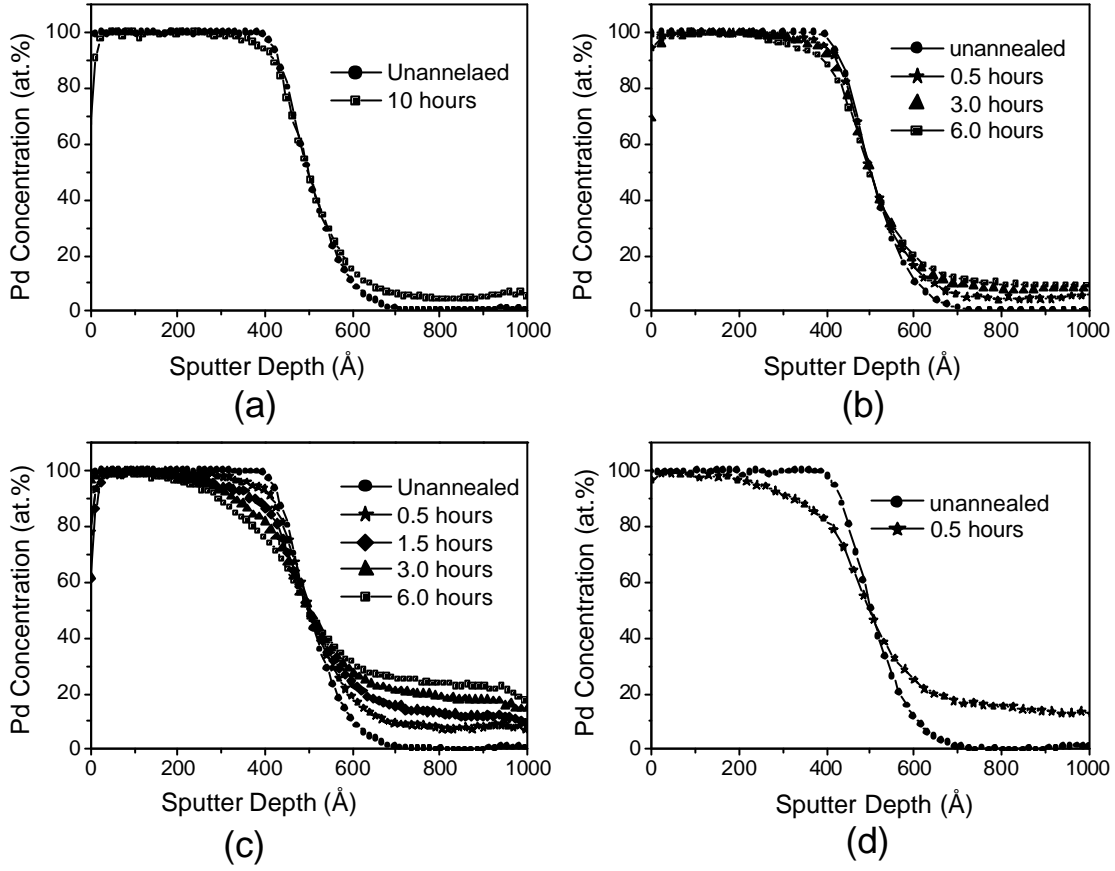


Fig. 3.2: Pd concentration versus sputter depth at different annealing temperatures and annealing times: (a) annealing temperature: 175°C., (b) annealing temperature: 200°C, (c) annealing temperature: 225°C and (d) annealing temperature: 250°C.

potential reasons could exist for the absence of Cu plateau on the Pd-rich side of the couple: (i) only very little grain boundary diffusion of Cu through Pd occurs due to a low grain-boundary density; or (ii) the volume diffusion coefficient on the Pd-side is low. Microstructural investigations indicate similar grain-boundary densities for both the Pd and Cu-sublayers (cf Section 3.4.1). The occurrence of grain-boundary diffusion is also confirmed by the following observation: At all temperatures and annealing times, Cu is present on the specimen surface (see Figs. 3.2(a)-(d) at small sputter-depths). It is remarkable that Cu on the surface also occurs even if the plateau concentration of Cu within the Pd layer is very small. The presence of Cu on the Pd surface after annealing has also been confirmed

### 3. Mechanisms of interdiffusion in Pd-Cu thin film diffusion couples

---

by measuring the Cu concentration accumulated on the Pd surface with annealing time during in-situ annealing of Pd-Cu bilayers at a temperature about 120°C, which is much lower than the lowest annealing temperature of 175°C. Unfortunately large error (as much as  $\pm 20^\circ\text{C}$ ) may be involved in the temperature measurement in ultra high vacuum as the temperature of the specimen holder has been taken as a measure of specimen temperature. This confirms that Cu diffuses through Pd grain boundaries following the so-called ‘C’ kinetics ( $\sqrt{\tilde{D}t} \ll d_{gb}$ ) [Harrison (1961)].

Considering these observations and the similarity of the microstructures of the two sublayers (cf. Section 3.4.1), it has to be concluded that the volume diffusion coefficients in the Pd- and Cu-sides of the couples must differ significantly. This finding is compatible with the experimentally observed concentration dependence of the interdiffusion coefficient  $\tilde{D}$  observed for macroscopic specimens [Thomas and Birchenall (1952)] and the expected concentration dependence, recognizing that the melting point of Pd is considerably higher than the melting point of Cu.

It is obvious from the concentration-depth profiles for annealed specimens shown in Fig. 3.2(c) that an apparent mass gain occurs for Pd (i.e. a corresponding mass loss occurs for Cu; compare, for example, the area under the profiles for the unannealed specimen and the specimen annealed for six hours at 225°C). This result is a consequence of the procedure employed for the calibration of the sputter rate (see Section 3.3.3.1; option (i) was adopted for the sake of the determination of the diffusion coefficient). If, instead of option (i), option (ii) is adopted (cf. Section 3.3.3.1), the depth of the point with a Cu/Pd concentration of 50 at.% shifts upon annealing. This is a consequence of the concentration dependence of the diffusion coefficient.

An example is shown in Fig. 3.3. This approach leads to significant improvement of the mass conservation in the profiles. However, for the analysis of diffusion coefficients presented in the following, the adoption of option (i), though in principle incorrect [see also, for example, Hall et.al, (1976)], is a prerequisite.

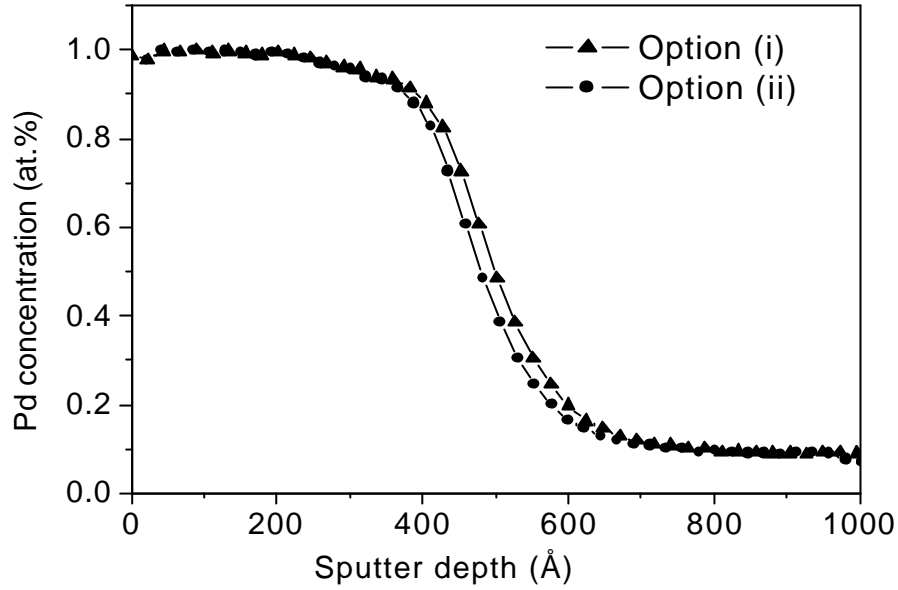


Fig. 3.3: Comparison of the concentration-depth profiles obtained employing different calibration schemes for the determination of the sputter rate: option (i) using the fixed point 50at.% at 500Å (Cu/Pd interface) and option (ii) using the fixed point 1000 Å at Cu/Si<sub>3</sub>N<sub>4</sub> interface. Annealing condition: 200°C, 6 hours.

#### 3.4.3. Determination of diffusion coefficients

##### 3.4.3.1. Centre-gradient (CG) method

The centre-gradient method relies on an error-function shape of the concentration profile near the interface. To verify this condition, the Pd concentrations profiles near the interface can be plotted on a linear probability scale. Such plots are given in Figs. 3.4(a)-(d); at a particular annealing temperature, the concentration-depth profiles show a linear dependence for all annealing times.

Values for  $G_0$  and  $G_t$  have been determined from the slope of the linear regions of the probability plots of unannealed and annealed specimens, respectively. Using these values, volume interdiffusion coefficients ( $\tilde{D}_{CG}$ ) have been calculated employing equation (3.2) and have been summarised in Table 3.1 for all annealing temperatures and times.

Obviously, the diffusion coefficients decrease with increasing annealing time. In Fig. 3.5(a), the interdiffusion coefficients (on a logarithmic scale) have been plotted versus



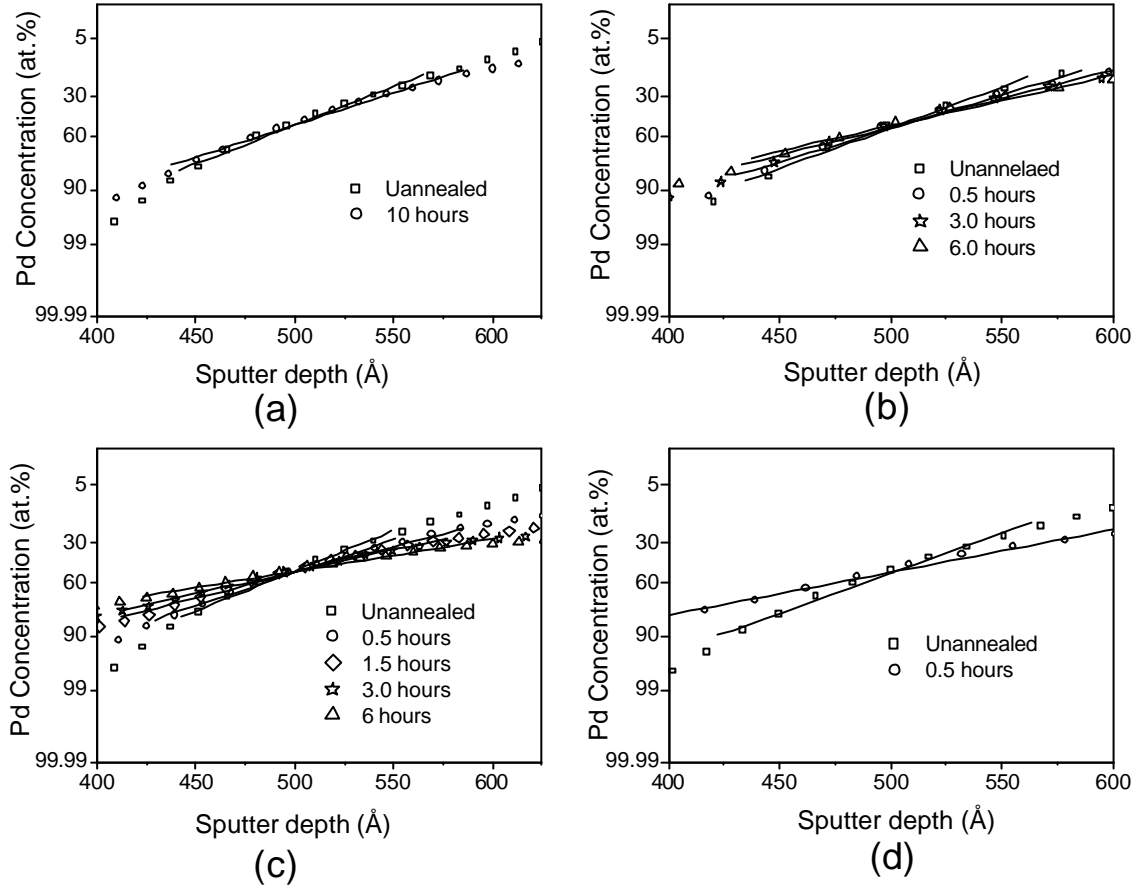


Fig. 3.4: Probability plots for the Pd concentrations of specimens annealed at different temperatures. (a) annealing temperature: 175°C., (b) annealing temperature: 200°C, (c) annealing temperature: 225°C and (d) annealing temperature: 250°C.

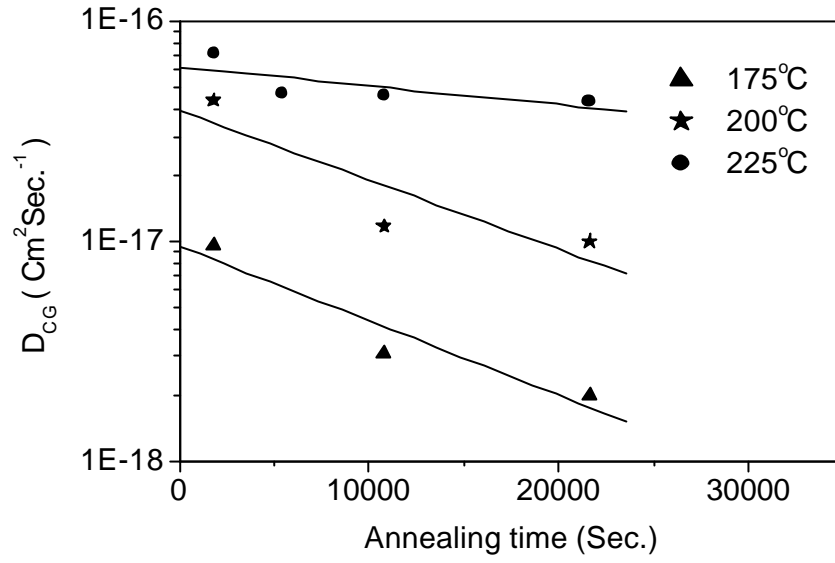
annealing time. It can be seen that the interdiffusion coefficients decrease approximately exponentially with increasing annealing time at a particular annealing temperature (i.e., a linear behaviour occurs in Fig. 3.5(a)). This decrease can be attributed to the annihilation of defects, which accelerate diffusional transport. This is true at least up to annealing temperature of 200°C and 3 hours annealing time. Annealing at 200°C, 6 hours and 225°C, formation of ordered phases have been detected which may complicate the diffusion process and it has been discussed later (see Section 3.4.7). Also, at 225°C, diffusion coefficient is a

### 3. Mechanisms of interdiffusion in Pd-Cu thin film diffusion couples

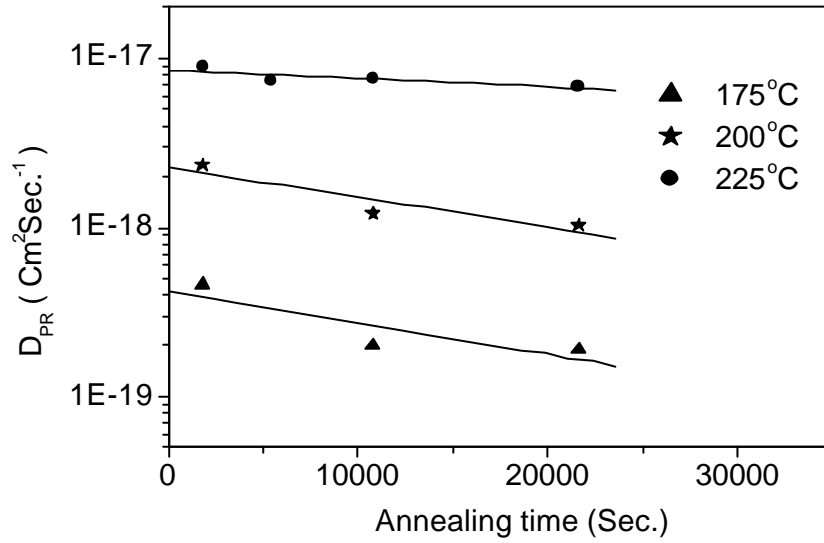
Table 3.1: Interdiffusion coefficients  $\tilde{D}$  obtained using the CG and PR methods. For details, see text.

Annealing temperature (°C)	Annealing time (hours)	$\tilde{D}$ by CG method (cm <sup>2</sup> Sec. <sup>-1</sup> )	$\tilde{D}$ by PR method (cm <sup>2</sup> Sec. <sup>-1</sup> )	Ratio $\tilde{D}_{CG} / \tilde{D}_{PR}$	$\tilde{D}$ from rise of plateau concentration (cm <sup>2</sup> Sec. <sup>-1</sup> )
175	0.5	$9.6 \times 10^{-18}$	$4.54 \times 10^{-19}$	21	$1.6 \times 10^{-19}$
175	3	$3.1 \times 10^{-18}$	$2 \times 10^{-19}$	15.5	
175	6	$2.0 \times 10^{-18}$	$1.9 \times 10^{-19}$	10.6	
175	10	$1.45 \times 10^{-18}$	$1.25 \times 10^{-19}$	11.5	
200	0.5	$4.37 \times 10^{-17}$	$2.35 \times 10^{-18}$	18.6	$1.1 \times 10^{-18}$
200	3	$1.16 \times 10^{-17}$	$1.2 \times 10^{-18}$	9.7	
200	6	$1.0 \times 10^{-17}$	$1.03 \times 10^{-18}$	9.7	
225	0.5	$7.14 \times 10^{-17}$	$8.9 \times 10^{-18}$	8	$7.15 \times 10^{-18}$
225	1.5	$4.75 \times 10^{-17}$	$7.4 \times 10^{-18}$	6.4	
225	3	$4.58 \times 10^{-17}$	$7.6 \times 10^{-18}$	6	
225	6	$4.34 \times 10^{-17}$	$6.7 \times 10^{-18}$	6.4	
250	0.5	$3 \times 10^{-16}$	$2.9 \times 10^{-17}$	10.4	

weak function of annealing time (Fig. 3.5). For a comparison of these results with literature data, see Section 3.4.6. For remarks concerning the time dependence found in this work, see also Section 3.4.7.



(a)



(b)

Fig. 3.5: Volume interdiffusion coefficients determined by CG method (Fig.3.5 (a)) and PR method (Fig. 3.5(b)) have been plotted as a function of annealing time ( $t$ ) at all annealing temperatures. The diffusion coefficients decrease approximately exponentially with  $t$ .

#### 3.4.3.2. Plateau-rise (PR) method

Volume interdiffusion coefficients have also been determined from the plateau rise method (cf. Section 3.2.2). To this end, the plateau concentrations have been estimated at a sputter depth of 850Å on the Cu-rich side of the couple. Fig. 3.6 shows the plateau concentrations of Pd as a function of annealing time in logarithmic scale. Straight lines with fixed slopes of 0.5 have been fitted to the data points at all annealing temperatures. A reasonably good, though not perfect, fit has been obtained. In particular at 175°C annealing temperature, deviations from a straight line occur. These deviations are largely due to statistical uncertainties in the low plateau concentration values.

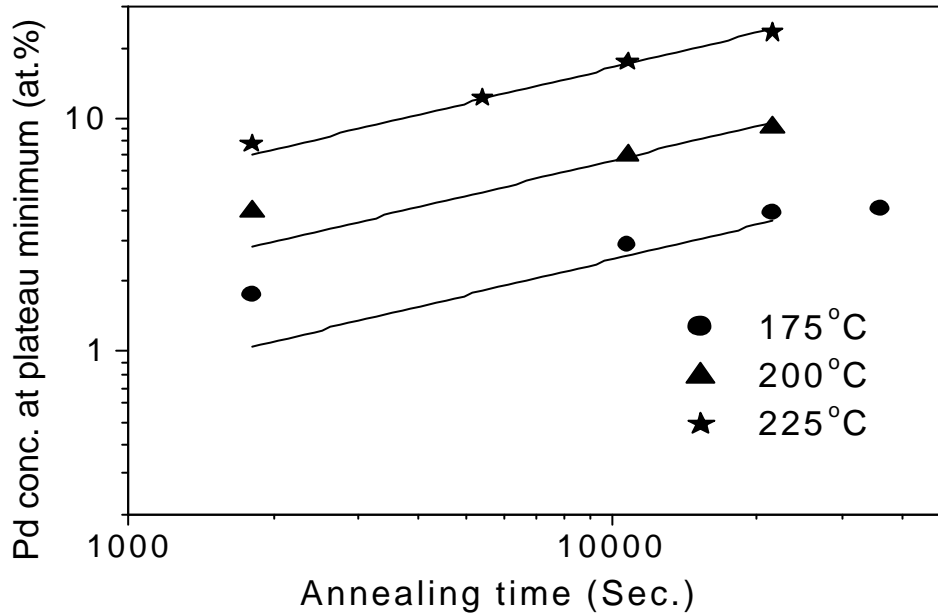


Fig. 3.6: Plateau concentrations (at  $y = 350 \text{ \AA}$ ) versus annealing time at all annealing temperatures. Straight lines fitting at all temperatures show approximate  $\sqrt{t}$  variation of plateau concentrations.

This approach presumes that the diffusion coefficient does not change with time, as concentrations corresponding to different annealing times are used simultaneously in the analysis. Employing equation (3.4) diffusion coefficients can also be determined individually for each annealing time. The results of this approach have been summarised in Table 3.1

### 3. Mechanisms of interdiffusion in Pd-Cu thin film diffusion couples

---

together with the corresponding diffusion coefficients determined from Fig. 3.6 (based on the rise of the plateau with time). To this end, an in-plane average grain size of Cu ( $L$ ) in the as-deposited specimen has been determined as 22nm from TEM (cf. Section 3.4.1).  $C_0$  is not known, but it will certainly be higher than 20 at.% up to which a reasonably good  $t^{\frac{1}{2}}$  dependence is followed (Fig. 3.6). It must also be less than 50 at.% which would correspond to a complete homogenization. In this work,  $C_0$  has been taken as 30 at.%, as suggested by Hall *et al.* (1976).

It is obvious that a decrease of the individually determined diffusion coefficient occurs. Thus, deviations from straight lines in Fig. 3.6 are also due to the time dependence of the diffusion coefficient.

Fig. 3.5(b) shows that the diffusion coefficients obtained by this approach decrease roughly exponentially with increasing annealing time which is similar to the results obtained by using CG method (see above discussion).

#### 3.4.3.3. Whipple-Le Claire method

Fig. 3.7(a)-(d) show so-called Whipple-plots, i.e. plots of  $\ln \bar{C}$  versus  $y^{\frac{6}{5}}$ , for the specimens annealed at different temperatures for different annealing times, respectively. These plots show two distinct regions: The first region, extending up to about 200Å from the interface is dominated by volume diffusion (through Cu grains). Beyond this point, the second region is due to grain boundary diffusion. Grain boundary diffusion coefficients ( $D'$ ) of Pd in Cu grain boundaries can be determined from the slope of this second region in the Whipple plots using equation (3.5) as described in section 3.2.3.  $d_{gb}$  has been taken as 5 Å and both time dependent volume diffusion coefficients  $\tilde{D}_{CG}$  and  $\tilde{D}_{PR}$  have been used to obtain corresponding grain boundary diffusion coefficients. The obtained GB diffusion coefficients have been summarized in Table 3.2.

At low annealing temperature (175°C and 200°C), both significant curvature and a concentration minimum occur in the second region, resulting from an increase of the concentration close to the interface to the substrate. This introduces a considerable

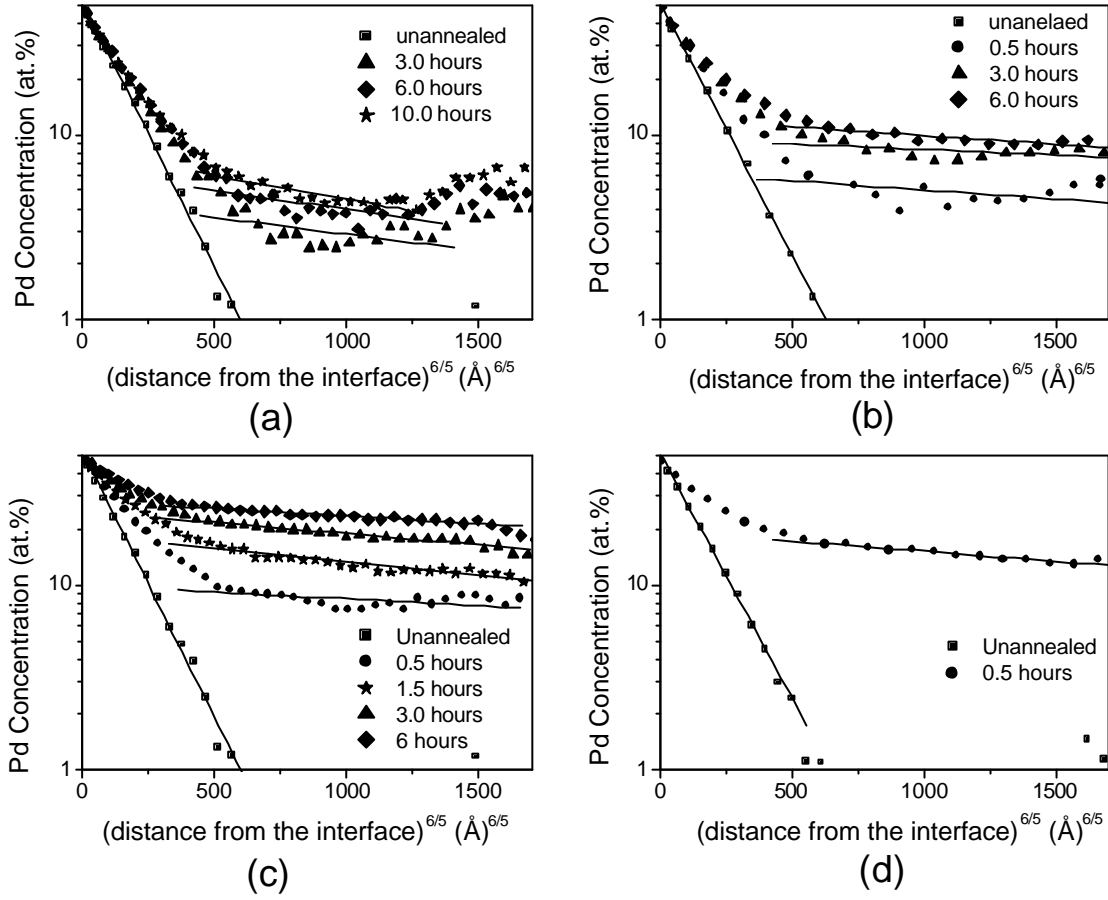


Fig. 3.7: Whipple-Le-Claire plots for different annealing temperatures. (a) annealing temperature: 175°C, (b) annealing temperature: 200°C, (c) annealing temperature: 225°C and (d) Annealing temperature: 250°C.

uncertainty in the determination of the diffusion coefficients from the slope, because the region for fitting a straight line is poorly defined.

The increase of the concentration close the interface to the substrate can also be seen in Figs. 3.2(a) and 3.2(b) and results from the rapid diffusion along the grain boundary and a spreading of the concentration along the interface close to the substrate. Of course, the seeming occurrence of 'up-hill' diffusion is a consequence of the lateral concentration averaging in the AES measurement. The violation of assumption (iv) (see Section 3.2; double-semi-infinite couple) leads to a reservoir for back-diffusion into the grain interior

### 3. Mechanisms of interdiffusion in Pd-Cu thin film diffusion couples

---

Table 3.2: Grain boundary diffusion coefficients  $D'$  obtained by the Whipple-Le Claire method as a function of annealing time and temperature.

Annealing temperature (°C)	Annealing time (hours)	GB diffusion coefficient using $\tilde{D}_{CG}$ cm <sup>2</sup> Sec. <sup>-1</sup>	GB diffusion coefficient using $\tilde{D}_{PR}$ cm <sup>2</sup> Sec. <sup>-1</sup>
175	0.5	$7.1 \times 10^{-14}$	$1.54 \times 10^{-14}$
175	3	$1.95 \times 10^{-14}$	$4.96 \times 10^{-15}$
175	6	$1.35 \times 10^{-14}$	$4.15 \times 10^{-15}$
175	10	$9.4 \times 10^{-15}$	$2.76 \times 10^{-15}$
200	0.5	$2.17 \times 10^{-13}$	$5.03 \times 10^{-14}$
200	3	$1.34 \times 10^{-13}$	$4.31 \times 10^{-14}$
200	6	$1.21 \times 10^{-13}$	$3.88 \times 10^{-14}$
225	0.5	$4.1 \times 10^{-13}$	$1.45 \times 10^{-13}$
225	1.5	$2.12 \times 10^{-13}$	$8.35 \times 10^{-14}$
225	3	$1.72 \times 10^{-13}$	$6.99 \times 10^{-14}$
225	6	$2.12 \times 10^{-13}$	$8.37 \times 10^{-14}$
250	0.5	$7.06 \times 10^{-13}$	$2.19 \times 10^{-13}$

from the interface to the substrate and introduces errors in both the volume (PR method) and GB diffusion coefficients.

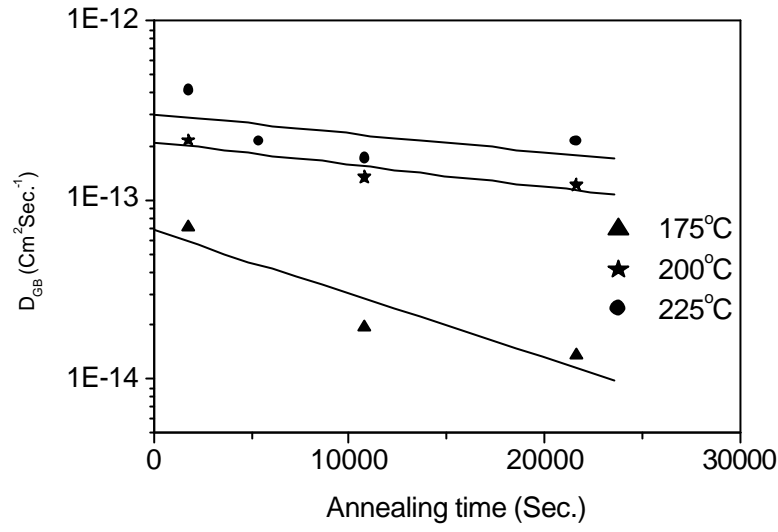
However, it is interesting to note that the concentration 'hump' at the interface to the substrate exists also for the unannealed specimen (see, e.g., Fig. 3.2). This indicates that already at room temperature, grain boundary and interface diffusion of Pd through Cu has occurred. With increasing annealing temperature, the relative importance/relevance of GB diffusion for diffusional intermixing decreases and the 'hump' gradually vanishes.

For certain limiting cases, Gilmer and Farrell have extended the Whipple treatment: (i) case of finite layer thickness with a diffusion barrier (Gilmer & Farrell, (1976a)); (ii) case of finite layer thickness with zero concentration boundary condition (Gilmer & Farrell, (1976b)) and (iii) case of finite layer thickness with rapid surface/interface diffusion at the terminal surface/interface (Gilmer & Farrell, 1976b).

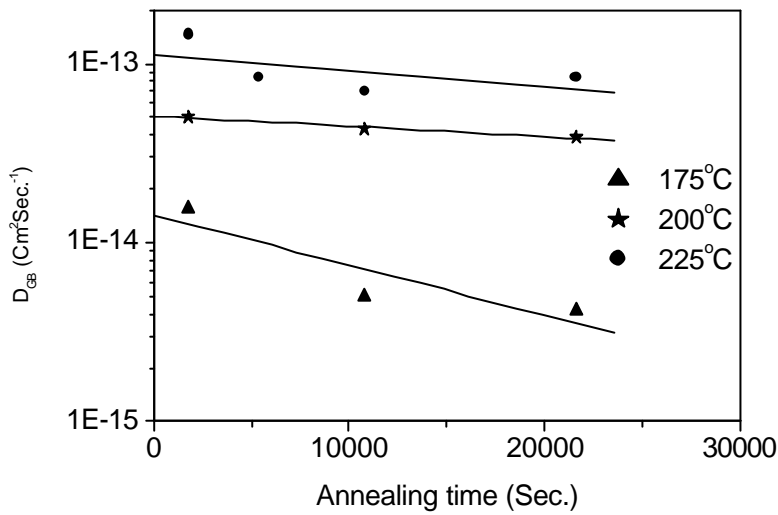
Unfortunately, the investigated specimens do not satisfy any of the above mentioned criteria: interface diffusion occurs, but it is not rapid (the interface concentration takes only small values). Thus, a more correct determination of GB diffusion coefficients is not possible.

Obviously, GB diffusion coefficients calculated from  $\tilde{D}_{CG}$  and  $\tilde{D}_{PR}$  enlisted in Table 3.2 show a decreasing trend with increasing annealing time. In Fig. 3.8, the grain boundary diffusion coefficients calculated using both  $\tilde{D}_{CG}$  and  $\tilde{D}_{PR}$  have been plotted with annealing time. It can be seen that the interdiffusion coefficients decrease roughly exponentially with increasing annealing time at a particular annealing temperature (i.e., a linear behaviour occurs in Figs. 3.8(a) and (b)). Such a decrease can be attributed to the relaxation of the GB structure upon annealing (see, for example, Nazarov, (2003), Ovidko & Reizis, (2001), Gleiter, (1989)) and parallels the decrease of the volume diffusion coefficients (cf. Section 3.4.3.1 and Fig. 3.5) at least up to annealing at 200°C for 3 hours. Beyond this temperature and time annealing leads to the formation of ordered phases which can create further complications (see Section 3.4.7). Also, from Table 3.2, it can be seen that the grain boundary diffusion coefficients obtained using  $\tilde{D}_{CG}$  are three times higher than those obtained using  $\tilde{D}_{PR}$  which is a consequence of the fact that  $\tilde{D}_{CG}$  is higher than  $\tilde{D}_{PR}$  (Table 3.1). For a comparison of these results with literature data, see Section 3.4.6





(a)



(b)

Fig. 3.8: Grain boundary diffusion coefficients ( $D'$ ) determined by Whipple-Le Claire method versus annealing time at all annealing temperatures. (a)  $\tilde{D}_{CG}$  have been used for the determination of  $D'$ . (b)  $\tilde{D}_{PR}$  have been used to determine  $D'$ . Approximate exponential time dependence is shown.

#### 3.4.4. Comparison of $\tilde{D}_{CG}$ , $\tilde{D}_{PR}$ and $D'$

The diffusion coefficients obtained as a function of time with the PR method are in reasonable agreement with the CG results, but there is a general tendency that coefficients determined by the PR method are up to one order of magnitude lower than those determined by the CG method (see Table 3.1). The ratio  $\tilde{D}_{CG}/\tilde{D}_{PR}$  has also been listed in Table 3.1.

It has to be recognized that both formalisms involve highly simplifying assumptions, which may not be satisfied under practical circumstances. In particular, grain boundary diffusion is neglected in the CG method; in the PR method, the assumption  $L \gg 4\sqrt{\tilde{D}t}$  has to be met. Both assumptions are violated in these investigations at higher temperatures for longer annealing times (see Table 3.3). However, it becomes obvious from the ratios listed in Table 3.1 that the differences in the diffusion coefficients decrease with increasing annealing temperature and time. This result makes it less likely that the differences are due to these simplifying assumptions. Rather, physical reasons may lead to these differences. In this context, it has to be remarked that, of course, the diffusion coefficients are determined at different regions within the couple employing the CG and PR methods. Thus, both differences in the microstructure (in particular with respect of defects enhancing diffusion) and the average solute concentration within the diffusion zone (note that the diffusion coefficient may be a strong function of concentration) can affect the so determined diffusion coefficient. Though grain growth during annealing also may complicate the interpretation (see, for example, De Bonte *et.al.* (1975)), the relevance in the present work can be excluded on the basis of the microstructural investigations (cf. Section 3.4.1).

Similar results have also been obtained by other authors for Cu-Pd diffusion couples (Bukaluk, (2001)), Au-Pd diffusion couples (Hall et al., (1976)) and Au-Ag diffusion couple (Bukaluk, (1983)). Hall *et al.* [Hall *et al.* (1976)] have suggested that the smaller diffusion coefficient (and higher activation energy; see Section 3.4.5) in the plateau region as compared to the interface region can be attributed to a larger defect density near the interface. In this context, it is worth noting that the time dependence of  $\tilde{D}_{PR}$  is a weaker function of annealing time than  $\tilde{D}_{CG}$ : if more defects are present in the proximity of the interface, the defect annihilation will have a more pronounced effect on  $\tilde{D}_{CG}$  rather than on  $\tilde{D}_{PR}$ .

### 3. Mechanisms of interdiffusion in Pd-Cu thin film diffusion couples

---

The GB diffusion coefficients (of Pd through Cu GBs) at any particular temperature (obtained using either  $\tilde{D}_{CG}$  or  $\tilde{D}_{PR}$ ) are about  $10^4$  times higher than the corresponding interdiffusion coefficients ( $\tilde{D}_{CG}$  or  $\tilde{D}_{PR}$ ) (cf. Table 3.1 and 3.2).

Table 3.3: Diffusion length  $4\sqrt{\tilde{D}t}$  as function of annealing time and temperature. Note that the condition  $L \gg 4\sqrt{\tilde{D}t}$  should be satisfied, where  $L$  is the in plane average grain size of Cu:  $L = 220 \text{ \AA}$ .

Temperature (°C)	Time (Hours)	$4\sqrt{\tilde{D}t}$ (Å) from CG method	$4\sqrt{\tilde{D}t}$ (Å) from PR method
175	0.5	52.6	11.4
175	3	73.2	18.6
175	6	83	25.5
175	10	91.4	27
200	0.5	112.2	26
200	3	141.6	45.5
200	6	186	60
225	0.5	143.4	50.7
225	1.5	202.5	80
225	3	281	114.3
225	6	387	152.6
250	0.5	294	91

#### 3.4.5. Determination of activation energies

It has been found (see Section 3.4.3.1- 3.4.3.3) that the diffusion coefficients are a function of time for a given temperature. This finding suggests that also a time dependence of the activations energies and pre-exponential factors should be considered. A source of error is thus introduced if diffusion coefficients corresponding to different times (and temperatures) are used simultaneously in an Arrhenius-type of plot.

The following two approaches have been adopted in order to determine activation energies:

(i) Activation energies have been determined at a particular time using diffusion coefficients obtained at various temperatures.

### 3. Mechanisms of interdiffusion in Pd-Cu thin film diffusion couples

(ii) Activation energies have also been determined using diffusion coefficients obtained by extrapolating an exponential time dependence of the diffusion coefficient at a particular temperature to zero annealing time.

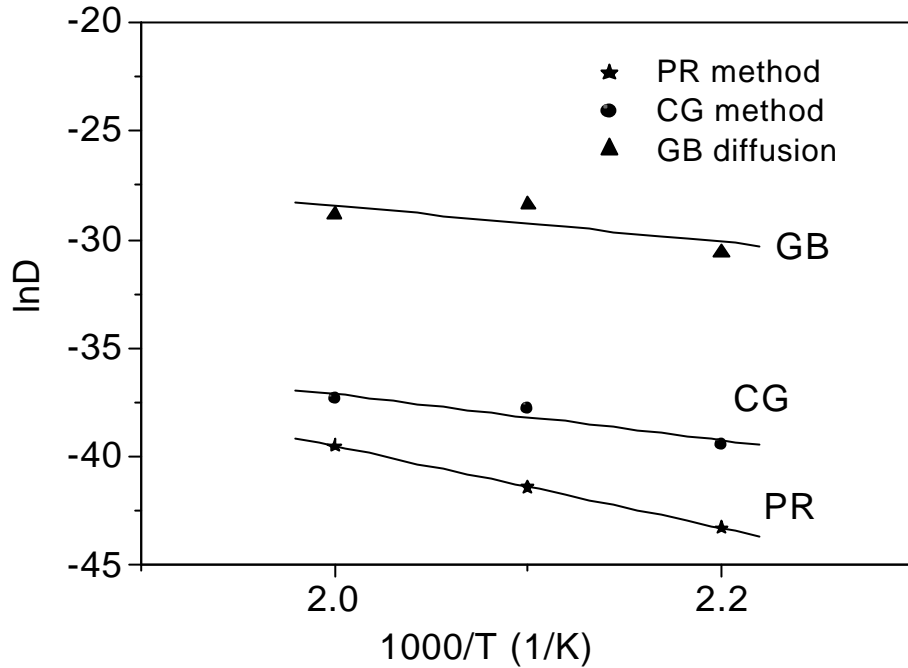


Fig. 3.9: Arrhenius plots for the determination of activation energies for volume and GB diffusion. Interdiffusion coefficients corresponding to zero annealing time (extrapolated values obtained from Fig. 3.5(a) in CG method and Fig. 3.8(a) for GB diffusion) at three annealing temperatures have been used in the Arrhenius plots. For PR method, diffusion coefficients obtained from the ‘rise of plateau concentrations’ at three annealing temperatures (last column in Table 3.1) have been used.

The activation energies obtained employed the different approaches have been gathered in Table 3.4. Arrhenius plots have been shown in Fig.3.9. In case of the PR method, the activation energy for volume diffusion has also been determined from the diffusion coefficients determined from the rise of plateau concentrations (Fig. 3.6 and Table 3.4).

Obviously, the activation energies for both GB and volume diffusion tend to increase upon continued annealing. This increase parallels the decrease of the diffusion coefficients at a

### 3. Mechanisms of interdiffusion in Pd-Cu thin film diffusion couples

particular temperature. For remarks concerning the time dependence found in this work, see Section 3.4.7.

Table 3.4: Activation energies for volume diffusion determined from  $\tilde{D}_{CG}$ ,  $\tilde{D}_{PR}$  and for grain boundary diffusion ( $D'$ ) determined from Whipple-Le Claire method.

Annealing time (hours)	Activation energy (eV) using $\tilde{D}_{CG}$	Activation energy (eV) using $\tilde{D}_{PR}$	Activation energy (eV) using $\tilde{D}$ from the rise of plateau concentration	Activation energy (eV) For GB diffusion ( $D'$ values determined from $\tilde{D}_{CG}$ values)
0	0.91	1.33	1.63	0.73
3	1.05	1.57		0.9
6	1.2	1.54		1.1

#### 3.4.6. Comparison with literature data

Interdiffusion coefficients ( $\tilde{D}$ ) obtained in the present work have been compared with their macroscopic counterparts reported in the literature [Neukam, (1970)]. Table 3.5 shows that the extrapolated macroscopic interdiffusion coefficients (in the annealing temperature range 175°C-250°C) are about seven to nine orders of magnitude smaller than the diffusion coefficients found in this work (cf. Table 3.1). Such findings are not unusual and similar values have been obtained for example in Pd-Cu multilayers by Bukaluk [Bukaluk, (1999)].

Activation energies for interdiffusion determined both using  $\tilde{D}_{CG}$  and  $\tilde{D}_{PR}$  in the present work (Table 3.4) are much less than those reported in the literature for the macroscopic Pd-Cu diffusion couples (Table 3.5) [Neukam, (1970)].

### 3. Mechanisms of interdiffusion in Pd-Cu thin film diffusion couples

---

In case of macroscopic specimens, the activation energy of gb diffusion can be taken as half of that of lattice diffusion (1.16eV). This value is still higher than the activation energy of gb diffusion reported in the present work (see Table 3.4).

Table 3.5: Comparison of the diffusion coefficients obtained in this work with literature data obtained for macroscopic specimens: Activation Energy = 223.89KJ/mole=2.321eV.

Pre-exponential factor:  $0.48 \text{ cm}^2 \text{Sec.}^{-1}$  . [Neukam (1970)]

Temperature (°C)	Diffusion Coefficient ( $\text{cm}^2 \text{Sec}^{-1}$ )	Annealing time (Sec.)	Diffusion length $\sqrt{Dt}$ (cm.)
175	$3.66 \times 10^{-27}$	21600	$8.9 \times 10^{-12}$
200	$8.78 \times 10^{-27}$	21600	$4.4 \times 10^{-11}$
225	$1.53 \times 10^{-24}$	21600	$1.8 \times 10^{-10}$
250	$2.03 \times 10^{-23}$	21600	$6.6 \times 10^{-10}$

#### 3.4.7. Phase formation

A detailed description of the X-ray diffraction phase analysis will be published elsewhere [Chakraborty *et al.* to be communicated]. Here, only the many findings relevant to this work will be summarized. Investigations of unannealed Pd-Cu bilayers revealed that all reflections corresponding to Pd and Cu appear in the diffractograms. A more detailed analysis based on pole figure measurements revealed that both layers are polycrystalline and have a {111} fibre texture. Diffusional intermixing is accompanied by the sequential formation of new phases. First, an ordering of the solid solution leads to the formation of  $\text{Cu}_3\text{Pd}$  at temperatures of 200°C and 225°C. At 250°C, CuPd forms: after a coexistence of CuPd and  $\text{Cu}_3\text{Pd}$  for short annealing times (up to 1.5 hours), CuPd grows at the cost of  $\text{Cu}_3\text{Pd}$ .

It has to be remarked that so far, no investigation of phase formation has been performed by other authors who have studied interdiffusion in Pd-Cu multilayers [Bukaluk (2001), Jeon *et al.* (1994)]. From the concentration-depth profiles obtained in the present work, no obvious effect of phase formation on interdiffusion has been noticed. However, the formation of new phases, in principle, can cause considerable complications in the determination of diffusion coefficients from concentration-depth profiles as:

### 3. Mechanisms of interdiffusion in Pd-Cu thin film diffusion couples

---

(i) the diffusion coefficients of the new phases formed can be expected to be different from those of the parent phases and

(ii) the formation of new interfaces (interphase boundaries) can accompany phase formation.

Up to an annealing temperature of 225°C, only Cu<sub>3</sub>Pd forms by an ordering of the Cu and Pd atoms in the disordered Cu-Pd solid solution. In Cu<sub>3</sub>Pd, Cu atoms can diffuse by nearest neighbour jumps without creating so-called antistructure defects. The situation is different for Pd atoms: their movement involves the creation of antistructure defects. Thus, the intrinsic diffusion coefficient of Pd is expected to be smaller than the intrinsic diffusion coefficient of Cu [Philibert (1991)]. Thus, the formation of Cu<sub>3</sub>Pd could considerably retard interdiffusion and thus account also, possibly together with a decrease of the density of defects, for the decrease of the diffusion coefficients (see Fig. 3.5 and 3.8) and a corresponding increase of the activation energy (see Table 3.4) with time.

At an annealing temperature of 250°C, CuPd forms. CuPd has a CsCl-type structure (B2 structure) and the movement of both Cu and Pd atoms is impossible without the creation of antisite defects [Philibert (1991)]. It could thus be expected that the formation of CuPd considerably retards interdiffusion. For this work, however, the formation of CuPd is not relevant for the determination of diffusion coefficients and activation energies as the results obtained at this temperature have not been employed for the determination of diffusion coefficients.

#### 3.5. Summary

- Pd-Cu diffusion couples (thickness of each sublayer: 50nm) were prepared by successive deposition of Cu and Pd onto single-crystalline Si wafers in a dc magnetron sputtering chamber. Transmission electron microscopy and X-ray diffraction investigations reveal that the layers are polycrystalline, consisting of columnar-shaped grains separated by grain boundaries oriented more or less perpendicular to the film surface.
- It has been found by Auger-electron spectroscopy in combination with ion sputter profiling that considerable interdiffusion occurs in the couples upon annealing in the temperature range 175°C-250°C.
- X-ray diffraction phase analysis indicates that diffusional intermixing is accompanied by the sequential formation of new phases. First, an ordering of the solid solution leads to the formation of Cu<sub>3</sub>Pd at temperatures of 200°C and 225°C. At 250°C, CuPd forms: after a coexistence of CuPd and Cu<sub>3</sub>Pd at short annealing times (up to 1.5 hours), CuPd grows at the cost of Cu<sub>3</sub>Pd.
- The (absolute value of the) concentration gradient at the initial interface decreases and a plateau develops on the Cu-rich side of the couple. It is remarkable that no plateau develops on the Pd-rich side even though grain boundary diffusion through Pd occurs: the occurrence of grain boundary diffusion is indicated by the presence of copper on the surface of annealed specimens. The absence of a plateau on the Pd-rich side has been interpreted as a consequence of the concentration dependence of the volume diffusion coefficient: the volume diffusion coefficient is low at high Pd concentrations.
- Volume diffusion coefficients have been determined employing the centre-gradient method. It was found that the diffusion coefficients decrease with increasing annealing time.
- Also, volume diffusion coefficients determined employing the plateau-rise method have been found to decrease with increasing annealing time.
- The volume diffusion coefficients determined employing the centre-gradient and the plateau-rise methods differ by about one order of magnitude. This difference is due a higher defect concentration in the proximity of the initial interface.



### 3. Mechanisms of interdiffusion in Pd-Cu thin film diffusion couples

---

- Grain-boundary diffusion coefficients determined employing the Whipple-Le Claire method using both  $\tilde{D}_{CG}$  and  $\tilde{D}_{PR}$  have been found to decrease with increasing annealing time.
- The activation energies for interdiffusion and grain boundary diffusion have been determined on the basis of Arrhenius-plots. Activation energies determined from the diffusion coefficients obtained by PR method are higher (see Table 3.4) than the activation energies determined using the diffusion coefficients obtained from CG method.
- The activation energies increase slightly with increasing annealing time. The time dependence of the activation energies (and diffusion coefficients) has been attributed both to a decrease of the concentration of defects accelerating interdiffusion and the formation of new phases retarding interdiffusion.
- Interdiffusion coefficients determined for Pd-Cu bilayers in the present work are in good agreement with literature values obtained by other authors from Pd-Cu multilayer specimens. Higher activation energies and lower values of diffusion coefficients as determined from PR method (compared to those from CG method) are also in agreement with reported works in the literatures. However, the observed time dependence of the volume and GB diffusion coefficients has not been reported so far in the literature. Also, the same statement is true in case of phase formation during interdiffusion.

## **4. Interdiffusion, phase formation and stress development in Pd- Cu thin film diffusion couples**

J. Chakraborty, U. Welzel and E. J. Mittemeijer

### **Abstract**

Pd-Cu thin film diffusion couples (individual layer thicknesses: 50nm) have been prepared by DC-magnetron sputtering on silicon substrates coated with a thin amorphous  $\text{Si}_3\text{N}_4$  layer. Stress evolution, microstructural development and phase formation during interdiffusion have been investigated employing Auger-electron spectroscopy (in combination with sputter-depth profiling), X-ray diffraction, wafer curvature measurements and transmission electron microscopy. Upon annealing at relatively low temperatures (175°C to 250°C) for durations up to 10 hours, considerable diffusional intermixing occurs. Interdiffusion is accompanied by sequential formation of new phases. First,  $\text{Cu}_3\text{Pd}$  forms; subsequently,  $\text{CuPd}$  forms and grows at the expense of  $\text{Cu}_3\text{Pd}$ . Annealing leads to a slight sharpening of the pre-existing {111}-fibre textures and a little increase in the average grain size. Ex-situ (X-ray diffraction) and in-situ (wafer curvature) stress measurements reveal that tensile stresses are generated during annealing. The stress results are discussed in the light of possible mechanisms of stress generation.

### 4.1. Introduction

Bilayer and multilayer thin films are key materials for many technical applications such as devices in microelectronics, sensors, actuators etc. One important concern regarding the thermal stability of these devices is the interdiffusion between two adjacent thin layers even at room temperature (if one (or both) layer is polycrystalline) via grain boundary diffusion. Interdiffusion can be both beneficial or detrimental for e.g. functional properties. Therefore, a fundamental understanding of diffusion processes is of major importance.

Often interdiffusion is accompanied by the formation of compound phases [Goesele and Tu (1982), Van Loo (1973), Tu (1977), Tu *et al.* (1983), d'Heurle (1998), d'Heurle *et al.* (1997), Hodaj and Gusak (2004)] However, it has been frequently found that not all phases expected on the basis of the phase diagram occur. The mechanism of this phase suppression may have both a thermodynamic or kinetic origin which is still a matter of debate [d'Heurle *et al.* (1995) ; d'Heurle *et al.* (2004)].

Thin films can have very high residual stresses arising from their growth [Windischmann (1992)], mismatch of the coefficient of thermal expansion between the film and substrate or from diffusion and phase formation. Interdiffusion can be a source of stress generation if the partial molar volumes of the diffusing species are different or if a net vacancy flux occurs due to a difference of the intrinsic diffusion coefficients of the diffusing species (Kirkendall effect) [Li (1978); Stevens and Powell (1977)]. However, systematic experimental investigations of the stress evolution in thin-film diffusion couples are lacking.

It has frequently been speculated that stress states influences diffusion. This is well known for the case of hydrostatic stresses, which affect the diffusivity via the so-called activation volume [Shewmon (1989),]. The case of non-hydrostatic stress states, however, has received much less attention both theoretically and, in particular, experimentally. The pioneering theoretical work in that field is due to Cahn and Larche [Larche and Cahn (1985)]. However, systematic experimental investigations are lacking.

In the present work, interdiffusion and phase formation in thin (50nm thick) bilayer diffusion couples of Cu and Pd have been investigated employing Auger-electron spectroscopy in combination with sputter depth profiling, transmission electron microscopy, X-ray diffraction and wafer curvature measurements.

#### 4. Interdiffusion, phase formation and stress development in Pd-Cu thin film diffusion couples

---

It has been found that interdiffusion is accompanied by the formation of new phases and considerable stress changes, as revealed by X-ray diffraction phase and stress analysis and in-situ stress measurements by the wafer curvature method.

## 4.2. Experimental

### 4.2.1. Preparation of Pd-Cu diffusion couples

Polycrystalline thin film Pd-Cu diffusion couples were prepared by successive deposition of Cu and Pd on Si/SiO<sub>2</sub>/Si<sub>3</sub>N<sub>4</sub> substrates in a dc magnetron sputtering chamber evacuated to a base pressure of  $1 \times 10^{-10}$  mbar. The substrates were commercially available single crystalline silicon (100) wafers of thickness 500  $\mu$ m with amorphous silicon oxide (50nm thickness) and amorphous silicon nitride (50nm thickness) layers on it. The Cu and Pd layers each had a thickness 50nm. Before deposition, the substrates were sputter cleaned for 1 minute with Ar<sup>+</sup> ions accelerated with -100V. During film deposition, the sample holder was rotated at 12 rpm and the chamber pressure was maintained at  $2 \times 10^{-4}$  mbar using Argon gas for producing a plasma. The magnetron power has been set to 200W for the deposition of the Cu layer and 100W for the deposition of the Pd layer. The substrate temperature increased slightly during the deposition due to the atomic bombardment. The maximum temperature did not exceed 40°C.

### 4.2.2. Annealing of Pd-Cu diffusion couples

The Pd-Cu diffusions couples were annealed in quartz ampoules initially evacuated to a pressure of  $1 \times 10^{-6}$  mbar and subsequently filled with Ar gas at a pressure of 300 mbar in order to avoid oxidation. Specimens were annealed at 175°C, 200°C, 225°C and 250°C annealing temperatures for various durations (0.5 hours to 10 hours).

### 4.2.3. Characterisation of Pd-Cu bilayers before and after diffusion annealing:

#### 4.2.3.1. Concentration-depth profiling

Concentration-depth profiles have been measured employing ion sputter profiling combined with Auger Electron spectroscopy (AES) in a JEOL JAMP 7830F field emission Auger

#### 4. Interdiffusion, phase formation and stress development in Pd-Cu thin film diffusion couples

---

microprobe. The energy of the Argon ions used for sputter-depth profiling was 1keV and a primary electron beam with energy 10keV was used for AES. These sputter conditions resulted in the best compromise of depth resolution and sputter time for the samples under investigation.

Auger lines of Cu (LMM, 920eV) and Pd (MNN, 330eV) were measured for the determination of the Cu and Pd concentrations. The sputter rates for pure elements (Pd and Cu) have been evaluated by total removal of the pure Pd and pure Cu layers in the unannealed (as-deposited) specimens. The ratio of their sputter rates was determined as 0.96. Sputter time can be converted into sputter depth if the sputter rate is known. However, the sputter rate can change with changing composition in a binary system when inter-diffusion takes place. In order to evaluate the sputter rate of the Pd-Cu binary system a simple kinetic sputter model originally developed by Ho et.al [Ho *et al.* 1977] has been applied.

The concentrations of Cu and Pd atoms were calculated using the following relationships:

$$C_{cu} = \frac{\frac{I_{Cu}}{S_{Cu}}}{\frac{I_{Cu}}{S_{Cu}} + \frac{I_{Pd}}{S_{Pd}}} \quad (4.1) \quad C_{Pd} = \frac{\frac{I_{Pd}}{S_{Pd}}}{\frac{I_{Cu}}{S_{Cu}} + \frac{I_{Pd}}{S_{Pd}}} \quad (4.2)$$

Where  $C_{cu}$  and  $C_{Pd}$  are the concentrations of Cu and Pd respectively.  $S_{Cu}$  and  $S_{Pd}$  are the (0.574 and 0.973) relative Auger yield of Cu and Pd respectively with respect to pure Cu [JEOL database].  $I_{Cu}$  and  $I_{Pd}$  are Auger peak-to-peak heights (APPH) of Auger peaks corresponding to Cu and Pd respectively.

##### 4.2.3.2. Phase analysis and measurement of macrostress

Both the unannealed and the annealed samples have been characterised by X-ray diffraction (XRD). Phase analysis has been performed in the Bragg-Brentano geometry using Cu  $K\alpha$  radiation in a Philips X'Pert MRD diffractometer equipped with an Eulerian cradle and parallel beam optics and also using Philips X'Pert MPD diffractometer equipped with a monochromator in the primary side (for selecting Cu  $K\alpha_1$  radiation) and a position sensitive detector (Panalytical X'Pert Accelerator) in the secondary side. A software 'ProFit' [ProFit for Windows Users's Guide, Philips Analytical X-ray, 1<sup>st</sup> edition, Almelo, 1996] provided by 'Philips' was used to determine the peak maximum position, full width at half maximum

(FWHM), peak asymmetry and peak shape parameter corresponding to each reflection by fitting Pearson VII function to the measured diffraction lines.

The measurement of the macrostress in the individual layer (Cu and Pd) has been performed using Cu K $\alpha$  radiation in a Philips X'Pert MRD diffractometer equipped with an Eulerian cradle and parallel beam optics. Details of x-ray diffraction stress measurement and analysis are given below:

#### 4.2.3.2.1. 'd-sin<sup>2</sup> $\psi$ ' method

In the 'd-sin<sup>2</sup> $\psi$ ' method,  $q/2q$  scans corresponding to a particular  $hkl$  reflection are conducted at various tilt angles ' $\psi$ ' where  $\psi$  is the angle between the sample normal and the diffraction vector [Noyan and Cohen (1987), Hauk (1997) and Welzel *et al.* (2004)]. The interplanar spacing  $d_y^{hkl}$  at each tilt angle was calculated from the corresponding observed  $2q$  position of the peak maximum using Bragg's law. In the present work, 111 and 311 reflections have been used for both Cu and Pd for stress analysis. Due to in-plane rotational symmetry of the biaxial stress (measurements at rotation angles  $\phi = 0^\circ$  and  $\phi = 90^\circ$  yielded the same stress values) in Cu and Pd films, the stress  $S_{\parallel}$  can be determined from the following formula:

$$d_y^{hkl} = \frac{1}{2} S_2^{hkl} d_0^{hkl} S_{\parallel} \sin^2 \psi + (1 + 2 S_1^{hkl} S_{\parallel}) d_0^{hkl} \quad (4.3)$$

where,  $d_0^{hkl}$  is the strain free lattice spacing of the  $\{hkl\}$  planes.  $S_1^{hkl}$  and  $\frac{1}{2} S_2^{hkl}$  are the so-called x-ray elastic constants (see, for example, Hauk, 1997 ; Welzel *et al.*, 2004). For polycrystalline Cu and Pd, Neerfeld-Hill (N-H) average (see, for example, Hauk 1997 and Welzel *et al.* 2004) values of  $S_1^{hkl}$  and  $\frac{1}{2} S_2^{hkl}$  have been calculated from the single crystalline elastic constants of Cu and Pd and have been summarised in Table 4.1. However, due to the presence of a  $\{111\}$  fibre texture (although not sharp, cf. Section 4.3.4) in both the Cu and Pd layers, the use of the so-called x-ray stress factors would have been a more accurate approach instead of using x-ray elastic constants, which are valid only in case of untextured specimens

#### 4. Interdiffusion, phase formation and stress development in Pd-Cu thin film diffusion couples

exhibiting isotropic grain interaction (Welzel and Mittemeijer (2003)). The use of equation (4.3) for stress analysis thus represents an approximation.

From equation (4.3) it can be seen that the stress ( $\mathbf{s}_{\parallel}$ ) can be calculated from the slope of the straight line fitted to the data obtained by plotting  $d_y^{hkl}$  versus  $\sin^2 \mathbf{y}$ .

By putting  $d_y^{hkl} = d_0^{hkl}$  (strain free) in equation (4.3), the following expression can be obtained for the tilt angle  $\mathbf{y}$  corresponding to zero strain ( $\mathbf{y}_0$ , 'strain-free direction):

$$\mathbf{y}_0 = \sin^{-1} \left( \sqrt{\frac{-2 S_1^{\{hkl\}}}{\frac{1}{2} S_2^{\{hkl\}}}} \right). \quad (4.4)$$

The strain-free directions  $\mathbf{y}_0$  have also been included in Table 4.1.

Table 4.1: Neerfeld-Hill (N-H) X-ray elastic constants and strain free directions for various Cu and Pd reflections.

Reflections	$S_1^{hkl} \text{ (Pa}^{-1}\text{)}$	$\frac{1}{2} S_2^{hkl} \text{ (Pa}^{-1}\text{)}$	$\mathbf{y}_0$
Cu 111	$-0.184 \times 10^{-11}$	$0.792 \times 10^{-11}$	$42.97^\circ$
Cu 311	$-0.313 \times 10^{-11}$	$1.179 \times 10^{-11}$	$46.77^\circ$
Pd 111	$-0.217 \times 10^{-11}$	$0.822 \times 10^{-11}$	$46.60^\circ$
Pd 311	$-0.33 \times 10^{-11}$	$1.157 \times 10^{-11}$	$49.05^\circ$

##### 4.2.3.2.2. Wafer curvature method

The measurement of the thickness-average macrostress in the Pd-Cu diffusion couples has also been performed *in situ* during annealing by the wafer curvature method to observe any possible stress change due to interdiffusion *in-situ*. From a wafer curvature measurement the film stress ( $\mathbf{s}_{film}$ ) can be determined from the following formula derived by Stoney [Stoney (1909)]:

$$\mathbf{s}_{film} = \frac{M_s \times t_s^2}{6t_f} \times (C_{f+s} - C_s) \quad (4.5)$$

#### 4. Interdiffusion, phase formation and stress development in Pd-Cu thin film diffusion couples

---

where,  $M_s$  is biaxial modulus of the substrate.  $t_s$  is the thickness of the substrate and  $t_f$  is the film thickness.  $C_{f+s}$  is the curvature of the film/substrate assembly and  $C_s$  is the curvature of the bare substrate (without a film on it). It can be noted that equation (4.5) depends only on the elastic properties of the substrate but not on those of the film deposited on it. Two important assumptions of Stoney's derivation are: the film stress strains the substrate and the substrate is much thicker than the film deposited on it. In the present

measurement, the average stress ( $\frac{t_{cu}S_{cu} + t_{pd}S_{pd}}{t_{cu} + t_{pd}}$ ) present in the unannealed bilayer deforms

the substrate (single crystalline silicon (100),  $M_s=180.5\text{GPa}$  [Nix (1989)]) elastically and any change in this average stress during annealing also bring changes in the elastic deformation of the substrate. The substrate ( $\sim 500\mu\text{m}$ ) is much thicker than the bilayer films ( $\sim 100\text{nm}$ ).

The substrate/Pd-Cu bilayer combination is thermally cycled between room temperature and the desired annealing temperature ( $175^\circ\text{C}$ ,  $200^\circ\text{C}$  and  $225^\circ\text{C}$ ) with a holding time of six hours at the desired annealing temperature.

The measurement of the curvature of the bilayer/substrate combination has been performed in a wafer curvature apparatus using a laser scanning method, the details of which can be found elsewhere [Nix (1989)]. The curvature can be extremely small and the technique is capable of detecting a maximum radius of curvature of  $10\text{km}$ , corresponding to a stress sensitivity of  $\sim 0.2\text{MPa}$ .

During the wafer curvature measurement, the bilayer/substrate combination was placed into a furnace which could be heated up to maximum  $600^\circ\text{C}$  at a controlled rate. In all the experiments, the heating rate was maintained at  $25^\circ\text{C}/\text{min}$ . and the cooling rate was maintained at  $5^\circ\text{C}/\text{min}$  down to  $40^\circ\text{C}$ .

A bare substrate (without bilayer films on it) has also been thermally cycled up to  $250^\circ\text{C}$  and the observed change in the curvature was of the order of  $0.0003\text{m}^{-1}$ , which is smaller by more than a factor of 10 with respect to the observed curvature change in cycling the bilayer/substrate combination. Thus, the changes in the curvature of the bare substrates during the cycling have been neglected.



#### 4. Interdiffusion, phase formation and stress development in Pd-Cu thin film diffusion couples

---

In the present analysis, in each case, the curvature of the bare substrate at room temperature has been back-calculated from equation (4.5) by using the measured value of curvature of bilayer/substrate combination at room temperature along with the measured average stress value in the unannealed Pd-Cu bilayer at room temperature by x-ray diffraction. Subsequently, this calculated value of bare substrate curvature has been used to calculate the absolute values of average biaxial stress from the measured curvature data of bilayer/substrate during thermal cycling and also during annealing.

##### 4.2.3.3. Texture

The crystallographic texture in the individual layers (Cu and Pd) has been investigated by measuring pole figures for 111 reflections of Cu and Pd using Cu K $\alpha$  radiation in a Philips X'Pert MRD diffractometer equipped with an Eulerian cradle and parallel beam optics.

##### 4.2.3.4. Microstructure

Microstructural investigations have been performed in a JEOL FX 2000 transmission electron microscope (TEM) using unannealed and annealed cross-sectional specimens. For specimen preparation, two pieces have been cut from the bilayer/substrate assembly and they have been sandwiched (bilayer films faces each other from both pieces) with epoxy glue. After mechanical thinning by grinding, this thin slice of materials has been embedded into a specially designed cylindrical polycrystalline Al<sub>2</sub>O<sub>3</sub> tube of 3mm diameter as a holder for the cross-sectional sample. Then the tube has been cut into slices of thickness ~350 $\mu$ m. The slices underwent mechanical grinding, dimpling from both sides and finally ion thinning (Ar<sup>+</sup> ions with 3.5 keV energy and 1mA ion current in BAL-TEC RES 010 with liquid nitrogen cooling) for several hours to achieve electron transparency. Details of the specimen preparation can be found elsewhere [Strecker *et al.* (2003)]. Bright field (BF) images have been taken using a 200keV electron beam. The possible presence of any ordered phase or epitaxy between Cu and Pd layers before after annealing has been investigated using selected area diffraction (SAD) patterns. The thicknesses of the films have been verified from the cross-sectional TEM (XTEM) micrographs.

### 4.3. Results

#### 4.3.1. Concentration-depth profiling

Figs. 4.1(a)-(d) show Pd concentration-depth profiles for the samples annealed in the temperature range 175°C-250°C for various annealing durations. Cu concentration-depth profiles can be generated by subtracting the palladium concentration values at each depth from unity.

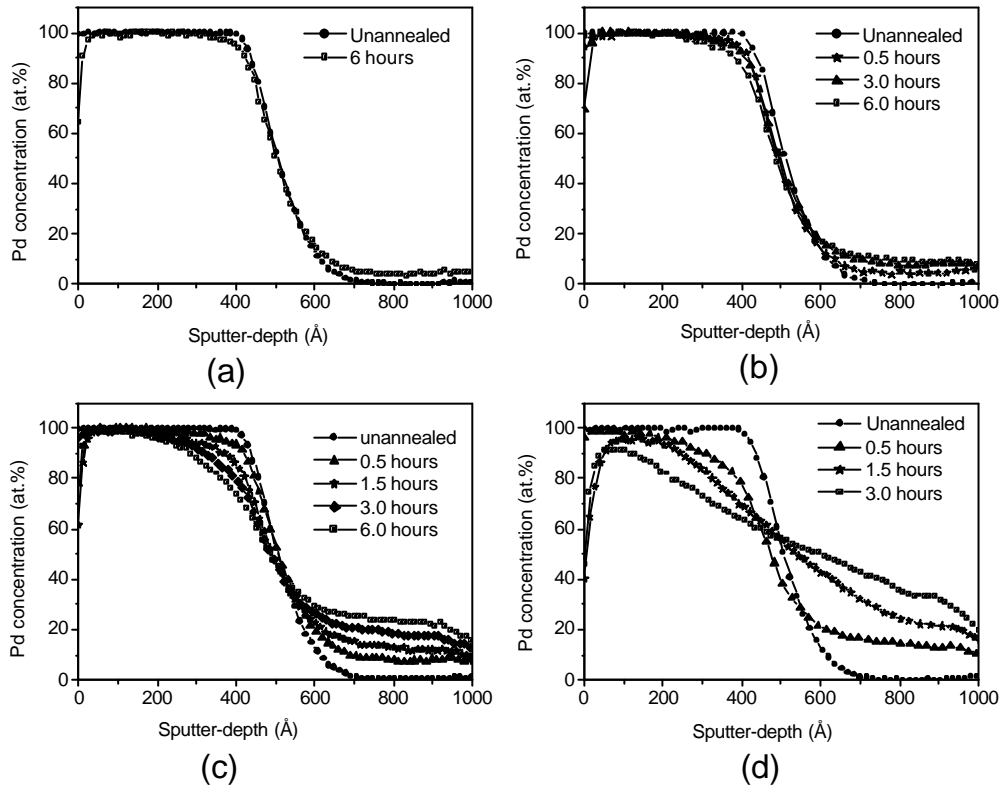


Fig. 4.1: Pd concentration versus sputter depth at different annealing temperatures and annealing times. (a) annealing temperature: 175°C, (b) annealing temperature: 200°C (c) annealing temperature: 225°C and (d) annealing temperature: 250°C.

The sputter-depth profile of the as-deposited sample does not show a sharp interface. The diffuseness of the interface is due to the following reasons: (1) the roughness of the interface, (2) the smearing of the 'true' concentration-depth profile due to instrumental effects during AES depth profiling [Hoffmann (1994)]. Interdiffusion in the unannealed diffusion couple

can be ignored as all depositions have been performed at temperatures far below the annealing temperature ( $T < 40^\circ\text{C}$ , cf. Section 4.2.1).

The sputter-depth profiles of annealed samples show considerable shift of the position for which the Pd concentration is 50 at. %. The depth profiles of annealed specimens do not have any point of inversion symmetry.

Inverse error function plots of Pd concentration profiles near the interface show straight lines for all the annealed samples. This confirms complementary error function dependence of Pd concentration profiles near the interface. The slopes of the straight lines can be used to determine the interdiffusion coefficients using the formalism developed by Hall *et al.* [Hall and Morabito (1976)]. At  $175^\circ\text{C}$ , straight lines slopes do not vary much with annealing time indicating extremely low Pd diffusion through Cu grains which is also clear from Pd concentration profiles (for 6 hours annealing time) near interface in Fig. 4.1(a). With increasing annealing temperature palladium diffuses more into copper grains (volume interdiffusion coefficient ( $\tilde{D}$ ) increases) and beyond  $250^\circ\text{C}$ , 1.5 hours, annealing condition, concentration-depth profiles get severely distorted indicating almost complete homogenisation within the bilayer. Also, the sputter depth profiles for the annealed samples show the existence of a plateau region with a few percent Pd concentration in Cu which varies with annealing time and temperatures. This is a combined effect of Pd diffusion through Cu grain boundaries and then sideways diffusion through Cu grains following so called 'B' kinetics of Harrison's classification [Harrison (1961)]. From the measured depth profiles by AES, it has been confirmed that at a particular annealing temperature the plateau concentration of Pd varies with annealing time following a  $\sqrt{t}$  behaviour. In contrast, one can notice presence of Cu atoms on the Pd surface with negligible Cu concentration in the plateau region. Therefore, there is relatively small volume diffusion of Cu through Pd grains and Cu diffusion through Pd follows the so-called 'C' kinetics [Harrison (1961)]. Volume interdiffusion coefficients (diffusion through lattice/grains) and grain boundary diffusion coefficients have been determined using the near interface and plateau regions which will be published elsewhere [Chapter 3, section 3.4.3].

### 4.3.2. X-ray diffraction phase analysis

X-ray diffraction patterns of the unannealed Pd-Cu diffusion couples show reflections of pure Cu and pure Pd. Figs. 4.2(a), 4.2(b) and 4.2(c) show the 111 reflections of Pd and Cu of the diffusion couples annealed at 175°C, 200°C and 225°C for different durations, respectively. Fig. 4.2(d) corresponds to 250°C annealing temperature and will be discussed later.

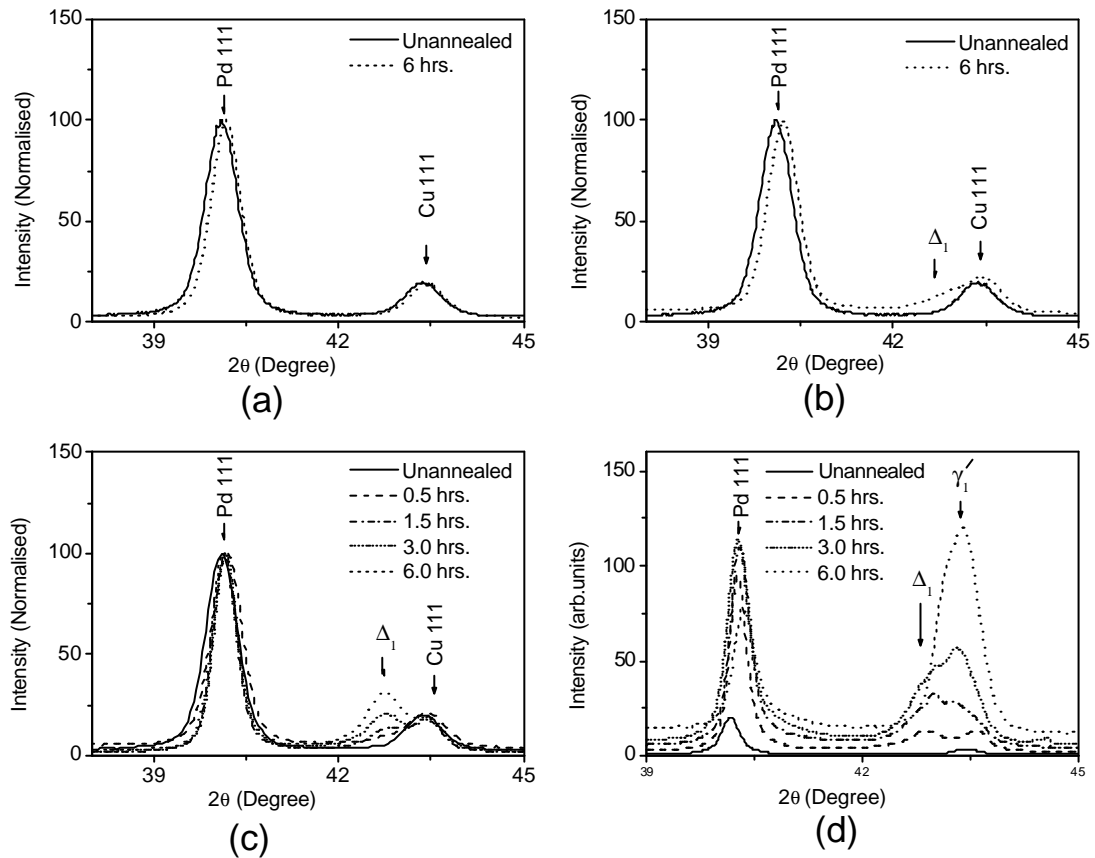


Fig. 4.2. 111 reflections of Pd and Cu in the unannealed specimen and the specimens annealed at: (a) 175°C, (b) 200°C, (c) 225°C and (d) 250°C for different annealing times. The developments of the new phases  $\Delta_1$  and  $\gamma'_1$  at different annealing temperatures and annealing times are shown. Measurements have been performed in Philips X'Pert MRD diffractometer for Figs. (a), (b) and (c) and in each case, the intensity has been normalised with respect to the maximum peak intensity. In Fig. (d), measurement has been performed in the Philips MPD diffractometer.

#### 4. Interdiffusion, phase formation and stress development in Pd-Cu thin film diffusion couples

---

It is reasonable to expect all reflections of Pd and Cu to broaden upon diffusion annealing due to continuous composition variation in the couple and finally to merge into reflections corresponding to the homogenized state. At 175°C, (Fig. 4.2(a)), there is only a very little shift of the 111 reflections of palladium and copper without much change in broadening, corresponding to only very little interdiffusion as seen from AES sputter-depth profiles in Fig. 4.1(a). However, in Fig. 4.2(b) a shoulder develops on the low-angle side of the Cu 111 reflection. Upon annealing at higher temperature (225°C), a similar shoulder develops for an annealing time of 0.5 hours. However, upon continued annealing it becomes evident that the shoulder is caused by an additional reflection (marked as  $\Delta_1$  in the following) increasing in intensity. The presence of additional reflections (named  $\Delta_2$ ,  $\Delta_3$  and  $\Delta_4$ ) has also been observed on the low-angle side of the Cu 200, 311 and 222 reflections (shown in Figs. 4.4(a) and 4.4(b)). The appearance of these additional reflections indicates the formation of a new phase. An attempt for the identification of this new phase has been undertaken as follows.

From the  $\Delta_1$  reflection, the strain-free lattice constant of the new phase has been determined employing equation (4.4) under the following assumptions: (i) the new phase has cubic symmetry and  $\Delta_1$  is the 111 reflection of the new phase; (ii) the strain-free direction  $y_0$  of the new phase is identical to the strain-free direction of Cu; (iii) the stress state for the new phase is also planar, rotationally symmetric. The strain-free lattice constant has been determined employing equation (4.4) also for the Cu 111 reflection. Using Vegard's law for the composition-dependent lattice parameter of the disordered Cu-Pd solid solution [Soutter and Hertz (1971)] the compositions corresponding to the observed strain free lattice parameters for the reflections  $\Delta_1$  and Cu 111 have been derived and presented as a function of the annealing time at 225°C in Fig. 4.3.

The Pd concentration derived from the Cu 111 reflection shows only a very small increase with continued annealing. This is a result of the dissolution of Pd in Cu by means of volume diffusion.

The Pd composition in the new phase is approximately constant for all observed  $\Delta_1$  reflections and the average lattice parameter has been determined as  $0.3674 \pm 0.001$  nm. The observed lattice parameter is very close to the reported literature value of the lattice

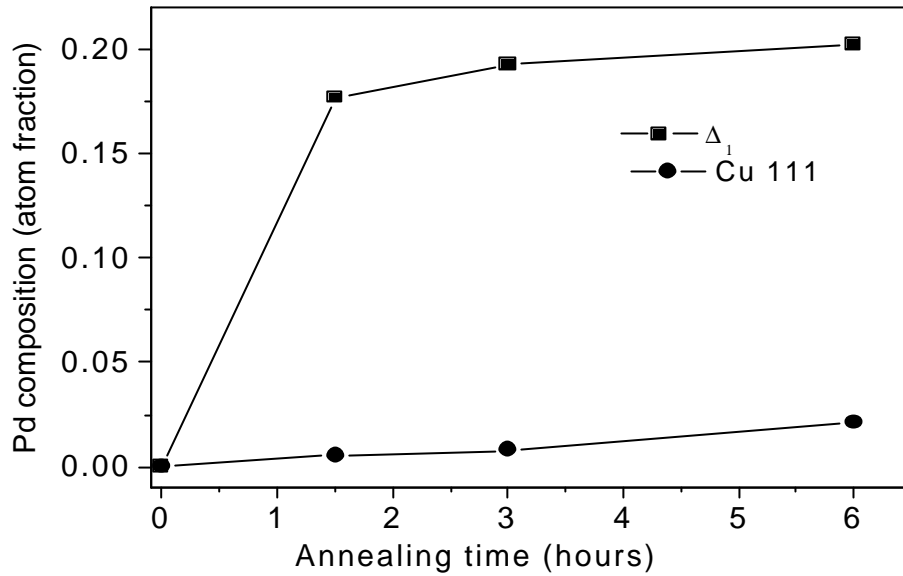


Fig. 4.3: Palladium composition from Vegard's law for both Cu 111 and  $\Delta_1$  reflections.

parameter ( $3.67 \text{ \AA}$ ) of an ordered phase  $\text{Cu}_3\text{Pd}$  observed below 20at% palladium [Jones and Sykes (1939), Guymont and gratias (1976)] having ordering like the prototype structure  $\text{Cu}_3\text{Au}$  (Strukturbericht designation  $\text{L1}_2$ ; space group  $Pm\bar{3}m$ ). Thus, these findings suggest that the newly formed phase is  $\text{Cu}_3\text{Pd}$ . However, the presence of  $\text{Cu}_3\text{Pd}$  ( $P4mm$ ) tetragonal phase can not be ruled out as it was not possible to resolve the tetragonal splitting for 200 and 311 reflections (due to compositional change) because of the intrinsic broadening of these reflections and extremely low tetragonality ( $c/a$  ratio) of  $\text{Cu}_3\text{Pd}$  phase [Guymont and gratias (1976)].

Also the occurrence and the observed positions of the reflections  $\Delta_2$ ,  $\Delta_3$  and  $\Delta_4$  are compatible with the formation of the phase  $\text{Cu}_3\text{Pd}$ . However, for this phase additional (superstructure) reflections are expected. These superstructure reflections (having mixed  $hkl$  values) have not been observed due to their extremely low intensities because of the close values of the atomic scattering factors of Pd and Cu. A rough estimation of the structure factor calculation shows that at low angle, superstructure reflections have about sixty times less intensity than the fundamental reflections. Also, compared to the observed diffracted

#### 4. Interdiffusion, phase formation and stress development in Pd-Cu thin film diffusion couples

intensities for fundamental reflections, the intensities of the superstructure reflections can not be distinguished from the background in the measured data.

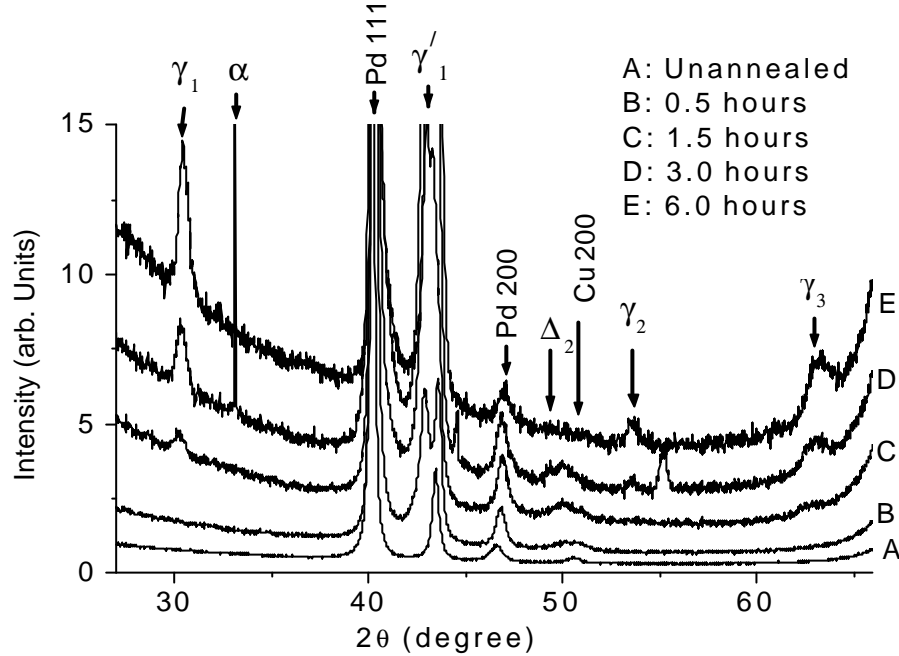


Fig. 4.4(a): Evolution of the new phase ( $\gamma$ ) with increasing annealing time at 250°C. Pd reflections are also shown. Si 400 reflection for  $\frac{1}{2}(\lambda_{\text{CuK}\alpha 1})$  has been marked as  $\alpha$  sign. Measurement has been performed in Philips MPD diffractometer.  $\Delta_2$  appears at low angle side of Cu 200 reflection which also appears after annealing at 225°C

At 250°C, diffraction lines corresponding to  $\text{Cu}_3\text{Pd}$  can be unambiguously identified only for an annealing time of 0.5 hours (see Figs. 4.2(d), 4.4(a) and 4.4(b)). At an annealing time of 6 hours, new reflections marked as  $g_i$  (see Figs. 4.4(a) and 4.4(b)) have developed. The existence of diffractions lines previously indexed as Cu 111 and  $\text{Cu}_3\text{Pd}$  111 and Cu 222 and  $\text{Cu}_3\text{Pd}$  222 cannot be confirmed. However, it is likely that the intensity of these reflections gradually decreases and new reflections marked as  $g'_i$  (Figs. 4.2(d) and 4.4(a)) appear and grow in intensity. The measured intensity distributions in the angular ranges 42°-44° and 93°-96.5° may thus originate from the presence of Cu,  $\text{Cu}_3\text{Pd}$  and the newly formed yet unidentified phase.

#### 4. Interdiffusion, phase formation and stress development in Pd-Cu thin film diffusion couples

All Pd reflections observed for the unannealed specimen are still present up to 6 hours annealing time and the Cu reflections are also present, at least up to 1.5 hours annealing time at 250°C. At longer annealing time, the existence of unreacted Cu cannot be unambiguously detected due to line overlap with reflections  $g_i'$ .

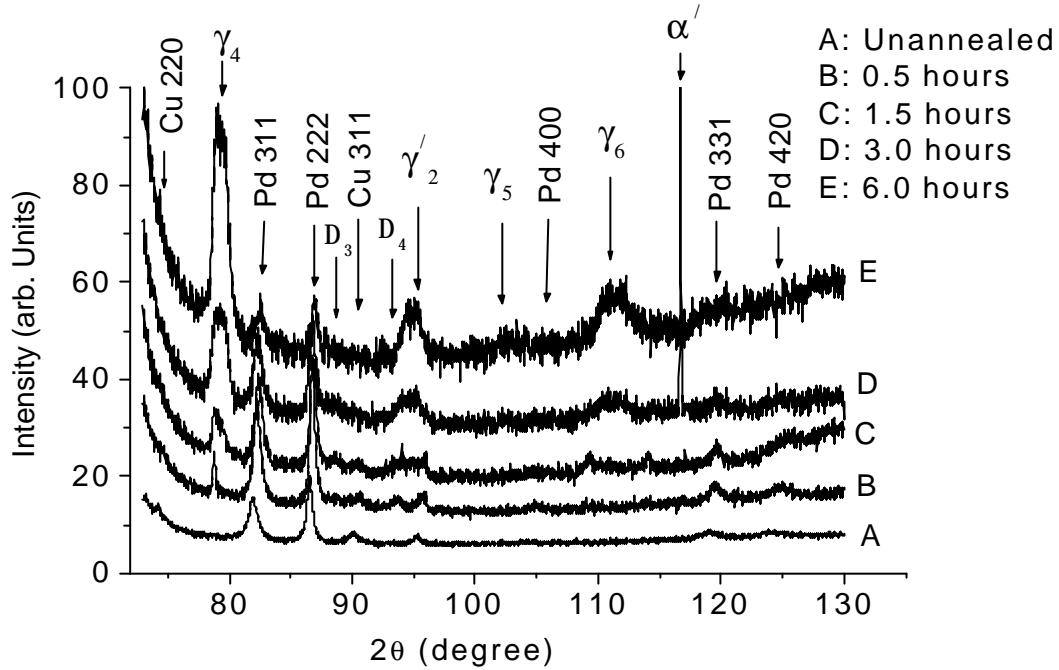


Fig. 4.4(b) : Evolution of the new phase ( $\gamma$ ) with increasing annealing time at 250°C. Cu and Pd reflections are also shown. Si 600 reflection for  $\lambda_{\text{CuK}\alpha 1}$  has been marked as  $\alpha'$  sign. Measurement has been performed in Philips MPD diffractometer.  $\Delta_3$  and  $\Delta_4$  appear at low side of Cu 311 and Cu222 reflections which are also present after annealing at 225°C.

An attempt has been made to index all reflections  $g_i$  and  $g_i'$  (Figs. 4.4(a) and 4.4(b)) assuming that they originate from a single phase. The result of this indexing is summarized in Table 4.2. A consistent indexing has been achieved assuming that the new phase has cubic symmetry. The obtained lattice parameter is 0.2952nm which is an average of the lattice parameter values calculated from the observed 'd' values for different reflections. This is in reasonable agreement with reported lattice parameter of 0.2988nm of the ordered phase CuPd



#### 4. Interdiffusion, phase formation and stress development in Pd-Cu thin film diffusion couples

---

Table 4.2: Results of indexing all reflections except Pd ones (after annealing at 250°C for 6 hours) in Fig. 4.4, Lattice parameter determined as 2.952 Å

h k l	calculated 'd' values (Å)	Observed 'd' values (Å)	Difference (Obs.-Cal.) (Å)	Integrated Intensity (counts)	Integral Breadth
1 0 0	2.952	2.93752	-0.0144	26650	0.6
1 1 0	2.08738	2.08568	-0.0017	313796	0.663
1 1 1	1.70434	1.70787	0.00353	3413.5	0.579
2 0 0	1.476	1.47286	-0.00314	45764.2	2.518
2 1 0	1.32017	*	*	*	
2 1 1	1.20515	1.20703	0.00188	45896.5	1.368
2 2 0	1.04369	1.04538	0.00169	14353.8	1.873
3 0 0	0.984	0.98434	0.00034	°	°
3 1 0	0.9335	0.93408	0.00058	20471.6	3.016
3 1 1	0.89006	°			
2 2 2	0.85217	°			

\* Peak position is very close to (400) Si single crystalline reflection.

° Accurate determination is difficult

having CsCl structure (1:1 ratio of copper and palladium), space group nomenclature  $Pm\bar{3}m$  (<http://www.chimdocet.it/solido/file11.htm>). However, it has to be remarked that the reflections, in particular at higher diffraction angles, show considerable broadening. This may indicate a very small size of the newly formed grains and large defect content. The phase composition at intermediate annealing times (1.5 and 3 hours) remains ambiguous due to the presence of a few unidentified reflections, which, upon continued annealing, disappear. Some reflections indicative of the presence of the CuPd gradually develop.

### 4.3.3. Residual stress

#### 4.3.3.1. X-ray diffraction stress analysis

The stresses before and after diffusion anneals in the Pd and Cu layers obtained employing the  $\sin^2\psi$ -method (cf. Section 4.2.3.2.1) have been presented in Fig. 4.5. After deposition, the stress in the Pd layer is compressive ( $\sigma_{\parallel} = -330$  MPa), whereas the stress in the Cu layer is tensile ( $\sigma_{\parallel} = 115$  MPa). After annealing, it has been found that the stresses in both layers have changed drastically: in both layers, annealing has lead to a tensile stress contribution increasing in magnitude with increasing annealing time and temperature. For the specimens annealed at 250°C, the stress can only be determined for the Pd layer in a straightforward manner for all annealing times. For the Cu layer, a stress determination is only possible for an annealing time of 0.5 hours, as only for this time a clear separation of the Cu 111 reflection from the peaks of newly developing phases is possible (cf. Section 4.3.2 and Fig. 4.2(d)). For the specimens annealed at 225°C an attempt has been made to determine the stress also in the Cu<sub>3</sub>Pd phase from the 111 reflection using the X-ray elastic constants of the Cu 111 reflection. The results have been included in Fig. 4.5(b).

The average stress of the bilayer has been calculated as the arithmetic average of the stresses of the Cu and Pd layers and has been presented in Fig. 4.5 (c). The averages stress is tensile after annealing and increases with increasing annealing time and temperature.

#### 4. Interdiffusion, phase formation and stress development in Pd-Cu thin film diffusion couples

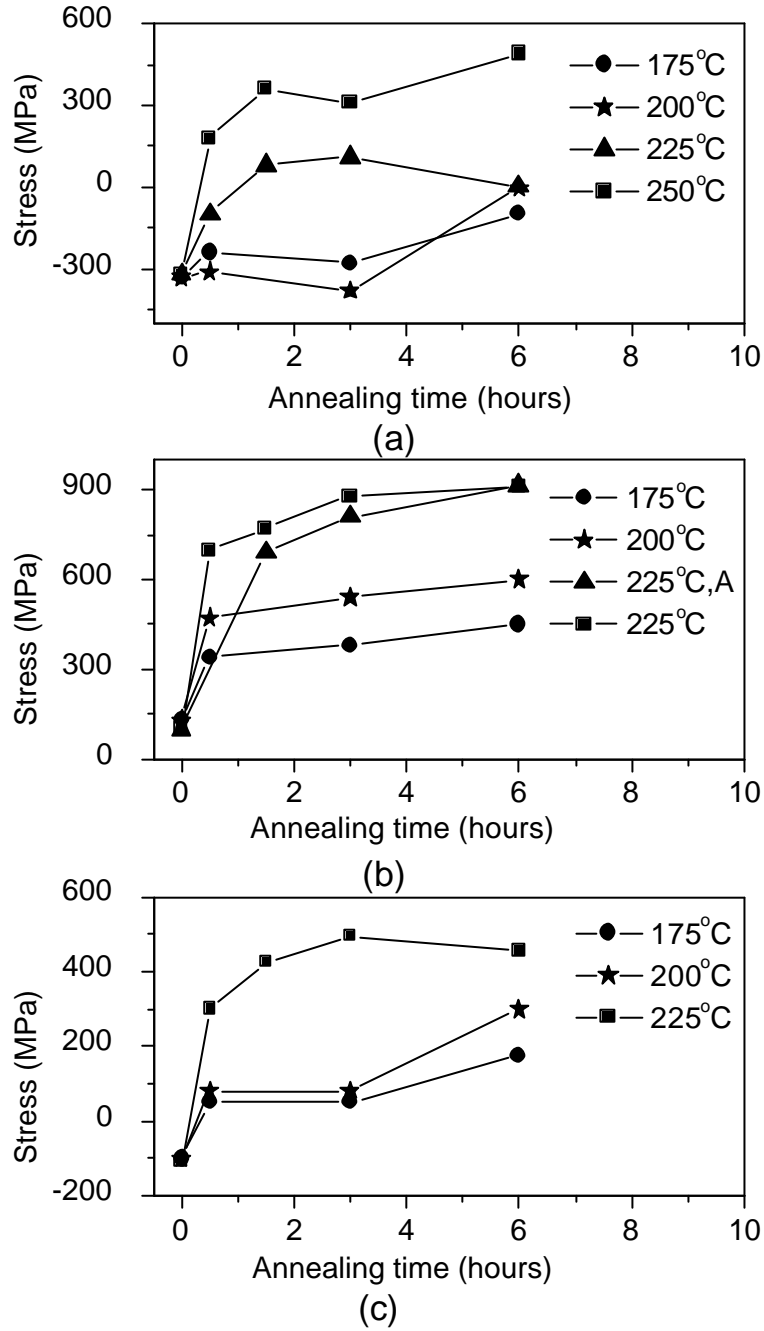


Fig. 4.5: Variation of stress with increasing annealing time at different annealing temperatures: (a) in Pd layers (b) in Cu layers and (c) average stress in Pd-Cu bilayers. 311 reflections of both Pd and Cu are considered at 175°C and 200°C. 111 Pd reflections are considered at 225°C, and 250°C. Also, Cu 111 reflections are considered at 225°C. In Fig. 4.5(b), '225°C, A' corresponds to stress in the  $\text{Cu}_3\text{Pd}$  phase using 111 reflections.

#### 4. Interdiffusion, phase formation and stress development in Pd-Cu thin film diffusion couples

---

##### 4.3.3.2. Stress by wafer curvature method

Specimens have been thermally cycled in a wafer curvature apparatus (cf. Section: 4.2.3.2.2) between room temperature and annealing temperatures of 175°C, 200°C and 225°C for in-situ measurements of the average stress in the diffusion couples. The desired annealing temperatures were maintained for a holding time of six hours.

Fig. 4.6 shows, as an example, the heating segment of the temperature cycle for the specimen annealed at 225°C.

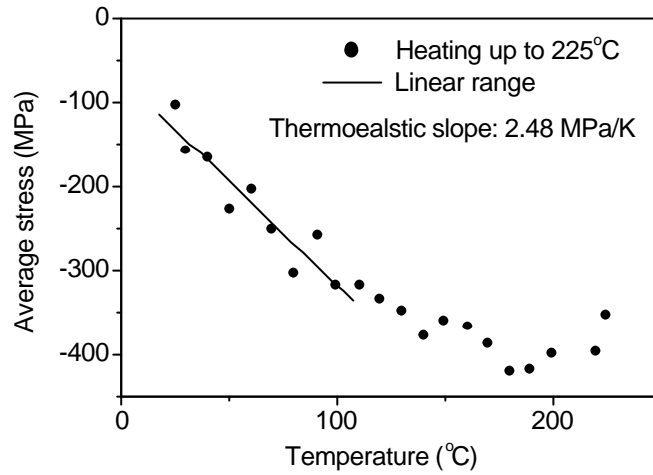


Fig. 4.6

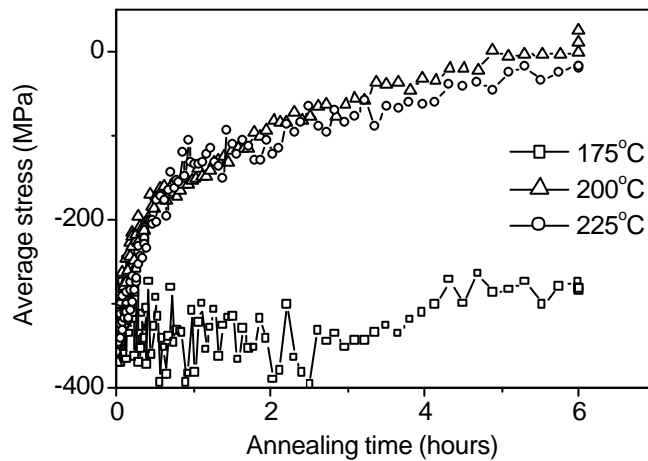


Fig. 4.7

Fig. 4.6: Average stress measured *in-situ* during heating cycle while annealing at 225°C for 6 hours. Thermoealstic slope has been determined using the linear region.

Fig. 4.7: Change in average stress measured *in-situ* during the period of annealing at different temperatures up to 6 hours annealing time.

#### 4. Interdiffusion, phase formation and stress development in Pd-Cu thin film diffusion couples

At temperatures below about 125°C, a linear region exists. From the slope of this linear region, the so-called thermoelastic slope  $\Xi$  ( $\Xi = \Delta S_{\parallel} / \Delta T$ )

can be determined, where  $\Delta S_{\parallel}$  is the change in the biaxial, rotationally symmetric stress resulting from the temperature change  $\Delta T$ . The results for diffusion couples annealed at different temperatures have been summarised in Table 4.3. For comparison, the expected thermoelastic slopes for couples consisting of polycrystalline, untextured Cu and Pd layers and couples consisting of perfectly {111}-fibre textured Cu and Pd layers have also been calculated and included in Table 4.3 (note that the layers exhibit a {111}-fibre texture, cf. Section: 4.3.4). Details of this calculation are presented in appendix 4A.

Table 4.3: Thermoelastic slopes ( $\Xi$ ) for Pd-Cu bilayer: theoretical and experimental values.

Temperature (°C)	$\Xi$ (MPa/K) Polycrystalline Pd and Cu	$\Xi$ (MPa/K) perfect {111} fiber textured Pd and Cu	Average Thermoelastic slope (MPa/K)	$\Xi$ (MPa/K) Experimentally Obtained values
175	-2.20	-3.04	-2.62	-2.45
200	-2.21	-3.04	-2.62	-2.45
225	-2.22	-3.04	-2.62	-2.48

Obviously, the experimentally obtained values of  $\Xi$  fall in between the calculated bounds and lie closer to the untextured case. These findings are compatible with the texture results, demonstrating that a relatively weak {111}-fibre texture occurs (cf. Section: 4.3.4).

During heating, at temperatures above about 125°C, the stress-temperature relation is no longer linear and the magnitude of the measured stress is lower than expected on the basis of the thermoelasticity.

The stresses measured during the holding time at the annealing temperatures are shown in Fig. 4.7. Upon annealing at 175°C, the stress is almost constant. Annealing at temperatures of 200°C and 225°C leads to almost complete relaxation of the average stress.

#### 4.3.4. Texture analysis

The diffractograms shown in Figs. 4.4(a) and 4.4(b) reveal that both layers are textured: the intensities of the 111 reflections, compared to intensities of other reflections, exceed the figures expected for the case of untextured specimens drastically. A more detailed investigation has been based upon the analysis of {111} pole figures (cf. Section 4.2.3.3). It has been found that the as-prepared Cu and Pd layers are {111}-fibre textured, as revealed by the presence of maxima at  $\psi = 0^\circ$  and  $\psi = 70.53^\circ$  in the {111} pole figure sections (Fig. 4.8(a) and (b)). However, the texture is relatively broad: diffracted intensity for the 111 reflection can be found at all tilt angles  $\psi$ .

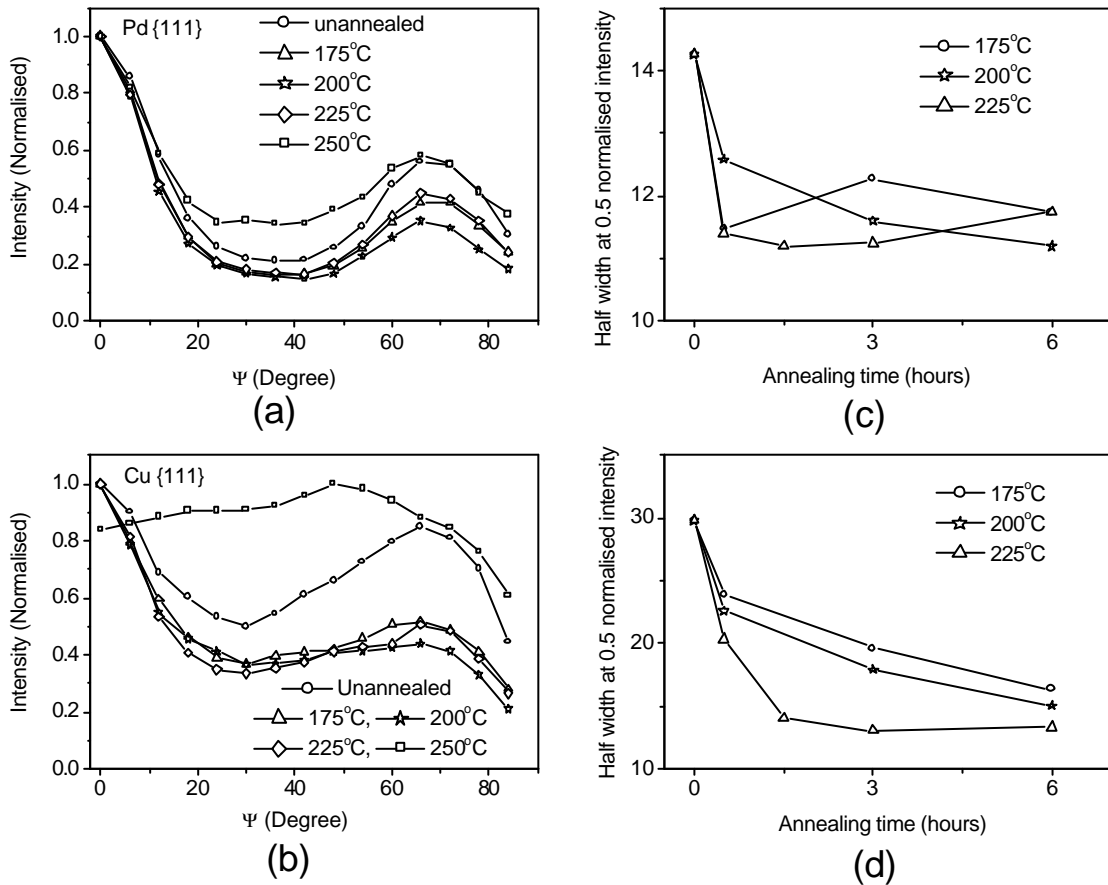


Fig. 4.8: {111} pole figure sections (a) for Pd and (b) for Cu from the specimens annealed at different temperatures for 6 hours annealing time. Also, pole widths have been plotted with annealing time at different annealing temperatures for (c) Pd 111 reflection and (d) Cu 111 reflection.

#### 4. Interdiffusion, phase formation and stress development in Pd-Cu thin film diffusion couples

---

Upon annealing at temperatures below 250°C, only minor texture changes occur. The width of the pole in the centre of the {111} pole figure decreases slightly (see Figs. 4.8 (c) and (d)). The effect is more pronounced for the Cu sublayer.

Also, {111}-fibre texture has been observed for Cu<sub>3</sub>Pd which does not change much with annealing time. At 250°C, the texture has been analysed for the Pd sublayer and a pole figure has also been measured by placing the detector at the position ( $2q$ ) of 110 reflection of CuPd phase. The texture of the Pd sublayer is comparable to results obtained at lower annealing temperatures (see Fig. 4.8(a)). The pole figure section in Fig. 4.8(b) suggests that the newly formed phase CuPd grows practically untextured.

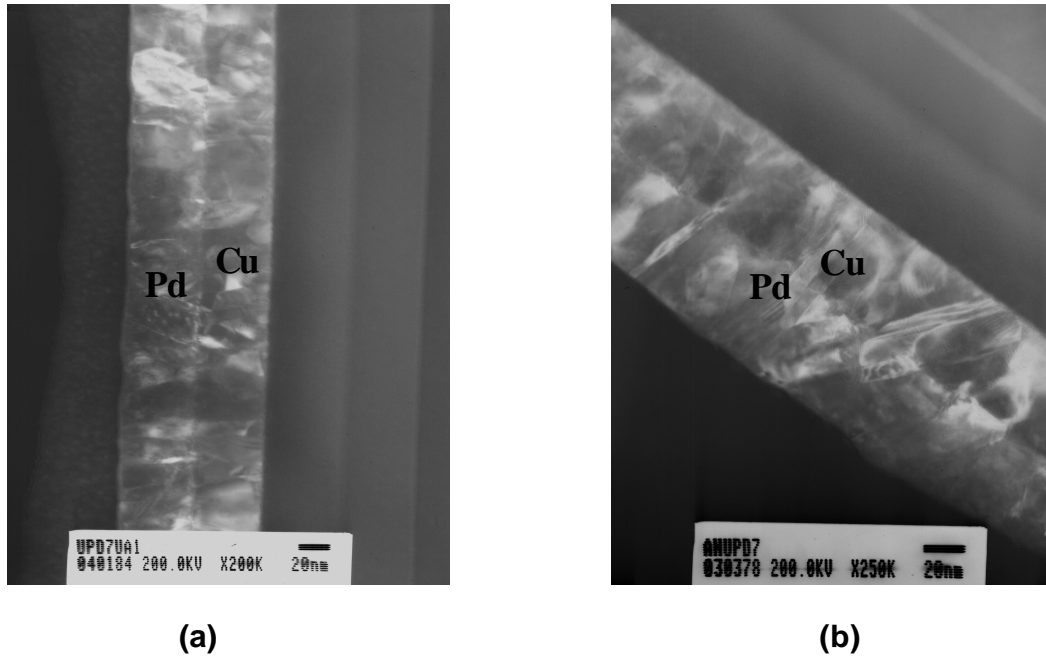


Fig. 4.9: (a) XTEM of an unannealed Pd-Cu bilayer. (b) XTEM of an annealed Pd-Cu bilayer, annealing temperature: 200°C, annealing time: 6 hours.

##### 4.3.5. Microstructure and selected area diffraction patterns

Cross-sectional TEM investigations have been performed both for the unannealed and the annealed specimens. Fig. 4.9(a) shows exemplary one of the cross-sectional micrographs of an unannealed specimen. It has been found from the inspection of a number of micrographs

#### 4. Interdiffusion, phase formation and stress development in Pd-Cu thin film diffusion couples

that a columnar microstructure prevails in both sublayers. However, a more irregular microstructure is also observed in some portions of the Cu sublayer. The interface of the two sublayers is clearly visible. The in-plane grain-sizes fall in the range from 10 nm to 25 nm (average: 22nm) for the Cu sublayer and in the range from 15 nm to 25 nm (average: 21 nm) for the Pd sublayer.

Up to 200°C annealing temperature, the interface of the two sublayers is still clearly visible (Fig. 4.9(b)). However, already after annealing at 200°C, a slight increase of about 5 nm to 6 nm of the average grain size has been noticed. Upon annealing at 225°C, the in-plane average grain size increases to about 26 nm for both the Cu and Pd sublayer. It appears that grains have grown normal to the interface (across the interface).

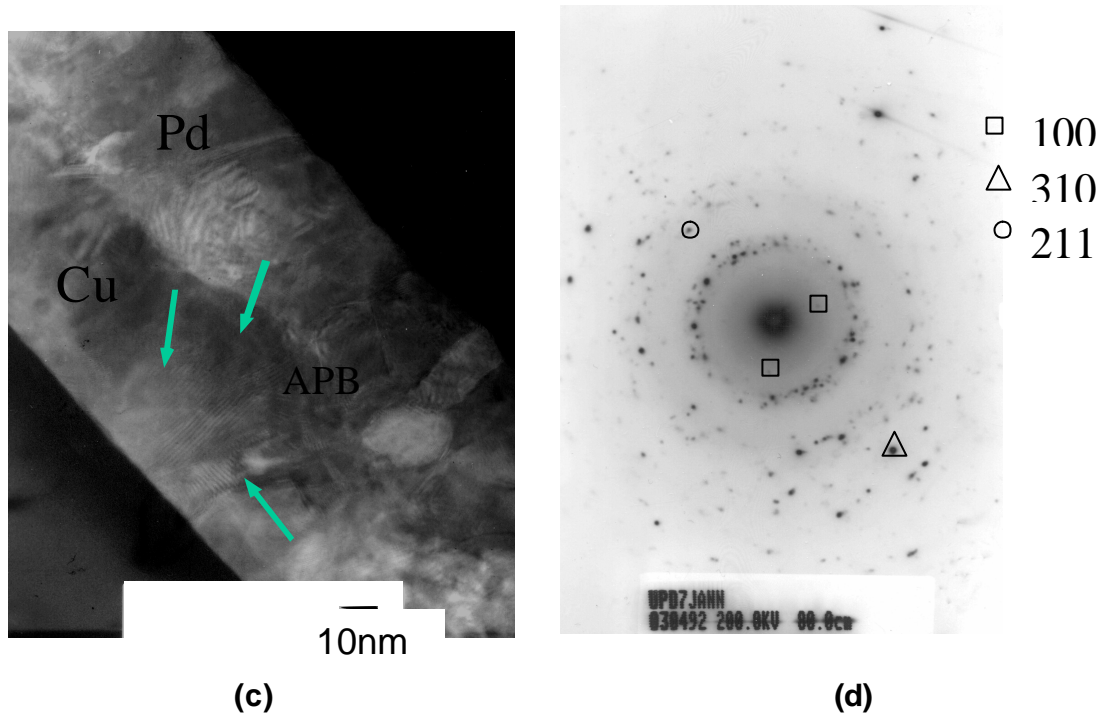


Fig. 4.9: (c) Antiphase boundaries from  $\text{Cu}_3\text{Pd}$  formed after annealing at 225°C. (b) SAD pattern of Pd-Cu bilayer after annealing at 250°C for 3 hours. CuPd reflections are shown.

High resolution TEM observation shows the presence of antiphase domain boundaries confirming the ordered phase formation (Fig. 4.9(c)). It has been noticed, that the initial interface is no longer clearly visible. After annealing at 250°C, neither the columnar microstructure nor the location of the initial interface can be observed. This indicates that



extensive interdiffusion has taken place, which is potentially accompanied by the migration of grain boundaries, extensive grain growth and the formation of new phases (see also Section 4.3.2).

Selected area diffraction (SAD) patterns of unannealed specimens show the presence of concentric diffraction rings only corresponding to pure Cu and pure Pd. After annealing at 250°C, 100, 211 and 310 reflections of CuPd have been identified unambiguously (see Fig. 4.9(d)). However, already after annealing at temperatures of 200°C (6 hours), additional diffraction spots (100 and 111 reflections of CuPd) have been observed. This indicates that, in principle, the onset of the formation of CuPd occurs already upon annealing at 200°C. However, it has been found by X-ray diffraction that CuPd grows with significant volume fraction only at elevated temperature (250°C). The onset of the CuPd phase formation at lower temperature has not been noticeable in the X-ray diffraction patterns due to (extremely) small volume fraction of CuPd and the severe overlap of some of the corresponding diffraction lines with diffraction lines of Cu and Cu<sub>3</sub>Pd.

## 4.4. Discussion

### 4.4.1. Phase formation

According to Pd-Cu equilibrium phase diagram [Subramanian and Laughlin (1990)],  $\text{Cu}_3\text{Pd}$  ( $a'$ , space group  $Pm\bar{3}m$ ),  $\text{Cu}_3\text{Pd}$  ( $a''$ , space group  $P4mm$ ) and  $\text{CuPd}$  (space group  $Pm\bar{3}m$ ) are in principle expected to form in the diffusion zone.

However, it has been found experimentally from X-ray diffraction phase analysis that the initial stage of diffusional intermixing is accompanied by the formation of  $\text{Cu}_3\text{Pd}$ . A distinction of the phases  $\text{Cu}_3\text{Pd}$  ( $a'$ ) and  $\text{Cu}_3\text{Pd}$  ( $a''$ ) was not possible (cf. Section 4.3.2) although from the available literature, formation of  $\text{Cu}_3\text{Pd}$  ( $a'$ ) is much more probable below 20at.% Pd composition as determined in the present case [Phase diagram and Jones and Sykes (1939)] Upon continued annealing,  $\text{Cu}_3\text{Pd}$  disappears and, simultaneously,  $\text{CuPd}$  grows. These findings suggest that not all phases expected from the phase diagram nucleate and grow simultaneously, i.e. a sequential phase formation occurs.

Sequential phase formation in sufficiently thin diffusion zones (as in thin film diffusion couples) has already been found experimentally and predicted theoretically in the past (see, for example, [Gösele and Tu (1982); Garcia *et al.* (2000); Heurle *et al.* (1997); Hodaj and Gusak (2004)]). As a rule, it is expected that, if the melting points of the two metals are sufficiently different, the first phases formed should be those with the highest concentration of the low melting point metal [Heurle *et al.* (1997)]. This expectation is met by the experimentally obtained results.

It has been found assuming a planar diffusion/reaction zone and neglecting the importance of nucleation problems that [see, for example, Gösele and Tu (1982)]:

- (i) either the formation of a second phase occurs after the phase formed first has reached a critical thickness and both phases then grow simultaneously or
- (ii) that the phase formed first grows until the supply of one of the components of the diffusion couple is exhausted and then, the second phase grows and the phase formed first shrinks.

However, in this work it has been found that  $\text{Cu}_3\text{Pd}$  forms first and, after exceeding a critical thickness,  $\text{CuPd}$  forms and grows while  $\text{Cu}_3\text{Pd}$  shrinks before either Cu or Pd have been fully consumed. Considering the potential relevance of nucleation problems, the non-planar

#### 4. Interdiffusion, phase formation and stress development in Pd-Cu thin film diffusion couples

---

structure of the diffusion/reaction zone (note that grain boundary diffusion is a dominant diffusion process) and the very small spatial extension of the diffusion zone (involving the occurrence of steep stress gradient), it can be anticipated that theoretical expectations based on the assumptions of planar reaction fronts and the unimportance of nucleation problems are not met here experimentally. Similar results have been obtained for example by Tu & Berry, (1972) for the Cu-Au thin film diffusion couples.

Also the following thermodynamics reasoning concerning specific interfacial energies (energy /area) supports that Cu<sub>3</sub>Pd should form first. Before annealing, there was only Pd/Cu interface and the interfacial energy ( $g_{<Pd>-<Cu>}$ ) ( presented in Table 4.4) has been calculated using the average surface energies of Pd ( $g_{<Pd>}$ ) and Cu ( $g_{<Cu>}$ ) from the following equation applicable in general [ Benedictus *et al.* (1996) ]:

$$g_{<A>-<B>} = \frac{\Delta H_{A \text{ in } B}^{\text{interface}}}{C_0 V_A^{\frac{2}{3}}} + \frac{1}{3} \left( \frac{g_{<A>} + g_{<B>}}{2} \right) \quad (4.6)$$

where, A is Pd and B is Cu.  $\Delta H_{A \text{ in } B}^{\text{interface}}$  ( $\Delta H_{Pd \text{ in } Cu}^{\text{interface}} = -62 \text{ KJ / mole}$ ) [Boer *et al.*, (1989)] is the increase of enthalpy per mole of Pd atoms due to the interaction with Cu atoms at the interface.  $V_A$  is the molar volume of A atoms ( $V_{Pd} = 8.91 \times 10^{-6} \text{ m}^3 / \text{mole}$ ).  $C_0$  is a constant which has been taken as  $4.5 \times 10^8$  [Benedictus *et al.* (1996)]. After annealing, the formation of either Cu<sub>3</sub>Pd ( $g_{<Cu_3Pd>}$ ) or CuPd ( $g_{<CuPd>}$ ) involves the creation of new interfaces: Pd/Cu<sub>3</sub>Pd/Cu or Pd/CuPd/Cu, respectively. The associated interfacial energies have been estimated from the following equation [Benedictus *et al.* (1996)]

$$g_{<A>-<AB>} = \frac{F_B^A \Delta H_{A \text{ in } B}^{\text{interface}}}{C_0 V_A^{\frac{2}{3}}} + \frac{1}{3} \left( \frac{g_{<A>} + g_{<AB>}}{2} \right) \quad (4.7)$$

Where, A (or B) can be either Pd or Cu and <AB> can be either Cu<sub>3</sub>Pd or CuPd.  $F_B^A$  is the degree to which A atoms are surrounded by the ‘B’ atoms. This can be calculated from the following equation [Benedictus *et al.* (1996)]:

#### 4. Interdiffusion, phase formation and stress development in Pd-Cu thin film diffusion couples

$$F_B^A = \frac{(1 - c)V_B^{\frac{2}{3}}}{cV_A^{\frac{2}{3}} + (1 - c)V_B^{\frac{2}{3}}} \quad (4.8)$$

where,  $c$  is the mole fraction of A atoms.  $g_{\langle Cu_3Pd \rangle}$  and  $g_{\langle CuPd \rangle}$  have been calculated as  $1953 \text{ mJ/m}^2$  and  $2026 \text{ mJ/m}^2$  respectively. Resulting interfacial energies have been summarised in Table 4.4. It can be observed that  $g_{\langle Pd \rangle - \langle Cu_3Pd \rangle}$  is much less than  $g_{\langle Pd \rangle - \langle CuPd \rangle}$ . Thus, energetically, the formation of  $Cu_3Pd$  in the diffusion zone is more favourable than the formation of  $CuPd$ , at least in an initial stage, where the energetics are largely controlled by the interface energies and not by volume contributions.

Table 4.4: Formation of new interfaces and associated energies.

Surface energy Cu	Surface energy Pd	Starting interface	Pd/Cu <sub>3</sub> Pd/Cu New interface formation		Pd/CuPd/Cu New interface formation	
$g_{\langle Cu \rangle}$	$g_{\langle Pd \rangle}$	Interface energy Pd/Cu	Interface energy Pd/Cu <sub>3</sub> Pd	Interface energy Cu <sub>3</sub> Pd/Cu	Interface energy Pd/CuPd	Interface energy CuPd/Cu
$\text{mJm}^{-2}$	$\text{mJm}^{-2}$	$g_{\langle Pd \rangle - \langle Cu \rangle}$ $\text{mJm}^{-2}$	$g_{\langle Pd \rangle - \langle Cu_3Pd \rangle}$ $\text{mJm}^{-2}$	$g_{\langle Cu \rangle - \langle Cu_3Pd \rangle}$ $\text{mJm}^{-2}$	$g_{\langle Pd \rangle - \langle CuPd \rangle}$ $\text{mJm}^{-2}$	$g_{\langle Cu \rangle - \langle CuPd \rangle}$ $\text{mJm}^{-2}$
1825	2060	325	436	549	531	448

The growth kinetics of  $Cu_3Pd$  at an annealing temperature of  $225^\circ\text{C}$  have been analysed by taking the integrated intensity of the  $Cu_3Pd$  111 reflection (measured at  $\gamma = 0^\circ$ ) as a measure for the volume fraction of  $Cu_3Pd$  (it has been confirmed that the texture of  $Cu_3Pd$  is also of the  $\{111\}$  type and does not change significantly during annealing). The results are shown in Fig. 4.10(a). The amount of  $Cu_3Pd$  formed is proportional to  $t^n$ , where the exponent  $n$  has been determined as  $0.56 \pm 0.03$ . This value is very close to 0.5 indicating that the growth kinetic of  $Cu_3Pd$  phase is diffusion-controlled, similar to parabolic growth kinetics in bulk materials due to lattice diffusion [Reed-Hill (1973)]. The growth kinetics of  $CuPd$  at an annealing temperature of  $250^\circ\text{C}$  have been analysed by taking the integrated intensity of the

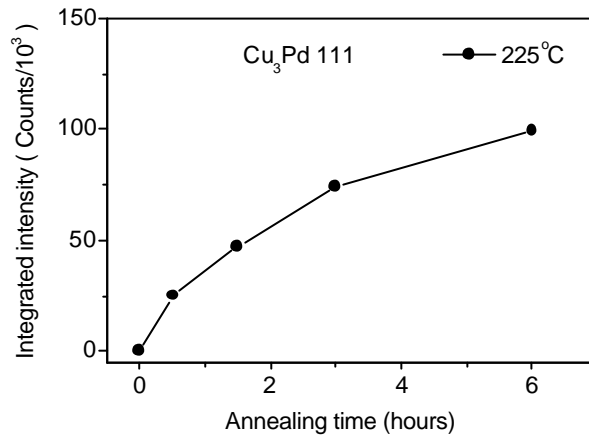
#### 4. Interdiffusion, phase formation and stress development in Pd-Cu thin film diffusion couples

---

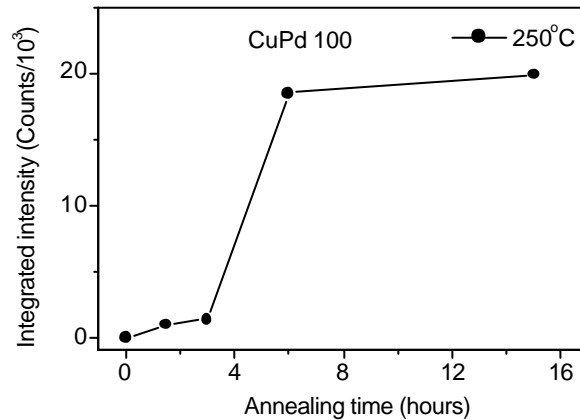
CuPd 100 reflection (measured at  $\psi = 0^\circ$ ) as a measure for the volume fraction of CuPd (it has been found that CuPd grows practically untextured during annealing). The results are shown in Fig. 4.10(b).

After an increase at low rate, a sudden drastic increase of the amount of CuPd has been found after annealing for 3 hours. The limited number of data points does not allow a reliable determination of the growth kinetics. It can only be speculated that two growth regimes (potentially reaction controlled / diffusion controlled) exist.

Finally, it has to be mentioned that at 175°C, and up to 200°C, 0.5 hours annealing conditions, no phase formation has been observed due to slow kinetics of the diffusion process.



(a)



(b)

Fig. 4.10: Integrated intensities have been plotted with annealing time for (a) 111 reflection of Cu<sub>3</sub>Pd at 225°C and (b) 100 reflection of CuPd at 250°C.

#### 4.4.2. Stress analysis

##### 4.4.2.1. Discussion of stress results

Diffraction stress analysis at room temperature (25°C) before and after annealing (see Fig. 4.5) suggests that annealing leads to a tensile stress contribution in both the Pd and Cu layers increasing with increasing annealing time and temperature. However, the direct interpretation of the results of the diffraction stress measurements (as stress change resulting from the

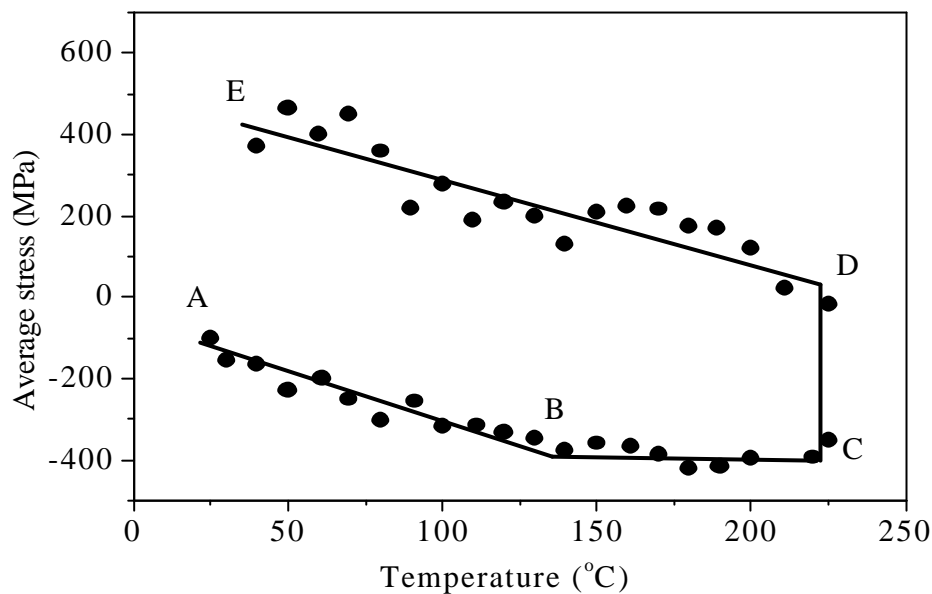


Fig. 4.11: Schematic of the thermal cycling (heating, annealing and cooling cycles) during annealing at 225°C.

annealing) is hindered by the fact that thermal stresses created during heating and cooling may not be accommodated purely elastically.

To overcome this problem, the results of the wafer-curvature measurements can be employed. Fig. 4.6 shows the average stress of the bilayer during the heating segment of a cycle with an annealing temperature of 225°C. From room temperature up to about 125°C, a linear region exists. Above 125°C, the curve shows non-linear behaviour with an increasing slope approaching approximately zero. This deviation from a purely elastic behaviour may be due to the onset of plastic deformation. This reasoning is supported by the following consideration: the heating rate was set to 25°Cmin<sup>-1</sup>. Thus, the time for heating from 125°C to the final annealing temperature of 225°C was only about 4min. During this short period, neither

#### 4. Interdiffusion, phase formation and stress development in Pd-Cu thin film diffusion couples

---

significant interdiffusion nor considerable grain growth can take place. This leaves plastic deformation as the only mechanism of stress relaxation. In the following discussion, consider the schematic diagram of a complete thermal cycle Fig. 4.11 and the abbreviations introduced therein. The stress values in the individual layers at the beginning of the annealing segment (point C in Fig. 4.11) have been calculated as follows: Known are the growth stresses in the individual layers at room temperature from diffraction stress measurements (point A in Fig. 4.11). It was then assumed that the stresses in both sublayers are accommodated purely elastically up to 125°C (point B in Fig. 4.11) and that no further stress changes occur upon heating from 125° up to the final annealing temperature (point C in Fig. 4.11). This assumption is based on the observation of (approximately) plateau levels (see Fig. 4.6) in the temperature range of 125°C to the annealing temperature for all annealing cycles (i.e., in between the points B and C in Fig. 4.11). For calculating the stresses in the individual layers in the points B (or C), assumptions about the biaxial moduli of the layers have to be made. In the present case, the arithmetic averages of the elastic moduli for polycrystalline and perfectly {111}-fibre textured specimens have been chosen, considering that the texture has {111}-fibre character but is neither very strong nor very sharp. On the basis of these assumptions, the average thermoelastic slope would be  $2.62 \text{ MPaK}^{-1}$  (see Appendix 4A and Table 4.3). This value matches well with the experimentally obtained values (e.g.  $2.48 \text{ MPaK}^{-1}$ , as determined from the fit shown in Fig. 4.6. The stress results of the calculations have been summarised in Table 4.5.

Table 4.5: Total stress in Cu and Pd layers at point B/C (Fig. 4.11), just before annealing.

Growth stress in Pd (MPa) at point A (MPa)	Growth stress in Cu (MPa) at point A (MPa)	Thermal stress in Pd at point B (MPa)	Thermal stress in Cu at point B (MPa)	Total stress in Pd at point B/C (MPa)	Total stress in Cu at point B/C (MPa)
-332	+131	-194	-328	- 526	-197

#### 4. Interdiffusion, phase formation and stress development in Pd-Cu thin film diffusion couples

The stresses in the layers upon completion of the annealing segment (point D in Fig. 4.11) can be back-calculated from the stresses measured by diffraction at room temperature (point E in Fig. 4.11) and the calculated tensile thermal stresses generated in the individual layers upon cooling to room temperature. It has been assumed that the full thermal stresses are accommodated elastically during cooling. The results for stresses in points D and E have been presented in Table 4.6.

Table 4.6: Stress in Cu and Pd layers just after annealing (immediately after interdiffusion).

Annealing temperature (°C) for 6 hours annealing time	Stress in Pd layer			Stress in Cu layer			Average Stress at point 'D' (after annealing) (MPa)
	Thermal stress at point 'E' (MPa)	Stress measured by XRD at RT (MPa)	Stress at point 'D' In Fig. 4.11 (MPa)	Thermal stress at point 'E' (MPa)	Stress measured by XRD at RT (MPa)	Stress at point 'D' in Fig. 4.11 (MPa)	
175°C	288	-100	-388	497	450	-47	-217.5
200°C	335	130	-205	583	780	197	-4.0
225°C	382	0	-382	671	912	241	-70.5

The (seeming) inequivalence of the treatment for the heating and cooling cycle (i.e. only partial elastic accommodation of thermal stresses upon heating, but full elastic accommodation of thermal stresses upon cooling) is supported by two arguments: (i) for all cooling cycles, the thermoelastic slope was never smaller than the slope obtained from the heating segment (part A-B). However, large data scatter was found during cooling when the temperature approached room temperature, rendering the results poorly reliable. (ii) Even though large stresses occur, in particular in the Cu layer, in the cooling segment, the largest stresses occur at room temperature and not at elevated temperature (about 125° C), thus making the occurrence of plastic deformation less likely.



#### 4. Interdiffusion, phase formation and stress development in Pd-Cu thin film diffusion couples

---

The reliability of the calculations adopted for the cooling segment can be judged by comparing the measured (by wafer curvature in Fig. 4.7 upon completion of annealing) and calculated (last column in Table 4.6, back-calculated from diffraction stress analysis at room temperature)

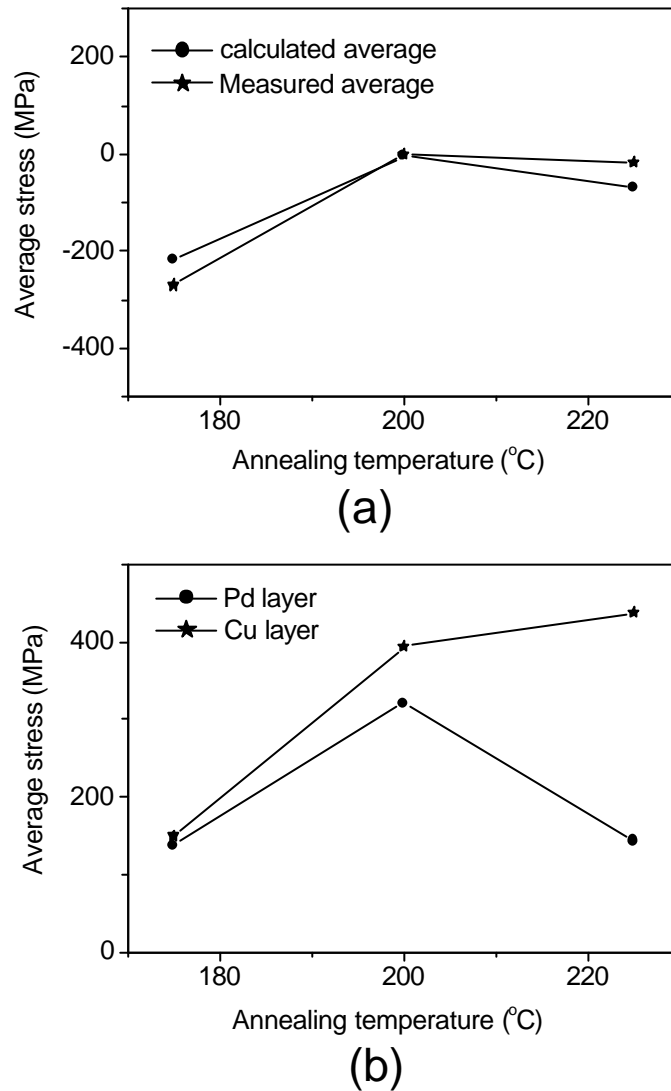


Fig. 4.12: (a) Calculated average stress at point 'D' (also shown in Table 4.5) and the measured average stress by wafer curvature (see Fig. 4.7) are in good agreement.

(b) Tensile stress generated in Cu and Pd layers during interdiffusion

average stress values at point D (see Fig. 4.12(a)). Obviously, a satisfactory agreement occurs. By comparing the stresses in the individual layers in points C (from Table 4.5) and D (from Table 4.6), the stress contribution arising from annealing can now be determined. The

#### 4. Interdiffusion, phase formation and stress development in Pd-Cu thin film diffusion couples

---

results have been presented in Fig. 4.12(b). Note that the stresses given in Fig. 4.12(b) are relative stress changes and not absolute stress values. It can thus be concluded that annealing leads to the generation of a tensile stress contribution in both sublayers. The potential sources of stresses will be discussed next.

##### 4.4.2.2. Discussion of stress generation during annealing

Various mechanisms which can alter the stress state during annealing can be conceived. In the following, all relevant mechanism will be briefly discussed. Then, an attempt will be made to identify the dominant mechanism relevant for the specimens investigated.

##### *Interdiffusion:*

During interdiffusion, stresses can be generated due to differences in the partial molar volumes and/or differences in the diffusion fluxes of the diffusing species. The effect of differences in the partial molar volumes will be discussed first.

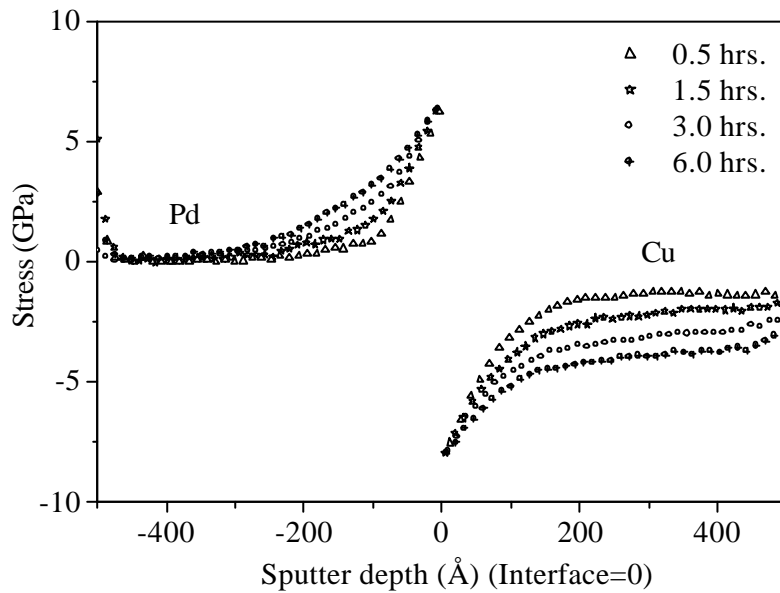


Fig. 4.13: Diffusion induced stress profiles due to partial molar volume difference at annealing temperature 225°C.

Consider the case of interdiffusion in a binary diffusion couple. In a volume element of the couple, a change of concentration would result in an associated volume change of the volume element if the partial molar volumes of the diffusion species are different and if the volume

#### 4. Interdiffusion, phase formation and stress development in Pd-Cu thin film diffusion couples

---

element would not be constrained by its surroundings. In a thin film diffusion couple attached to a rigid substrate, however, the extension of the volume element parallel to couple/substrate interface is constraint and thus stress is generated. The calculation of the stresses associated with concentration changes in a thin film diffusion couple attached to a rigid substrate is straightforward and has been outlined in the Appendix 4B.

As an example, the (in-plane) stress-depth profiles for the specimens annealed at 225°C have been gathered in Fig. 4.13.

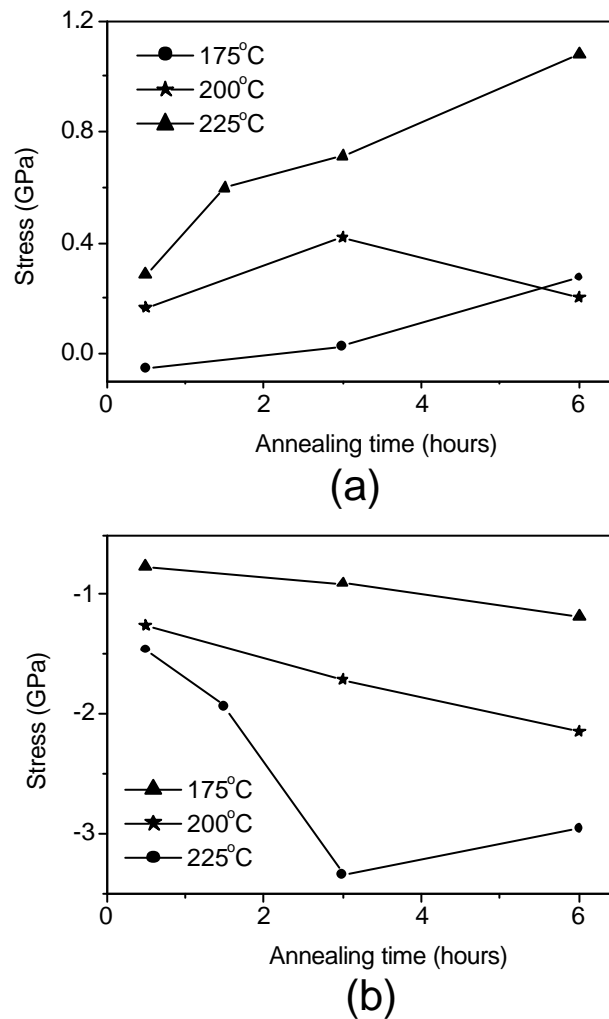


Fig. 4.14: Calculated average diffusion induced stress at various annealing temperatures (a) for Pd and (b) for Cu layers.

The averages stresses in the individual sub-layers as a function of time and temperature have been summarised in Fig. 4.14 (a) and (b). It follows that interdiffusion is accompanied by the

#### 4. Interdiffusion, phase formation and stress development in Pd-Cu thin film diffusion couples

---

generation of tensile stresses in the Pd sublayer ('larger Pd atoms are replaced by smaller Cu atoms') and of compressive stresses in the Cu sublayer ('smaller Cu atoms are replaced by larger Pd atoms'). Note that the calculated stresses can be in the order of some hundred/thousand MPa. This mechanism thus should contribute considerably to the stress evolution of the investigated specimens.

Next, the effect of differences in the diffusion fluxes of the diffusing species will be discussed. In this context, even qualitative predictions are difficult. In principle, stresses would result as a consequence of a net vacancy flux due to differences in the intrinsic diffusion coefficients of the two species. However, the following uncertainties fully hinder quantitative and even qualitative predictions: (i) for the thin film specimens investigated, intrinsic diffusion coefficients of Cu and Pd are not known. (ii) The rate at which vacancies can be created and annihilated in the diffusion zone is unknown. (iii) For diffusion fluxes through grain boundaries, the vacancy flux cannot be estimated. Thus, the effect of differences in the diffusion fluxes cannot be predicted.

##### *Phase formation:*

In principle, the formation of new phases in a specimen can lead to the generation of both tensile and compressive stresses if the phase transformation is associated with volume changes. In the present case, the unit cell volumes of  $\text{Cu}_3\text{Pd}$  (disordered) and  $\text{Cu}_3\text{Pd}$  (ordered) have to be compared (note that differences in the partial molar volumes of Cu and Pd have already been taken care of in the previous subsection; see above). Based on literature data (see, for example, Hirabayashi and Ogawa 1957) it can be concluded that no considerable volume effect is associated with the ordering. Thus, the formation of ordered  $\text{Cu}_3\text{Pd}$  should not lead to considerable stress changes in the investigated specimens.

##### *Grain growth:*

Grain growth can be a major source of tensile stress generation in thin films. The driving force for grain growth is the reduction of the total grain boundary energy. Grain growth results in the shrinkage of the film volume due to the reduction of total interfacial area which in turn generates tensile stress within the film if the film is constrained by a substrate. In this case, the maximum achievable grain size is limited by a balance between the strain energy

#### 4. Interdiffusion, phase formation and stress development in Pd-Cu thin film diffusion couples

---

and the interfacial energy (see Chaudhari (1971); see also Doerner and Nix (1988)). A model developed by Chaudhari (1971) and extended by Doerner and Nix (1988) allows the calculation of the rate of grain growth and stress development and the limiting size and stress values. The limiting grain sizes and stress values for an initial grain size of 20 nm are 35 nm and 3 GPa for Cu and 38 nm and 3.4 GPa for Pd, respectively. For these calculations, the grain boundary energies ( $\sim 1/3$  of the surface energy of a crystal) ( $0.6 \text{ J/m}^2$  for Cu and  $0.68 \text{ J/m}^2$  for Pd; see Boer *et al.* (1989)), and the biaxial moduli (see Appendix 4A) have been used. Note that these values would only be reached in equilibrium. However, reaching equilibrium may take a long time, depending on the temperature.

The estimation of the kinetics of grain growth and stress generation requires an assumption with respect to the activation energy for grain-boundary migration. Doerner and Nix (1988) suggested to use one third of the lattice self diffusion activation energy. However, this choice is quite arbitrary. It turns out, that the growth rate is highly sensitive to the choice of the activation energy and thus, quantitative predictions of the growth kinetics are of poor reliability. The situation is complicated by the fact that interdiffusion and phase formation occur simultaneously with the grain growth, which could enhance or suppress the growth process (see, for example, King and Harris (1994)). Also diffusion-induced grain-boundary migration can suppress grain growth and has been observed in Cu-Pd thin film diffusion couples (see Nakahara *et al.* (1983) and King & Harris (1994)).

For the specimens investigated, the initial grain sizes are about 20 nm for both sub-layers. After annealing, a slight increase of the grain size of about 5-7 nm had been noticed for specimens annealed at temperatures at and above  $200^\circ\text{C}$ . This observation is also reflected by the texture analysis, which indicated slight texture sharpening upon annealing (see Section 4.3.4). In conclusion, these findings suggest that grain growth should lead to considerable tensile stress generation in both sublayers at temperatures of  $200^\circ\text{C}$  and above. Adopting the above discussed model, the observed increase of the grain size would result in tensile stresses of about 1.6 GPa for both sublayers.

#### *Excess vacancy annihilation and shrinkage of grain-boundary (gb) voids*

The vacancy concentration in thin films after their production can deviate significantly from its equilibrium value. The annihilation of excess vacancies (at grain boundaries oriented

#### 4. Interdiffusion, phase formation and stress development in Pd-Cu thin film diffusion couples

---

perpendicularly to the film surface) is a source of stress generation due to associated volume changes, if the film is attached to a substrate. For films deposited at room temperature, however, the stress generation due to vacancy annihilation should be insignificant (for details, see Doerner and Nix (1988)).

The growth of a thin film from the vapour phase is usually associated with the formation of pores or voids at the grain boundaries. The shrinkage of the voids in grain boundaries (oriented perpendicularly to the film surface) also leads to the generation of tensile stress for films on substrates (for details, see Nix (1988)). The stress associated with the shrinkage of gb voids cannot be estimated without making estimates of the volume fraction of voids. In principle, considerable tensile stresses could be generated (for details, see Doerner and Nix (1988)).

##### *Plastic deformation:*

For the last several years, yield stresses of thin films have been investigated extensively. These investigations have revealed that the film thickness, the grain size and the temperature are significant factors affecting the strength of films (Nix, (1989); Arzt (1998); Weiss (2001)). However, quantitative predictions of the yield stress and yielding kinetics, in particular at elevated temperatures, still are a matter of debate. The following two processes, which could be relevant for stress changes in the specimens investigated, can be conceived: (i) thermally activated dislocation glide (Flinn (1987)) and (ii) constraint diffusional creep (Gao *et al.* (1999)). However, quantitative descriptions are difficult, if not impossible. It can only be noted that plastic deformation in any case can only lead to a relaxation of stresses towards zero. We suggest that plastic deformation is responsible for the stress development in the heating segment (Fig. 4.6 and Fig. 4.11).

##### *Concluding remarks:*

From the above discussion it is clear, that the net (observed) stress change can result from a combination of a number of, possibly competing, sources of stress generation. For the Cu sublayer, the stress changes its sign during annealing. As a consequence, at least one mechanism leading to tensile stresses must be operative. For the Pd sublayer, on the other hand, the stress does not change its sign; rather, the tensile stress contribution arising from annealing relaxes the compressive stress towards zero stress.

#### 4.5. Summary

- Annealing of Pd-Cu thin film (thickness of each sublayer: 50nm) diffusion couples at temperatures in the range of 175°C to 250°C leads to considerable diffusional intermixing.
- From AES depth profiling it has been found that a considerable plateau concentration develops on the Cu side of the couple but not on the Pd side.
- It has been found on the basis of X-ray diffraction phase analysis that diffusional intermixing is accompanied by the sequential formation of new phases. First, an ordering of the solid solution leads to the formation of Cu<sub>3</sub>Pd at temperatures of 200°C and 225°C. At 250°C, CuPd forms: after a coexistence of CuPd and Cu<sub>3</sub>Pd at short annealing times (up to 1.5 hours), CuPd grows at the cost of Cu<sub>3</sub>Pd.
- The crystallographic texture of the specimens has been investigated by X-ray diffraction pole figure measurements. After deposition, both sublayers have a weak {111}-fibre texture. Diffusion annealing results in a slight texture sharpening.
- The microstructural investigation by transmission electron microscopy reveals columnar grains of Cu and Pd in all unannealed specimens. Diffusion annealing also leads to a moderate increase of the average grain sizes in both sublayers from about 20 nm to about 26 nm.
- The stress evolution was investigated by X-ray diffraction stress analysis (ex-situ) in combination with wafer curvature measurements (in-situ). Upon annealing, tensile stresses are generated in both sublayers. Important sources of stress can be differences in partial molar volumes of the diffusing species, Kirkendall effect, grain growth and plastic deformation. This is the first time that stress changes resulting from interdiffusion have been monitored in-situ.

## Appendix 4A

### 1. Estimation of thermoelastic slopes presented in Table 4.3

In the present work both Cu and Pd have {111} fiber texture which is neither sharp nor strong. In view of this, the biaxial modulus ( $M_i$ ) of Cu (or Pd) film has been calculated as arithmetic average of the biaxial modulus of perfectly polycrystalline Cu (or Pd) [<http://www.webelements.com/>] and that of perfect {111} fiber textured Cu (or Pd). Biaxial modulus of {111} fiber textured Cu and Pd have been calculated from the following formula [Nix (1989)]:

$$M_{\{111\}} = \frac{6C_{44}(C_{11} + 2C_{12})}{C_{11} + 2C_{12} + 4C_{44}} \quad (4A1)$$

where,  $C_{11}$ ,  $C_{12}$  and  $C_{44}$  are the elastic stiffness for single crystalline Cu or Pd [Smithell's metal reference book, chap.15, 7<sup>th</sup> Editon].

For Pd:  $C_{11} = 2.24 \times 10^{11} \text{ Pa}$   $C_{12} = 1.73 \times 10^{11} \text{ Pa}$  and  $C_{44} = 0.72 \times 10^{11} \text{ Pa}$  and

For Cu :  $C_{11} = 1.7 \times 10^{11} \text{ Pa}$   $C_{12} = 1.23 \times 10^{11} \text{ Pa}$  and  $C_{44} = 0.76 \times 10^{11} \text{ Pa}$

The calculated biaxial moduli for Cu and Pd are presented in Table 4A. Thermoelastic slopes for the diffusion couples annealed at various temperatures (presented in Table 4.3 in section 4.3.3.2) have been calculated using the following formula:

$$\Xi = \frac{M_{cu} \times (a_{cu} - a_{substrate}) + M_{pd} \times (a_{pd} - a_{substrate})}{2} \quad (4A2)$$

where  $M_i$  are the biaxial moduli and  $a_i$  are the coefficients of thermal expansion of the individual layers and the substrate. Thermal expansion coefficients of Pd, Cu and Si have been taken from the literature [<http://bell.mma.edu>, <http://www.webelements.com/>]. For example, at 498K,  $a_{Cu} = 1.821 \times 10^{-5} / K$ ,  $a_{Pd} = 1.151 \times 10^{-5} / K$  and  $a_{Si} = 3.62 \times 10^{-6} / K$ .

For the diffusion couple consisting of perfectly polycrystalline Pd and Cu, corresponding values of  $M_{Cu}$  (or  $M_{Pd}$ ) from Table 4A have been used during calculation. Similarly, thermoelastic slopes for the diffusion couple consisting of perfect {111} fiber textured Cu and Pd have been calculated using the  $M_{Cu}$  (or  $M_{Pd}$ ) value for {111} fiber textured specimen from Table 4A. Thus calculated thermoelastic slopes are already presented in Table 4.3. This can be easily calculated from the data in Table 4.3, that at any annealing temperature, the



#### 4. Interdiffusion, phase formation and stress development in Pd-Cu thin film diffusion couples

arithmetic average of the thermoelastic slopes for the perfect polycrystalline case and that for the {111} fiber textured case is close to 2.6 MPa/K which is very close to the experimental slopes (Table 4.3) determined from the heating segments corresponding to different annealing temperatures.

Therefore, this results also supports the calculation of biaxial moduli for weekly textured Cu and Pd.

#### 2. Calculation of thermal stress in Cu and Pd for the determination of stresses at points A, B, C, D and E (Fig. 4.11).

Also, values of thermal stresses ( $s_{th}$ ) generated during heating (from room temperature (RT) up to various temperatures tabulated below in Table 4A) and cooling (from any tabulated temperature to RT ) have been calculated from the equation 4A3 using these average biaxial moduli of Cu and Pd films and they are presented in Table 4A.

$$s_{\parallel th} = M_i (a_{film} - a_{substrate})(T_a - T_m) \quad (4A3)$$

Table 4A : Calculation of thermal stresses in Pd and Cu layers.

Biaxial Modulus $M_i$ (GPa)	Cu	Pd	Temperature $T_a$ (K)	$s_{\parallel th}$ in Pd (MPa)	$s_{\parallel th}$ in Cu (MPa)
Polycrystalline	196.97	198.36	398 (125°C)	194	328
Perfect {111} Fiber textured	262.8	285.93	448 (175°C)	288	382
Average value (used for the calculation of thermal stress)	230	242	473 (200°C)	335	583
			498 (225°C)	382	671

$T_m$  is the temperature at which the stress was measured (room temperature 25°C). During heating thermal stress will be compressive (− sign before stress values in Table 4A) and during cooling thermal stress will be tensile (+ sign before stress values in Table 4A). Tensile stresses are generated during cooling because, the metallic films shrink more than the

#### 4. Interdiffusion, phase formation and stress development in Pd-Cu thin film diffusion couples

---

substrate and the substrate will try to stretch the films to fit them in its size. During heating the opposite will happen.

### Appendix 4B

#### Diffusion induced stress due to partial molar volume difference of the diffusing species

This kind of stress also has been named as chemical stress in the literature [Li (1978)]. Stress caused by concentration inhomogeneity is similar to those caused by temperature gradients in an otherwise unstressed body. Timoshenko has derived an expression for the stresses in a thin plate in which the temperature varies only along the thickness of the plate (Y) and temperature is independent of X and Z coordinate [Timoshenko and Goodier]. In the present work, interdiffusion between Pd and Cu is taking place in the direction normal to the films surfaces (Y say) whereas X and Z directions are constrained by the thick and rigid substrate (semi-infinite). Therefore, after annealing a continuous (assuming) film results due to interdiffusion with varying concentration of Cu (or Pd) along the thickness (Y direction) of the film. In Timoshenko's equation, the thermal strain can be replaced by the corresponding compositional strain in the continuous film due to concentration distribution which is the following:

$$\frac{1}{3} \left( \frac{V_m \{ X_{Pd}(y) \} - (V_m)_{ref.}}{(V_m)_{ref.}} \right) \quad (4B1)$$

Where, the strain expression corresponds to mean strain (assuming a hydrostatic strain component).  $V_m\{X_{Pd}(y)\}$  is the molar volume of the system at a particular palladium composition expressed in mole fraction ( $X_{Pd}$ , ( $= 1 - X_{Cu}$ )) which is obviously a function of 'y' along the thickness of the continuous film. It is also known that the molar volume ( $V_m$ ) varies linearly with composition in Cu-Pd binary system following Vegard's law [Soutter *et al.* (1971)]. The following expression for the molar volume has been obtained from the lattice parameter data of disordered Cu-Pd solid solution with varying palladium composition:

$$V_m\{X_{Pd}(y)\} = (7.12811 + 1.7878X_{Pd})\text{cm}^3/\text{mole} \quad (4B2)$$

$(V_m)_{ref.}$  is the molar volume in the reference state (before diffusion) which is different for Cu ( $7.12\text{cm}^3/\text{mole}$ ) and Pd ( $8.91\text{cm}^3/\text{mole}$ ). Therefore, considering the bilayer films on a rigid

#### 4. Interdiffusion, phase formation and stress development in Pd-Cu thin film diffusion couples

---

substrate (as in the present case) and thereby neglecting the terms associated with the tensile stress (due to relaxation) and stress causing the bending of the diffusion couple in Timoshenko's equation, the diffusion induced biaxial stress ( $\mathbf{s}_{xx} / \mathbf{s}_{zz}$ ) within the continuous film can be written as follows:

$$\mathbf{s}_{xx} = \mathbf{s}_{zz} = -\frac{1}{3}M \left( \frac{V_m \{X_{Pd}(y)\} - (V_m)_{ref.}}{(V_m)_{ref.}} \right) \quad (4B3)$$

$M$  has been taken as 198GPa which is the precisely the calculated average of the biaxial moduli for polycrystalline Cu and Pd. Therefore, for each annealing time  $t$ , it is possible to calculate a stress profile from equation (4B3) varying with  $y$ . Stress calculations have been performed numerically for all diffusion couple annealed in the temperature range 175°C-250°C using the experimentally obtained Pd sputter-depth profiles from AES (Figs. 4.1(a)-(d)). For the stress calculation, the interface in all the AES sputter-depth profiles was so adjusted that 50at.% Pd (or 50at.% Cu) corresponds to 500 Å. Example of the calculated diffusion induced stress profiles are shown in Fig. 4.14(a) for 225°C annealing temperature for different annealing time where the interfacial position (originally at 500Å) has been set to zero in all stress profiles. However, it can be noted that the absolute values of the diffusion induced stress (at each depth) can be erroneous as the instrumental effects (smearing of the Pd (or Cu) concentration profiles even in AES sputter-depth profile for unannealed specimen) in AES sputter-depth profiles of annealed specimens (Figs. 4.1(a)-(d)) are not corrected (deconvolution and extraction of real concentration-depth profile). This is the reason, stress profile and the corresponding average stress for Pd (or Cu) have also been calculated corresponding to the sputter-depth profile of unannealed specimen. Then this average stress for Pd (or Cu) of unannealed specimen has been subtracted linearly from the average stress value for Pd (or Cu) layer calculated for the annealed specimen for a particular annealing time and temperature (presented in Figs. 4.14(a) and 4.14 (b)).

**Acknowledgements:** We would like to thank Dr P. Wellner and Dr T. Wübben (Max Planck Institute for Metals Research, Stuttgart, Germany, Dept. of Prof. Arzt) for their assistance in performing the wafer curvature measurements.

## 5. Kurzfassung der Dissertation in deutscher Sprache

### 5.1. Einleitung und Überblick

Dünne Schichten sind von großer technologischer Bedeutung, z.B. als Schutzschichten oder in der Mikroelektronik. Diffusion und Phasenumwandlungen können in dünnen Schichten bereits bei viel niedrigeren Temperaturen ablaufen als in 'makroskopischen' Systemen, da dünne Schichten eine große Dichte von kristallinen Defekten und Korngrenzen enthalten können, die zu einer starken Beschleunigung von Diffusionsvorgängen führen. Diffusion und Phasenumwandlungen können sich positiv oder negativ auf die Eigenschaften eines Schichtsystems auswirken. Einerseits können diese Mechanismen zur Einstellung und Optimierung von Eigenschaften genutzt werden, andererseits können aber auch unerwünschte Effekte auftreten, die die Eigenschaften eines Schichtsystems erheblich verschlechtern oder sogar zur Zerstörung eines Bauteils führen könnten. Es besteht deswegen ein großes Interesse, ein grundlegendes Verständnis für Diffusion und Phasenumwandlungen in dünnen Schichten zu erlangen.

Die Auswirkungen einer hohen Dichte von kristallinen Defekten und Korngrenzen auf die Diffusion waren in der Vergangenheit der Gegenstand von zahlreichen Untersuchungen [Balluffi and Blakely (1975), Gilmer and Farrell (1976), Poate *et al.* (1978), Hwang and Balluffi (1979), Bukaluk (2000)]. Sehr viel weniger Aufmerksamkeit hat der Einfluß von nicht-hydrostatischen Spannungszuständen auf die Diffusion (und Phasenumwandlungen) erhalten. Es gibt nahezu keine quantitativen experimentellen Untersuchungen zum Einfluß von Spannungszuständen auf Diffusion in Schichtsystemen obgleich in zahlreichen Arbeiten der mögliche Einfluß von Spannungen zwar erwähnt, aber weder qualitativ noch quantitativ interpretiert wird [Balluffi and Blakely (1975), Ostrovsky *et al.* (2001), Balandina *et al.* (1998)]. Die wenigen Ansätze zur Quantifizierung leiden unter völlig unzureichenden Abschätzungen der auftretenden Spannungen und/oder der Benutzung von unzureichenden theoretischen Überlegungen zum Einfluß von Spannungen auf Diffusion [Balandina *et al.* (1998), Ostrovsky *et al.* (2001)].

Es muß an dieser Stelle erwähnt werden, daß die Spannungen in dünnen Schichten ausgesprochen groß sein können und im allgemeinen mehrere verschiedene Ursachen haben können. Neben Eigenspannungen, die aus der Herstellung der Schichten resultieren [siehe z.B. Ohring (2002)], können weitere Spannungen während Temperaturänderungen (durch die Fehlpassung der thermischen Ausdehnungskoeffizienten der Schichten untereinander oder bezüglich des Substrates) oder durch externe mechanische Belastungen von Schichtsystemen entstehen.

Auch Diffusion selbst kann zur Entwicklung von Spannungen führen wenn die partiellen Molvolumina der diffundierenden Spezies unterschiedlich sind: in diesem Fall können Konzentrationsänderungen, abhängig von den jeweils auftretenden Randbedingungen (z.B. freistehendes Schichtsystem, Schichtsystem auf einem rigiden Substrat), zu sehr großen Spannungen führen.

Es sollte deswegen nicht vom Einfluß von Spannungen auf die Diffusion, sondern vielmehr von der Wechselwirkung zwischen Spannungen und Diffusion gesprochen werden.

Es muß nochmals ausdrücklich darauf hingewiesen werden, daß die in Schichtsystemen auftretenden Spannungen im allgemeinen nicht hydrostatisch sind. Während der Einfluß von hydrostatischen Spannungszuständen auf die Diffusion in der Literatur wohl bekannt ist [Shewmon (1989), Philibert (1991)] und bereits zum Standard-Lehrbuchwissen gehört, ist dies für den Einfluß von nicht-hydrostatischen Spannungszuständen nicht der Fall.

Im Kapitel 2 dieser Arbeit wird der Einfluß von nicht-hydrostatischen (insbesondere: ebenen, rotationssymmetrischen) Spannungszuständen auf die Interdiffusion in einem binären, substitutionellen Diffusionspaar theoretisch betrachtet.

In den Kapiteln 3 und 4 werden experimentelle Ergebnisse vorgestellt, die an einem Kupfer-Palladium Dünnschicht-Diffusionspaar erhalten wurden. Insbesondere wurden Diffusionskoeffizienten, die Bildung neuer Phasen und die Entwicklung der Spannungen im Diffusionspaar während der Glühbehandlung untersucht.

## 5.2. Wechselwirkung von Spannungen und Diffusion in binären, substitutionellen Legierungen - Kapitel 2

### 5.2.1. Grundlagen

Das erste Ficksche Gesetz stellt die grundlegende Transportgleichung für die Beschreibung von Diffusionsvorgängen dar: gemäß dem ersten Fickschen Gesetz ist die Flußdichte  $j$  dem Konzentrationsgradienten  $\partial c / \partial x$  proportional:

$$j = -D \frac{\partial c}{\partial x}, \quad (5.1)$$

wobei  $D$  der Diffusionskoeffizient ist.

Die Grenzen der Anwendbarkeit des ersten Fickschen Gesetzes werden in vielen Fällen nicht beachtet. Es muß an dieser Stelle erwähnt werden, daß das erste Ficksche Gesetz so abgeleitet werden kann, daß die Flußdichte proportional zu dem Gradienten des chemischen Potentials gesetzt wird (siehe z.B. Shewmon (1989)):

$$j \propto \frac{\partial m}{\partial x}. \quad (5.2)$$

Diese Ableitung setzt zweierlei voraus:

- (i) Das das chemische Potential einer Atomsorte eine im System eindeutig definierbare Größe ist.
- (ii) Das das chemische Potential im thermodynamischen Gleichgewicht im betrachteten System konstant ist, d.h. der Gradient des chemischen Potentials identisch Null ist.

Das Konzept des chemischen Potentials basierte ursprünglich auf der thermodynamischen Betrachtung von Flüssigkeiten und ist nicht ohne weiteres auf (kristalline) Festkörper anwendbar. Festkörper unterscheiden sich von Flüssigkeiten dadurch, daß ihnen ein sogenanntes „Netzwerk“ zugeordnet werden kann [siehe z.B. Larche & Cahn (1973)]. Der Fall einer substitutionellen Legierung soll als Beispiel dienen: dann besteht das Netzwerk aus dem Kristallgitter. Jeder Platz im Netzwerk kann durch verschiedene Atome oder durch eine Leerstelle besetzt werden. Das Hinzufügen eines Atoms zum System ist nun offensichtlich nicht ohne weiteres möglich; vielmehr muß angegeben werden, wie das Hinzufügen geschehen soll: z.B. durch Entfernung eines Atoms von einem Platz im Netzwerk etc.

Die Existenz des Netzwerkes führt nun dazu, daß die Konzentrationen der verschiedenen Atomsorten im Netzwerk nicht mehr unabhängig voneinander sind. Gibt es  $N$  Atomsorten, so existieren nur  $(N-1)$  unabhängige Konzentrationsvariablen. Larche und Cahn [Larche und Cahn (1985)] konnten durch Betrachtungen des thermodynamischen Gleichgewichtes zeigen, daß in diesem Fall die chemischen Potentiale keine Größen sind, die im thermodynamischen Gleichgewicht konstant im System sind. Statt dessen müssen die sogenannten Diffusionspotentiale verwendet werden, die nun im thermodynamischen Gleichgewicht konstant sind. Anschaulich kann das Diffusionspotential  $M_{il}$  als Änderung der freien Energie interpretiert werden, die bei dem Ersetzen eines Atoms vom Typ  $l$  durch ein Atom vom Typ  $i$  entsteht.

Es muß an dieser Stelle erwähnt werden, daß von Larche und Cahn [Larche und Cahn (1973), (1985)] gezeigt werden konnte, daß das Konzept der Diffusionspotentiale im Falle von hydrostatischen Spannungszuständen äquivalent zum Konzept der chemischen Potentiale ist, im Falle nicht-hydrostatischer Spannungszustände jedoch das Konzept der chemischen Potentiale versagt.

Als Ausgangspunkt für die Ableitung einer Transportgleichung wird nun analog zur Gleichung (5.2) der folgende Ansatz gemacht:

$$j_i \propto \frac{\partial M_{il}}{\partial x}. \quad (5.3)$$

Dabei kann  $l$  jede andere Atomsorte (Leerstellen werden hierbei auch als Atomsorte betrachtet, d.h. der Index  $l$  kann auch für die Leerstellen stehen) im System sein.

Im Kapitel 2 der Arbeit werden ausgehend von Gleichung (5.3) Transportgleichungen analog zum ersten Fickschen Gesetz hergeleitet. Dazu wird die Interdiffusion in einem binären, substitutionellen System betrachtet, welches unter einem ebenen, rotationssymmetrischen Spannungszustand steht. Währenddessen die Gleichungen im am Kristallgitter fixierten Koordinatensystem schon in der Literatur bekannt sind, wird in dieser Arbeit nun erstmals eine vollständige Ableitung der Transportgleichungen im Laborsystem angegeben. Es zeigt sich, daß die Flußdichte nun nicht nur proportional zum Konzentrationsgradienten ist. Vielmehr tritt additiv ein weiterer Term in der Gleichung für  $j$  auf: danach ist die Flußdichte nun auch proportional zu dem Produkt aus der Differenz der partiellen Molvolumina der

interdiffundierenden Spezies (im Falle eines binären Systems) und dem Gradienten der Spur des Spannungstensors.

### 5.2.2. Exemplarische numerische Berechnungen

Zur Veranschaulichung der theoretischen Überlegungen wurden Berechnungen für ausgewählte Modellsysteme durchgeführt. Insbesondere wurden ausgehend von Daten für das System Kupfer-Palladium Berechnungen von Konzentrationsprofilen in einem Dünnschicht-Diffusionspaar durchgeführt. Dabei wurden sowohl extern angelegte Spannungsfelder als auch auf Grund der Diffusion entstehende Spannungsfelder berücksichtigt.

Eine analytische Lösung der zu Grunde liegenden Gleichungen ist im allgemeinen nicht möglich. Für eine numerische Lösung wurden die Grundgleichungen (d.h. die Transportgleichung (analog zum ersten Fickschen Gesetz) und die Kontinuitätsgleichung (d.h. das zweite Ficksche Gesetz) diskretisiert und die Berechnung numerisch auf Basis der sogenannten ‚finite-difference‘-Methode unter Verwendung dimensionsloser Variablen ausgeführt [Crank (1973)].

Ein Beispiel ist in der Abbildung 5.1 dargestellt. Es wurden zwei extern angelegte Spannungsfelder betrachtet. Die Spannungsgradienten, die in der Nähe der ursprünglichen Grenzfläche auftreten, unterscheiden sich dabei im Vorzeichen.

Im ersten betrachteten Fall führt der Spannungsgradient zu einer sehr auffälligen Verzerrung des Konzentrations-Tiefenprofils in der Mitte des Diffusionspaares. Dies kann wie folgt verstanden werden: der Beitrag zur Flußdichte, welcher vom Spannungsgradienten herrührt, ist in der Nähe der ursprünglichen Grenzfläche sehr groß (da dort der Spannungsgradient sehr groß ist); dadurch ist der Fluß sehr groß. In etwas größerem Abstand von der Grenzfläche ist die Spannung jedoch konstant, der Gradient der Spannung also Null; dort können Atome also nur auf Grund von Konzentrationsgradienten transportiert werden. Dieser führt zu einer Aufstauung von Atomen in den Bereichen, in denen der Spannungsgradient Null wird und damit zu der auffallenden Verzerrung des Konzentrationsprofils.

Im zweiten betrachteten Fall wirken der Konzentrationsgradient und der Spannungsgradient in der Nähe der ursprünglichen Grenzfläche einander entgegen und dadurch wird die Interdiffusion verlangsamt.



Qualitativ kann der Einfluß von Spannungen (genauer gesagt Spannungsgradienten) so verstanden werden, daß Atome mit kleinerem partiellem Molvolumen sich bevorzugt in Bereiche mit Druckspannungen, Atome mit größerem partiellem Molvolumen sich hingegen bevorzugt in Bereiche mit Zugspannungen begeben.

Weitere Beispiele für Berechnungen und eine ausführlichere Diskussion können im Kapitel 2 der Arbeit nachgelesen werden.

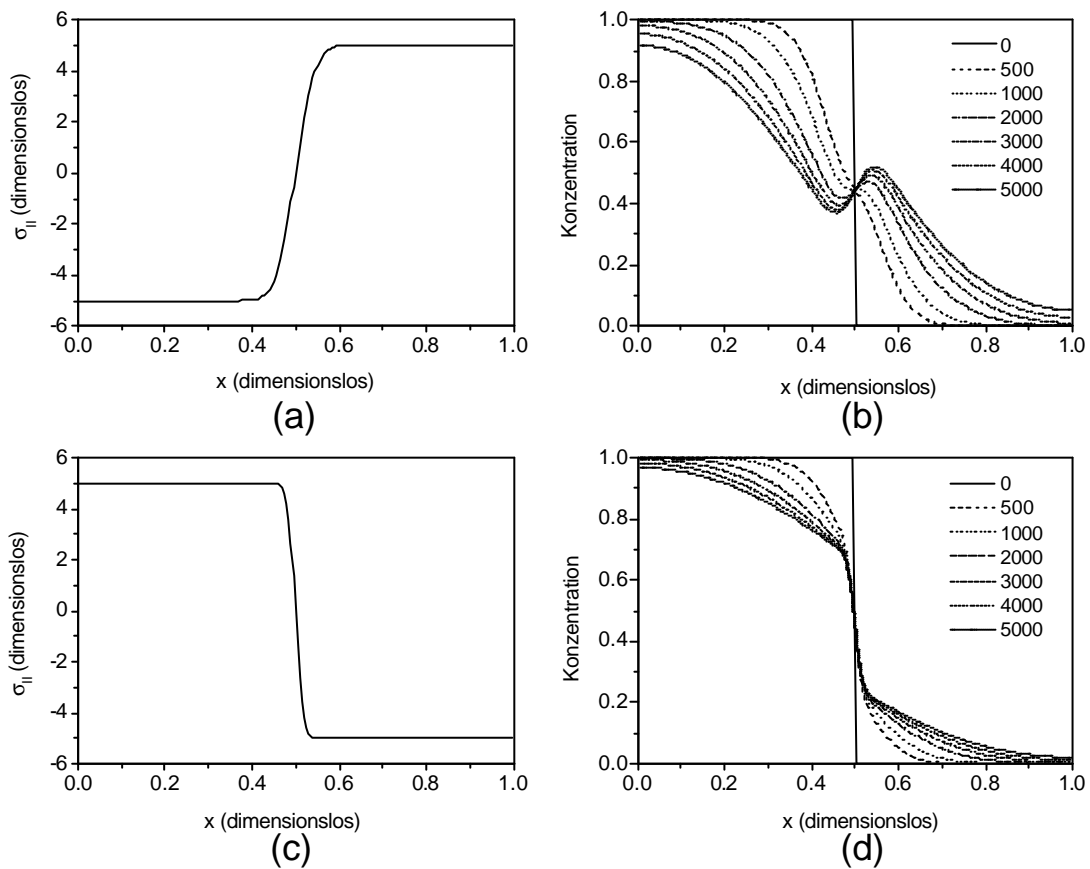


Abbildung 5.1: Spannung  $\sigma_{||}$  als Funktion der Position  $x$  in der Probe (a und c; es wird von einem ebenen, rotationssymmetrischen Spannungszustand ausgegangen) und zugehörige Palladium Konzentrationstiefenprofile für verschiedenen Zeiten (b) und (d); Legende im Bild: Anzahl der Zeitschritte). Für die Definition der dimensionslosen Größen, siehe Kapitel 2 der Arbeit.

### **5.3. Untersuchungen der Diffusion in Palladium-Kupfer Dünnschicht-Diffusionspaaren: Bestimmung und Diskussion von Diffusionskoeffizienten - Kapitel 3**

#### **5.3.1. Einleitung: untersuchte Proben und experimentelle Durchführung**

Durch Magnetronspuiten in einer UHV-Kammer wurden Palladium-Kupfer Diffusionspaare (Schichtdicke jeweils 50nm) auf Silizium-Wafern, welche an der Oberfläche mit einer amorphen  $\text{Si}_3\text{N}_4$ -Schicht belegt waren, hergestellt. Die Diffusionspaare wurden in Quarzampullen unter Schutzgas in einem Ölbad bei Temperatur von 175°C bis 250°C wärmebehandelt.

Die Schichten wurden vor und nach der Wärmebehandlung mit Röntgendiffraktometrie zur Phasenanalyse, Transmissionselektronenmikroskopie zur Untersuchung der Mikrostruktur und Auger-Elektronen-Spektroskopie (in Kombination mit Sputterabtragung) zur Bestimmung von Konzentrationstiefenprofilen untersucht.

Aus den Ergebnissen der Auger-Elektronen-Spektroskopie wurden Volumendiffusionskoeffizienten auf Basis der ‚Centre-gradient‘- (CG-Methode, Hall and Morabito(1976)), und ‚Plateau-rise‘-(PR-Methode, Hall *et al.* (1976)) Methoden ermittelt. Korngrenzendiffusionskoeffizienten von Palladium in Kupfer-Korngrenzen wurden mit Hilfe der ‚Whipple-Le Claire‘- [WLC-Methode, Whipple (1954), Le Claire (1963)] Methode bestimmt.

#### **5.3.2. Ergebnisse und Diskussion**

Die Untersuchungen der Mikrostruktur mit Transmissionselektronenmikroskopie ergaben, daß im wesentlichen eine kolumnare Mikrostruktur in den Schichten vorliegt. Bei der Wärmebehandlung treten bis 225°C keine wesentlichen Änderungen in Mikrostruktur auf. Bei den Wärmebehandlungen bei 250°C kommt es jedoch zum Wachstum von Körnern und auch die ursprüngliche Grenzfläche kann in der Mikrostruktur nicht mehr eindeutig lokalisiert werden.

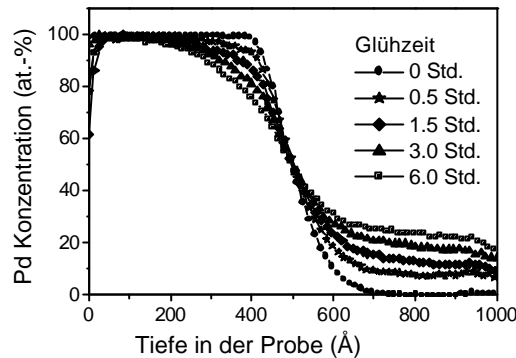


Abbildung 5.2: Pd Konzentrationstiefenprofile als Funktion der Glühzeit bei einer Temperatur von 225°C. Auffallend ist die Ausbildung eines Plateaus auf der Cu-reichen Seite der Probe.

Bei der Wärmebehandlung tritt erhebliche Interdiffusion auf. Abbildung 3.1 zeigt exemplarisch Konzentrations-Tiefenprofile für eine bei 225°C ausgelagerte Probe.

Es fällt auf, daß die Profile auf der Cu-reichen Seite ein deutliches Konzentrationsplateau aufweisen, welches auf der Pd-reichen Seite nicht auftritt. Ein Plateau entsteht im allgemeinen durch die Zusammenwirkung von schneller Korngrenzendiffusion und Volumendiffusion in Proben mit

kolumnarer Mikrostruktur. Die Abwesenheit eines Plateaus auf der Pd-reichen Seite der Probe kann nicht in der Abwesenheit von Korngrenzendiffusion begründet sein, denn es konnte nachgewiesen werden, daß durch Korngrenzendiffusion Kupfer zur Oberfläche der Probe gelangt. Aus den Untersuchungen zur Mikrostruktur ist bekannt, daß die Dichte der Korngrenzen in den beiden Subschichten ähnlich ist. Folglich muß der Volumendiffusionskoeffizient eine starke Konzentrationsabhängigkeit aufweisen und auf der Pd-reichen Seite deutlich kleiner als auf der Cu-reichen Seite sein.

Die mit den verschiedenen Methoden erhaltenen Diffusionskoeffizienten sind in den Tabellen 5.1 und 5.2 zusammengefaßt.

Tabelle 5.1: Zusammenstellung der Volumendiffusionskoeffizienten  $\tilde{D}$  (CG...’centre-gradient’-Methode, PR...’plateau-rise’-Methode).

Temperatur (°C)	Zeit (Stunden)	$\tilde{D}$ CG- Methode (cm <sup>2</sup> Sec. <sup>-1</sup> )	$\tilde{D}$ PR- Methode (cm <sup>2</sup> Sec. <sup>-1</sup> )
175	0.5	$9.6 \times 10^{-18}$	$4.54 \times 10^{-19}$
175	3	$3.1 \times 10^{-18}$	$2 \times 10^{-19}$
175	6	$2.0 \times 10^{-18}$	$1.9 \times 10^{-19}$
175	10	$1.45 \times 10^{-18}$	$1.25 \times 10^{-19}$
200	0.5	$4.37 \times 10^{-17}$	$2.35 \times 10^{-18}$
200	3	$1.16 \times 10^{-17}$	$1.2 \times 10^{-18}$
200	6	$1.0 \times 10^{-17}$	$1.03 \times 10^{-18}$
225	0.5	$7.14 \times 10^{-17}$	$8.9 \times 10^{-18}$
225	1.5	$4.75 \times 10^{-17}$	$7.4 \times 10^{-18}$
225	3	$4.58 \times 10^{-17}$	$7.6 \times 10^{-18}$
225	6	$4.34 \times 10^{-17}$	$6.7 \times 10^{-18}$
250	0.5	$3 \times 10^{-16}$	$2.9 \times 10^{-17}$

Tabelle 5.2: Zusammenstellung der Korngrenzendiffusionskoeffizienten (CG...’centre-gradient’-Methode, PR...’plateau-rise’-Methode).

Temperatur (°C)	Zeit (Stunden)	Korngrenzendiff.- Koeffizient (benutzt: $\tilde{D}_{CG}$ ) (cm <sup>2</sup> Sec. <sup>-1</sup> )	Korngrenzendiff.- Koeffizient (benutzt: $\tilde{D}_{PR}$ ) (cm <sup>2</sup> Sec. <sup>-1</sup> )
175	0.5	$7.1 \times 10^{-14}$	$1.54 \times 10^{-14}$
175	3	$1.95 \times 10^{-14}$	$4.96 \times 10^{-15}$
175	6	$1.35 \times 10^{-14}$	$4.15 \times 10^{-15}$
175	10	$9.4 \times 10^{-15}$	$2.76 \times 10^{-15}$
200	0.5	$2.17 \times 10^{-13}$	$5.03 \times 10^{-14}$
200	3	$1.34 \times 10^{-13}$	$4.31 \times 10^{-14}$
200	6	$1.21 \times 10^{-13}$	$3.88 \times 10^{-14}$
225	0.5	$4.1 \times 10^{-13}$	$1.45 \times 10^{-13}$
225	1.5	$2.12 \times 10^{-13}$	$8.35 \times 10^{-14}$
225	3	$1.72 \times 10^{-13}$	$6.99 \times 10^{-14}$
225	6	$2.12 \times 10^{-13}$	$8.37 \times 10^{-14}$
250	0.5	$7.06 \times 10^{-13}$	$2.19 \times 10^{-13}$

Beim Vergleich mit Literaturwerten, die an Bulk-Vielkristallen erhalten wurden, stellt man fest daß die hier ermittelten Diffusionskoeffizienten, wie erwartet, sehr viel größer sind (typischerweise acht Größenordnungen).

Es fällt auf, daß die mit der CG-Methode bestimmten Diffusionskoeffizienten größer als die mit der PR-Methode bestimmten Koeffizienten sind. Dies wurde in Literatur bereits berichtet und liegt daran, daß im allgemeinen die Dichte kristalliner Defekte in der Nähe der Grenzfläche der Subschichten größer ist.

Es fällt weiterhin auf, daß die Diffusionskoeffizienten zeitabhängig sind: sie nehmen mit zunehmender Dauer der Wärmebehandlung ab. Dies liegt zum einen daran, daß auch die Dichte der kristallinen Defekte (welche ja die Diffusion beschleunigen) mit der Zeit abnimmt. Eine weitere mögliche Ursache ist die Phasenbildung: Durch die röntgenografische Phasenanalyse konnte gezeigt werden, daß die Interdiffusion von der Bildung der Phasen  $\text{Cu}_3\text{Pd}$  und  $\text{CuPd}$  begleitet wird. Zunächst bildet sich die Phase  $\text{Cu}_3\text{Pd}$ . Erst bei der Temperatur von  $250^\circ\text{C}$  tritt merklich die Bildung von  $\text{CuPd}$  auf. Die Diffusion ist in den Phasen  $\text{Cu}_3\text{Pd}$  und  $\text{CuPd}$  verlangsamt. Die Diffusionskoeffizienten nehmen deswegen ab.

Es muß betont werden, daß die Möglichkeit der Bildung von neuen Phasen bei Diffusionsstudien in dünnen Schichten oft keine Beachtung findet: falls die Konzentrations-Tiefenprofile keinen Hinweis auf Phasenumwandlungen geben, wird meist davon ausgegangen, daß keine Phasenumwandlungen auftreten. In dieser Arbeit konnte jedoch gezeigt werden, daß die auftretenden Phasenumwandlungen sich nicht in den Konzentrations-Tiefenprofilen widerspiegeln, sondern nur durch sorgfältige Röntgenbeugungsuntersuchungen nachzuweisen waren.

## **5.4. Untersuchungen der Diffusion in Palladium-Kupfer Dünnschicht-Diffusionspaaren: Phasenumwandlungen und Entwicklung der Spannungen im System - Kapitel 4**

### **5.4.1 Einleitung: untersuchte Proben und experimentelle Durchführung**

Die Probenherstellung sowie die Charakterisierung der Phasenzusammensetzung und der Mikrostruktur erfolgten gemäß der in Kapitel 5.3.1 angegebenen Beschreibung. Die mechanischen Spannungen der Palladium- und Kupfer-Schichten wurden stets vor und nach einer Wärmebehandlung mittels der röntgenografischen  $\sin^2\psi$ -Methode gemessen [Welzel *et al.* (2004)]. Zusätzlich wurde die mittlere Spannung des Schichtsystems während der Wärmebehandlung in-situ gemessen, indem die Wärmebehandlung in Stickstoff in einer Apparatur durchgeführt wurde, die die Messung der Substratkrümmung erlaubt. Aus der Krümmung läßt sich bei Kenntnis der elastischen Eigenschaften des Substrates, der Dicke des Substrates und der Dicke der Schicht die mittlere Spannung des Schichtsystems berechnen.

Die mittels Röntgenbeugung gemessenen Spannungswerte beziehen sich auf Raumtemperatur. Auch wenn die Spannungen in den Schichten vor und nach der Wärmebehandlung vorliegen, läßt sich nicht auf die Spannungsveränderungen während der Wärmebehandlung zurückschließen, da beim Aufheizen und Abkühlen Spannungen plastisch relaxiert werden könnten (d.h. die Spannungsveränderungen beim Aufheizen und Abkühlen können nicht aus den thermischen Ausdehnungskoeffizienten von Schichten und Substrat berechnet werden).

Durch die Kombination von röntgenografischer Spannungsmessung (ex-situ) und Spannungsmessung mittels der Substratkrümmungsmethode (in-situ) war es jedoch möglich, die Spannungsveränderungen während der Temperaturbehandlung zu ermitteln.

### 5.4.2. Ergebnisse und Diskussion

Für die Kurzfassung der Ergebnisse zur Interdiffusion, Phasenumwandlungen und zur Entwicklung der Mikrostruktur sei der Leser auf Kapitel 5.3.2 verwiesen. Im folgenden

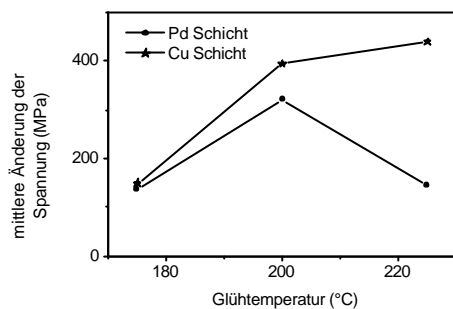


Abbildung 5.3: Spannungsänderungen in den Schichten während der Wärmebehandlung (Dauer: 6 Std.).

werden nur die Ergebnisse der Untersuchungen zur Spannungsentwicklung diskutiert.

Die Abbildung 5.3 zeigt die Änderungen der Spannungen in der Palladiumschicht und der Kupferschicht als Funktion der Temperatur (die Dauer der Wärmebehandlung war für alle Proben: 6 Stunden Haltezeit bei der angegebenen Temperatur). Die Spannungsänderungen wurden (siehe Kapitel 4.1) durch eine

Kombination von Ergebnissen der röntgenografischen Spannungsmessungen und der Spannungsmessungen mittels der Substratkrümmungsmethode ermittelt. Die Wärmebehandlung führt in beiden Schichten zur Erzeugung signifikanter Zugspannungsbeiträge.

Eine ausführliche Diskussion der möglichen Einflußgrößen wird in Kapitel 4. dieser Arbeit gegeben. Es stellt sich heraus, daß mehrere, konkurrierende Einflußfaktoren existieren und nur ein einzelner Prozeß nicht ausreicht, um die gewonnen Ergebnisse zu erklären. Die folgenden Einflußfaktoren können für das untersuchte Probensystem von Bedeutung sein:

- (i) Unterschiede in den partiellen Molvolumina von Kupfer und Palladium führen bei der Diffusion zu Spannungen (siehe auch Einleitung zur Kurzfassung, Kapitel 5.1.). Für das betrachtete Probensystem entstehen bei der Interdiffusion Druckspannungen in Kupfer und Zugspannungen in Palladium.
- (ii) Kornwachstum führt zur Zugspannungen, da Korngrenzen, die Regionen geringerer Dichte darstellen, annihiliert werden.
- (iii) Die Stromdichten für Kupfer- und Palladiumatome können unterschiedlich groß sein; In diesem Fall tritt ein Leerstellenstrom in der Probe auf. Die Erzeugung und Annihilation der

Leerstellen ist mit der Entstehung von Spannungen verknüpft. Leider können die einzelnen Stromdichten (genauer: die partiellen Diffusionskoeffizienten) nicht aus Konzentrationstiefenprofilen bestimmt werden: dazu wären Marker-Experimente nötig. Wenn also auch dieser Mechanismus als spannungsverursachend betrachtet werden muß, so sind quantitative Aussagen nicht möglich.

(iv) Plastische Deformation kann auftreten wenn die Spannungen in den Schichten die jeweiligen Fließgrenzen überschreiten. Plastische Deformation führt in jedem Fall zum Abbau von Spannungen.

Aus der Auflistung von möglichen Einflußfaktoren wird deutlich, daß eine einfache Einschränkung auf einen (dominanten) Mechanismus nicht ohne weiteres möglich ist. In-situ Untersuchungen der Spannungsentwicklung in dünnen Schichten während der Interdiffusion, wie sie in dieser Arbeit erstmals durch die Kombination von zwei Methoden realisiert wurden, stellen in jedem Fall Schlüsselexperimente dar, die benötigt werden um ein besseres Verständnis für die Spannungsentwicklung in dünnen Schichten während der Interdiffusion zu erreichen.



## REFERENCES

- Arzt E. (1998), *Acta Mater.*, 46, 561
- Balandina N., Bokstein B and Ostrovsky A. (1998), *Defect and Diffusion Forum*, 156, 181
- Balluffi R. W. and Blakely J. M. (1975), *Thin Solid Films*, 25, 363
- Baranowski B. (1989), *J. Less-Common Metals*, 154, 329
- Benedictus R., Bottger A. and Mittemeijer E. J. (1996), *Phys. Rev. B*, 54, 9109
- Boer F. R., Boom R, Mattens W.C.M, Miedema A.R. and Niessen A.K. (1989), Cohesion in metals: Cohesion and structure, Vol.1 Eds. Boer F. R., de and Pettifor D. G., North Holland
- Bukaluk A.(2001), *Appl. Surf. Sci.*, 175-176, 790
- Bukaluk A.(1999), *Vacuum*, 54, 279
- Bukaluk A. (1983), *Surf. and Interface Anal.*, 5, 20
- Bukaluk A. (2000), *Surf. and Interface Anal.*, 30, 597
- Chaudhari P. (1971), *J. Vac. Sci. and Tech.*, 9, 520
- Crank J. (1973), *The Mathematics Of Diffusion*, Second edition, (Clarendon Press. Oxford,)
- Darken L.S. (1948), *Trans. AIME*, 175, 184
- DeBonte W. J. (1975), Poate J. M., Melliard-Smith C. M. and Levesque R. A., *J. Appl. Phys.*, 46, 4284
- De Groot S.R. and Mazur P., *Non-equilibrium Thermodynamics* (Amsterdam, North Holland, 1962)
- d'Heurle F.M. (1998), *J. Mater. Res.*, 3, 167
- d'Heurle F.M., Gas P. and Philibert J. (1997), *Defect and Diffusion Forum*, 143-147, 529
- d'Heurle F.M., Gas P. and Philibert J. (1995), *Solid State Phenomena*, 41, 93
- d'Heurle Francois M. Gas Patrick, Lavoie Christian and Philibert Jean (2004), *Zeitschrift fur Metallkd*, 95, 10
- Doerner Mary F.and Nix William D. (1988), *Critical Reviews in Solid state and Materials Sciences*, 14, 3
- Flinn P. A., Gardner D.S. and Nix W.D. (1987), *IEEE Trans. Electr. Dev*, 34, 689
- Gao H., Zhang L., Nix W.D., Thompson C.V. and Arzt, E. (1999), *Acta Mater.*, 47, 2865
- Garcia V. H. Mors P.M. and Scherer C. (2000), *Acta Mater.* 48, 1201

## References

---

- Gibbs Willard J. (1928), *The collected Works*, Vol. I Thermodynamics, (Longmans, Green And CO, New York), pp.55
- Gilmer G. H. and Farrell H. H. (1976a), *J. Appl. Phys.*, 47, 3792
- Gilmer G. H. and Farrell H. H. (1976b), *J. Appl. Phys.*, 47, 4373
- Gleiter H. (1989), *Prog. Mater. Sci.* 33, 79
- Goesele U, and Tu K.N. (1982), *J. Appl. Phys.*, 53, 3252
- Grant J. T. (1989), *Surf. and Interface Anal.*, 14, 271
- Guymont M., and gratias D. (1976), *Phys.Stat.Sol.(a)* 36, 329
- Hall P.M., Morabito J.M. and Poate J. M. (1976), *Thin Solid Films*, 33, 107
- Hall P. M. and Morabito J. M. (1976), *Surf. Sci.*, 54, 79
- Harrison L.G. (1961), *Trans. Faraday Soc.* 57, 1191
- Hauk V. (1997), *Structural and Residual stress Analysis by Nondestructive Methods*, (Elsevier, Amsterdam).
- Hirabayashi M. and Ogawa S. (1957), *J. Phys. Soc. Japan*, 12, 259
- Hodaj F. and Gusak A.M. (2004), *Acta Mater.*, 52, 4305
- Ho P. S., Lewis J. E. and Howard L. K. (1977), *J. Vac. Sci. Technol.*, 14, 322
- Hofmann S., (1992), *J. Vac. Sci. Technol. B*, 10, 316
- Hofmann S. (1994), *Surf. And Interface Anal.*, 21, 673
- <http://www.chimdocet.it/solido/file11.htm>
- <http://bell.mma.edu>
- <http://www.webelements.com/>
- Hultgren R., Desai P.D., Hawkins D.T., Gleiser M. and Kelley K.K. (1973), *Selected Values of the Thermodynamic Properties of Binary Alloys* (American Society For Metals, Metals park, Ohio).
- Hwang J.C.M. and Balluffi R.W. (1979), *J. Appl. Phys.*, 50, 1339
- JEOL JAMP 7830F Field Emission Auger Microprobe Database.
- Jeon I. J., Hong J. H. and Lee Y. P. (1994), *J. Appl. Phys.*, 75, 7825
- Jones F.W. and Sykes C. J. (1939), *Inst. Metals*, 65, 419.
- Kandasamy K. (1988), *Script. Metall.* 22, 479
- King Alexander H. and Harris Karen E., *Polycrystalline Thin Films: Structure, Texture, Properties and Applications*, Eds. Barmak K., Parker M.A., Floro J.A.,

## References

---

- Sinclair R and Smith D.A. (1994), *MRS Symposium Series* 343, 33
- Larche F. and Cahn J.W. (1973), *Acta Metall.* 21, 1051
- Larche F. and Cahn J.W. (1982), *Acta Metall.* 30, 1835
- Cahn J.W. and Larche F.C. (1983), *Script. Metall.* 17, 927
- Larche F.C. and Cahn J.W. (1985), *Acta Metall.*, 33, 331
- Larche F. C. and Cahn J.W. (1992), *Acta Metall.* 40, 947
- Le Claire A. D.(1963), *Br. J. Appl. Phys.*, 14, 351
- Li J.C.M. (1966), Oriani R.A. and Darken L.S., *Zeitschrift Fur Physikalische Chemi Neue Folge*, Bd.49, S, 271
- Li J., Strane J. W., Russell S. W., Hong S. Q. and Mayer J. W. (1992), *J. Appl. Phys.* 72, 2810
- Li, J.C.M. (1978), *Metall. Trans. A*, 9A, 1353
- Lo C.C. and Schuele D. E. (1975), *J. Appl. Phys.*, (46), 5005
- McLellan A.G. (1968), *Proc. Roy. Soc. (London)*, A307, 1
- Nazarov A.A. (2003), *Phys. of the Sol. St.*, 45, 1166
- Nakahara S., Abys J.A. and Abys S.M. (1983), *Mat. Lett.*, 2, 155
- Neukam O. (1970), *Galvanotechnik (Saulgau/Wurt)*, 61, 626
- Nix W. D. (1989), *Metall. Trans. A*, 20A, 2217
- Nolfi F.V, Jr. (1973), *J. Appl. Phys.*, 44, 5245
- Noyan Ismail C. and Cohen Jerome B. (1987), *Residual Stress*, Springer-Verlag NeW York. Inc., pp. 118
- Nye J.F. (1955), *Physical Properties of Crystals*, (Clarendon Press, Oxford,) pp. 145
- Ohring M. (2002), *Materials Science of Thin Films, Deposition and Structure*, 2<sup>nd</sup> edition. Academic Press. pp. 703
- Onsager L. (1931a), *Phys. Rev.* 37, 405
- Onsager L. (1931b), *Phys. Rev.* 38, 2265
- Ostrovsky AS and Bokstein BS (2001), *Appl. Surf. Sci.*, 175, 312
- Ovid'ko I. A. and Reizis A. B. (2001), *Phys. of the Sol. St.*, 43, 35
- Pearson W.B. (1967), *Handbook of Lattice Spacings and Structures of Metals*, (Pergamon Press, Vol.II)
- Periodic Table of Elements* (Wiley-VCH Verlag GmbH, 1992, 2<sup>nd</sup> edition)

## References

---

- Philibert J. (1991), *Atom movements diffusion and mass transport in solids*, Les editions de Physique pp.190.
- Philibert J. (1991), *Atom Movements Diffusion and Mass Transport in Solids*, Les Editions De Physique, pp. 233
- Philibert J. (1991), *Atom Movements Diffusion and Mass Transport in Solids*, Les Editions De Physique, pp. 312
- Poate J.M., Tu K.N. and Mayer J.W. (1978), *Thin Films-Interdiffusion And Reactions*, John Wiley and Sons. pp. 161
- Pretorius R. (1984), *Mater. Res. Soc.Proc.*, 25, 10.
- ProFit for Windows Users's Guide, *Philips Analytical X-ray*, 1<sup>st</sup> edition, Almelo, 1996
- Prussin S (1961). *J. Appl. Phys.* 32, 1876
- Reed-Hill Robert E. (1973), *Physical Metallurgy principles*, Litton Educational Publishing INC.
- Residual Stress, Ismail C. Noyan and Jerome B. Cohen (1987), Springer-Verlag NeW York Inc., pp.72
- Shewmon, P.G. *Diffusion of solids*, (1989), The Minerals ,Metals and Materials Society Warrendale, Pennsylvania pp.85
- Shewmon, P.G. *Diffusion of solids*, (1989), The Minerals, Metals and Materials Society Warrendale, Pennsylvania, pp.137
- Simon A. M. and Grzywna (1992), Z. J., *Acta Metall.* 40, 3465
- Sinfelt. J. H. (1983), *Bimetallic catalysts: discoveries, concenpts and applications*. New York: Wiley ,
- Smith G. D. (1965), *Numerical solution of partial differential equations* (Oxford University Press)
- Smithell's Metals Reference Hand Book, Chap.15, 7<sup>th</sup> edition (1992), Series Eds. Gale W.F. and Totemeier T.C.
- Soutter A., Colson A., and Hertz J., (1971), *Memoires Scientifiques Rev. Metallurg.LXVIII*, N<sup>o</sup> , 9
- Stevens D.W. and Powell G.W. (1977), *Metall. Trans.* 8A, 1531
- Stoney G.G. (1909), *Proc. Roy. Soc.*, A82, 172
- Strecker A., Baeder U., Kelsch M., Salzberger U., Sycha M., Gao M., Richter G. and

## References

---

- Bentham K.V. (2003), *Z. Metallkd.*, 94, 3
- Subramanian P.R. and Laughlin D.E. (1990) , *Binary Alloy Phase Diagram*, Ed. Massalski T.B., ASM Int. Mat. Park Ohio, 2, 1454
- Thomas Donald E. and Birchenall C. Ernest, (1952), *J. of Metals*, 867
- Timoshenko S.P. and Goodier, J. N., *Thermal stress*, Theory of Elasticity, McGraw-Hill Book Company, pp.433
- Tu, K. N. (1977), *J. Appl. Phys.*, 48, 3400
- Tu K. N., Ottaviani G., Goesele U. and Foell H. (1983), *J. Appl. Phys.*, 54, 758
- Tu K.N. and Berry B.S. (1972), *J. Appl. Phys.* 43, 3283
- Van Loo F. J. J. and Rieck G. D. (1973), *Acta Metall.*, 21, 61
- Wang W.L., Chou Y.T. and Lee S. (2001), *J. Mater. Res.*, 16, 1967
- Weiss D. Gao H. and Arzt E. (2001), *Acta Mater.*, 49, 2395
- Welzel U., Ligot J., Lamparter P., Vermeulen A.C. and Mittemeijer E. J. (2004), Topical review: Stress analysis of polycrystalline thin films and surface regions by X-ray diffraction, accepted for publication in *J. Appl. Cryst.*
- Welzel U. and Mittemeijer E. J. (2003), *J. Appl. Phys.*, 93, 9001
- Whipple R. T. P. (1954), *Phil. Mag.*, 45, 1225
- Windischmann H. (1992), *Crit. Rev. in Sol. St. and Mat. Sci.*, 17, 547
- Zhang Wu-Shou, Zhang Zhong-Liang and Zhang Xin-Wei (2002), *J. Alloys and Comp.* 336, 170

## Curriculum Vitae

<i>Name</i>	Jay Chakraborty
<i>Date of birth</i>	16.10.1970
<i>Place of Birth</i>	Calcutta
<i>School</i>	1980-1986 : Naktala Govt. High School West Bengal Board Of Secondary Education 1986-1988 : Nabagram Vidyapith West Bengal Council Of Higher Secondary Education
<i>College</i>	1988-1991: B. Sc. (Physics) Ramkrishna Mission Residential College Narendrapur University of Calcutta, India
<i>University</i>	1991Sept. - 1994 March, M. Sc. (Physics) University of Kalyani, India 1995 -1997: M.Tech. (Materials Sc. & Tech.) Banaras Hindu University, India
<i>Research experience</i>	1994 August -1995August : Research Scholar Department of Physics (I.I.T. Kharagpur, India) 1998 April – 2001 July 31 <sup>st</sup> : Scientist-SC Institute For Plasma Research, Gandhinagar, India Under extraordinary leave since July 31 <sup>st</sup> 2001.
<i>Ph. D Study</i>	Since 1 <sup>st</sup> August, 2001: Ph.D Student at Max Planck Institute for Metals Research and Institut für Metallkunde, University of Stuttgart, Stuttgart.



## **Acknowledgements**

First of all I would like to thank Prof. Dr Ir. E. J. Mittemeijer for accepting me as a PhD student in his department. I would also like to thank him for his outstanding commitment, the continuous supervision and the numerous scientific discussions, which have considerably contributed to the completion of this work. Finally, I would like to thank him for writing the main opinion ('Hauptbericht') for the thesis.

I would like to thank Prof. Dr F. Aldinger for writing the second opinion ('Mitbericht') for the thesis.

Dr U. Welzel, my daily supervisor, has considerably contributed to the successful completion of this work. I would like to thank him for many advices, the constant supervision and the numerous scientific discussions.

I would also like to thank all colleagues in the Department Mittemeijer and the Max Planck Institute for the cooperation, their help with respect to many technical problems and the constructive and pleasant working atmosphere.

Last but not least I would like to acknowledge the continuous support and the encouragement provided by my parents, my wife and my son. Without their help I would not have been able to achieve this goal.